Gravity Separator Revamping

by

Richard Arntzen

A Thesis Submitted for the Degree of Dr.Ing.

to

Department of Chemical Engineering
Norwegian University of Science and Technology
Trondheim, Norway

March 2001

Thesis Comittee

Prof. Dr.	Christophe Gourdon	ENSIGNC (France)
Dr.ing.	Einar Eng Johnsen	Statoil a.s (Norway)
Prof. II Dr.ing.	Arne Grislingås	NTNU (Norway)

Summary

A pilot separator for oil/water separation by gravity has been studied in a variety of experiments, to investigate the effects of mechanical design and increasing water feeds, as typically found in the tail production phase of oil producing facilities. Bench-scale experiments have also been performed, and some data from full-scale gravity separators have been studied. New model fluid systems have been composed in co-operation with the University of Bergen, and one of them (called fluid system 3, batch 1) with Exxsol D-60 added Grane crude oil showed desirable characteristics.

The water quality has been measured for several fluid systems and for both the oil- and water continuous regime. When water is the dispersed phase, the oil concentration at the water outlet increases with increasing choke pressure drop, increasing water rate and increasing coalescence rate. When water is the continuous phase, the oil concentration at the water outlet increases with increasing pressure drop, increasing water rate and decreasing dispersed phase [oil] concentration at the inlet. There is a coupling between the water continuous dispersed phase concentration and the water rate regarding water outlet quality.

The dispersion layer shows a near-linear increase in volume with dispersed phase fraction, and the coalescence rate is different for the two regimes of continuity. For fluid system 3, batch 1, oil continuous, the linear fit approaches zero dispersion layer thickness for zero water rate, and all the water is transported through the dispersion layer. For the water continuous regime, the linear fit has a negative intercept and coalescence in the inlet region is appreciable. A model found in the literature [21] was fitted to the measured dispersion layer heights, with good results after an adjustment of the model.

An alternative model to the plug-flow approach has been presented, for the dispersed phase flow field. This approach directs part of the flow through the interface, as opposed to routing the bulk flow through the flow diffuser. The effect of this approach has been discussed in terms of grade efficiencies. Numerical flow simulations have been performed with both laminar- and turbulent models, and the effect of these models are discussed.

The flow through the flow diffuser has been studied in detail, and it has been shown that in a region directly behind the diffuser, a vertical velocity component is induced that may have effect on outlet qualities.

Microscale mechanisms have a profound effect on separator performance. In a fluid system partly stabilised by indigeneous components, as fluid system 3 batch 1, there is an

aggregation of these components in the dispersion layer as shown by UV/vis absorbance measurements. This results in a water release rate from the dispersion layer which is less than predicted from inlet samples, and the mass balance within the separator cannot always be determined from these inlet samples.

The separation profile from bottle tests for samples obtained at different points in the separator, more specifically from the inlet and the dispersion layer, show different separation characteristics. The SRTCA (Shell Research and Technology Center in Amsterdam) model was utilised for these bottle tests, and the results were in the expected range regarding water release.

Experimentally obtained DSDs (Droplet Size Distributions) were combined with ideal grade efficiencies and compared to outlet quality for water continuous cases. There were large discrepancies between predicted and experimental results, and these are believed to be caused by effects that cannot be predicted sufficiently with the existing model framework. For oil continuous results, the water quality showed no direct correlation with the oil continuous DSDs, which was expected.

Three different mechanical alterations have been tested on a pilot-scale gravity separator, and the effects on water quality and dispersion layer thickness have been measured. The entrance height of the liquid (the cyclone liquid outlet height) is important for cyclone-type inlets, as the dispersion layer thickness will increase unnecessarily if the liquids exit in a phase region different than the continuous phase. This is believed to be due to mechanical mixing, and will therefore depend on the liquid momentum exiting the cyclone.

It is possible to remove a water-rich flow from beneath the inlet, upstream the flow diffuser, that will reduce the average water velocity, or "unload" the water phase. This stream contains typically 95%–99% water, and is suitable for post-processing by a special hydrocyclone, known as a pre-deoiler. The effect depends on the incoming drop sizes, and also the coalescence rate of the system, but will be ideal for very-high water cuts as typically found in tail production.

"Dispersion dividers", a rack of horizontal plates filling the width of the separator, was tested, inspired by the work of Hartland and Panoussopoulos [19]. The purpose was to increase the area available for coalescence, and hence increase the separation. This effect, if present, was difficult to identify because of two other effects:

1. Due to the constraint on the dispersion flow, a "lump" was formed downstream the dividers. This increased the sensitivity towards fluctuations in level control, and also decreased the separator overall tolerance for dispersed phase.

2. For water continuous feeds, the water quality was significantly improved. This is believed to be due to reduction of the vertical mixing component through the flow diffuser as the dividers form a channel downstream the flow diffuser, reducing the effective Reynolds number.

A data body consisting of test results from full-scale separators in operation at the Statoil operated fields Gullfaks and Statfjord have been reviewed. The focus of the tests have been to investigate the liquid qualities resulting from inlet design changes,

particularly for the KPS Compact Cyclone Inlet. It has been found that the water (i.e. dispersed phase) quality was improved when the liquid outlet of the cyclone was raised to the oil phase (above NIL) as opposed to when it was below, or in the vicincity of NIL. The oil quality (or rather the water separation efficiency) was also improved when the liquid outlet was raised to well above NIL. The reason for these improvements is believed to be that the release of an oil continuous flow into a water-dominated region causes unnecessary mixing of the two liquid phases, and that this causes the creation of more dispersion, and also more oil drops into the water phase.

> "Strength is measured in kilograms. Velocity is measured in seconds. Bravery ... one cannot measure bravery." *The [translated] overdub from a teaser for the 2000 Olympics in Sydney, broadcasted by TV2 (a Norwegian television channel)*
>
> "Somehow, this (... lack of ability to measure bravery ...) does not surprise me." *Dag T. Kvamsdal*

Acknowledgements

The work contained in this thesis is the result of four years of interaction with advisors, co-workers, friends and family, and many thanks are due for the final results.

First of all I wish to thank my supervisor, Hallvard Svendsen, and current and past co-workers at the Kværner Process Systems R&D facility in Trondheim: Bjørn Christiansen, Jo Jernsletten, Dag T. Kvamsdal, Knut Sveberg, and Bjørnar Svingen. Through the development of this thesis, they have aided and supported me in my work and provided valuable input through discussions. I also wish the best for Bjørn, Dag, Knut, and Inge in their new venture in Trondheim.

I further acknowledge the co-operation and valuable input from Johan Sjöblom (Statoil, Norway), Per Arild K. Andresen (Ementor, Norway), Harald Kallevik (Statoil, Norway) and the other students who I met through the Flucha Programme at the University of Bergen. Spending weeks in various laboratorys with Per created fruitful discussions, to common enlightment and enjoyment. Johan, for theoretical and moral support, and Harald, for performing the UV/Vis-analysis (when he really didn't have to). I thank Gunnar Vangen (Statoil, Norway) for giving me access to the field performance data from the Statfjord and Gullfaks fields, and accompanying me on my trip to Gullfaks C.

Thanks also goes to my employer through all this time, Kværner Process Systems, for giving me the opportunity to perform and finish this work.

Finally, the financial support from Kværner ASA and the Research Council of Norway is gratefully acknowledged.

Contents

List of Figures

List of Tables

List of Symbols

Latin symbols

Symbol	Unit	Description
a	varies	Slope in linear fits
A	m^2	Area
b	varies	Intercept in linear fits
C		Constant
d	m	Particle diameter
e		Empiric exponent in equation (3.2)
E	J	Energy
f		Friction factor
F	N	Force
g	m/s^2	Acceleration by gravity
k	m^2/s^2	Turbulent kinetic energy
l	m	Lenght scale
m		Multiplyer found by least-square fitting
M	kg	Mass
n		Counter. Also: exponential parameter in the Rosin-Rammler distribution (4.5)
p		Interfacial coalescence index, $0 < p \leq 1$
Q	m^3/s	Volumetric flow rate
R	m	Radius
s		Relative standard deviation for m
t	s	Time
v	m/s	Velocity
V	m^3	Volume
x	m	Unit length, horizontal and perpendicular to cylinder axis
y	m	Unit length, vertical
Y	m	Vertical length
z	m	Unit length, horizontal and parallel to cylinder axis
Z	m	Axial length
å		Open fraction (porosity)

Greek symbols

Symbol	Unit	Description
α		Absorbance
β	s, s/m	Constants in SRTCA design theory
ϵ	m^2/s^3	Turbulent dissipation
η		Efficiency
μ	Pa s	Kinematic viscosity
ξ		Geometric conversion factor
ρ	kg/m^3	Density
σ	mN/m	Interface tension
τ	Pa	Stress
ϕ		Phase fraction
Ψ	m/s	Coalescence rate (i.e. flux)
ω		The omega function (also: the LambertW function)

Latin subscripts

Symbol	Description
0	Initial condition
$*$	Dense (packed) layer
$*i$	Inflection point
B	Buoyancy
c	Continuous phase
d	Dispersed phase
D	Drag
g	gas
i	Counter
I	Bulk interface
j	Counter
k	Kinetic
KH	Kumar & Hartland settling
l	Liquid
max	Maximum
N	Normalized
o	Oil
p	Particle
R	Residence
St	Stoke's settling
sep	Separation length
T	Thermal
w	Water
x	Spatial dimension, horizontal and perpendicular to cylinder axis

Symbol	Description
y	Spatial dimension, vertical
z	Spatial dimension, horizontal and parallel to cylinder axis

Greek subscripts

Symbol	Description
μ	Viscosity
σ	Surface

Superscripts

Symbol	Description
$'$	Turbulent fluctuation
$-$	Average value
c	Coalescence

Dimensionless numbers

Number	Description
Re	Reynolds number
We	Weber number

List of Abbreviations

Abbreviation	Description
2D	Two-dimensional
3D	Three-dimensional
BV	Bottom of vessel
CCI	Compact Cyclone Inlet
CFD	Computational Fluid Dynamics
DSD	Droplet Size Distribution
GFCI	Gullfaks C Inlet separator
GFCT	Gullfaks C Test separator
KPS	Kværner Process Systems
LR	Linear regression
NIL	Normal Interface Level
NLL	Normal Liquid Level
NTNU	The Norwegian University of Science and Technology
oiw	Oil in water
op	Operation
REM	Removed
SFBI	Statfjord B inlet separator
SFCT	Statfjord C test separator
Sp#	Sample point (see table 2.1)
SRTCA	Shell Research & Technology Centre, Amsterdam
Std	Standard
STP	Standard Temperature and Pressure (15°C, 1 atm)
UiB	The University of Bergen, Norway
UV	Ultra Violet
vis	Visible
WC	Water cut (water fraction in a liquid flow)
wio	Water in oil
ZDLT	Zero Dispersion Layer Thickness

Chapter 1

Introduction

Oil production on the Norwegian shelf saw major changes in the 1980's. The introduction of enhanced oil recovery methods made the expected lifetime of existing production facilities far longer than was anticipated when the original specifications were made. During this extended lifetime, the separator trains have had to perform at feed conditions far outside their original specifications. As an example, the Gullfaks C field at the Norwegian shelf, operated by Statoil a.s, had a maximum water cut (maximum water content in the liquid phase) of approx. 35% at design of the primary (1. stage) separators (1985). In December 1998 the feed water cut was well above 60%. The increase in field lifetime has had an enormous impact on profitability, but the necessity of the separator train to handle feed streams for which it was not built for, often requires a revamping of the equipment. In particular, the primary separator will usually need an upgrade to be able to manage the new conditions (for example: [1]). As such, the primary separator and the processes concerning its performance at high water cuts, is the core of this thesis.

A primary gravity separator is a very simple design and serves multiple purposes. It should remove a considerable amount of water, to make the effluents correspond to the inlet specifications of the subsequent steps. These are typically a compressor on the gas side, a water treatment package on the water side and subsequent gravity separators on the oil side (possibly an electrostatic coalescer as the final step). Typical feed specifications for these steps are given in table 1.1. The number of steps will depend on the required pressure reduction throughout the train, as the oil is delivered at ambient conditions, coupled with minimising compressor work.

In addition to performance as a separator, the primary separator also provides a safety volume for slugs, and must provide sufficient time for operators/control systems to shut down the process in the case of an emergency. Such design criteria are equally important to the separation criteria, and may be the determining factor in sizing the separator.

Revamping is normally not concerned with these factors, but only with the separation matter. The size of the vessel can be regarded as given, as the costs of major alterations here are effectively prohibitive. Typical revamping problem definitions (and some hypothesises regarding the cause) are:

Separator train component	Typical feed specification	Downstream components		
		Gas	Oil	Water
1. stage separator	ANY	Compressor	2. stage separator	Deoiler hydrocyclones
2. stage separator	$< 5\%$ oil in water	Compressor	3. stage separator	Deoiler hydrocyclones
3. stage separator (electrostatic coalescer)	$< 0.5\%$ oil in water	Compressor	Sales	2. stage separator
Compressor	<0.1 gal/MMSCF (1.3E-5 m^3/Sm^3)	Transport pipe		
Deoiler hydrocyclones	<1000 ppm oil in water		2. stage separator	waste

Table 1.1: Overview of process components, typical three-stage separator train.

1. Too much liquid carry-over to compressors, caused by:
   (a) Excessive foaming (gas is mixed into the liquid).
   (b) Incomplete settling of liquid drops in the gas phase.
   (c) Re-entrainment of liquid in the gas phase.
2. Too much water carry-over to 2. stage separator, caused by:
   (a) Incomplete settling of water drops in the oil.
   (b) Incomplete coalescence of the water drops that have settled, the dispersion layer (a layer formed by the settled drops) flows over weir.
3. Too much oil in the water phase, caused by:
   (a) Incomplete creaming of oil drops in the water.
   (b) Oil is being drawn from the dispersion layer through the water outlet, caused by too low interface setting or incomplete coalescence.

Item 1, concerning the gas phase quality, has received much attention and several devices exist to remedy the situation. In particular, a de-foaming device as the inlet has been the starting point for this thesis. This device, the CCI (Compact Cyclone Inlet) by Kværner Process Systems a.s has been used in all the studies that are shown here. This does not imply that de-foaming is a central part of the work - it is rather neglected as the CCI has shown very good results in this respect. This device does, however, change the manner that the liquids enter the separator, and the liquid-liquid separation is affected by this.

Traditionally, the function of the inlet has been to re-distribute and quell the incoming fluid momentum and, as early as possible, to create an even mass flux along the flow direction. The simplest form of inlets are the "momentum breaker" which is an obstruction mounted at the end of the inlet tube, directing the incoming flow into the vessel wall. More sophisticated inlets are of the vane-type, having a more specific guiding of the liquid into the walls or a special deflector. The third type is the cyclonic inlet, seeking to separate the gas- and liquid phases prior to entering the vessel. In conjunction with the inlet, a flow distributor is often required to establish an even velocity profile. It is therefore appropriate to define an inlet section, where the momentum is distributed and reduced as much as possible, prior to entering the settling section where the conditions are optimised for settling/creaming and separation. The final subdivision is the outlet section(s) where the suction from the relevant outlets will affect the flow pattern. Additionally, other internals such as vanes, cartridges and plates may affect the flow patterns within the separator. Figure 1.1 shows this general subdivision of a horizontal gravity separator with an end inlet.

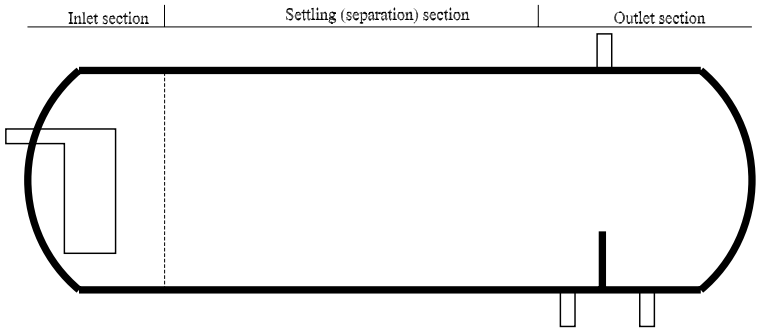

Figure 1.1: Subsectioning of a gravity separator

As mentioned initially, an issue for many oil fields that have been producing for some years, is the increase in feed water content due to enhanced oil recovery by water injection. This increase has several effects that concern the primary separator. Starting at the choke valve, the high pressure drop normally induced here will set up a turbulent field. The characteristic surviving drop diameter of this field will increase with increasing dispersed phase concentration. This is true for any strong turbulent fields. The collision frequency between drops in turbulent fields will also increase with increasing concentration. The coalescence rate for single drops will decrease with increasing diameter. In addition, the increase in concentration will give a tendency to form a dispersion layer near the oil/water interface, consisting of water drops that have settled, but not yet coalesced

with the water bulk phase. Finally, when the water content in the feed stream crosses the "inversion point", the liquid feed becomes water continuous consisting of oil drops in water.

It should be mentioned that in the oil industry it is customary to differentiate between "emulsions" and "dispersions", in the way that emulsions are liquid-liquid dispersions that are "difficult to separate" while "dispersions" are liquid-liquid dispersions that "separates readily". A time criteria of 4 minutes for dispersion break-down is customary in this respect (mirroring a common residence time in gravity separators [2]), although for heavy oils this criteria may stretch to 30 minutes. Hence, a gravity separator is supposed to handle "dispersions" but not "emulsions". Although the definition of an emulsion is a liquid-liquid dispersion, these terms will be used in this thesis (or rather only the term "dispersion" as "emulsions" are outside the scope).

Crude oils are a highly heterogeneous class of fluids, with large variations in compositions. When performing pilot-size experimental work, the approach in model system selection will greatly affect the results. The model systems investigated here correspond to light crude oils, as generally found on the Norwegian shelf. A considerable effort has been made to find a model system that shows some of the features that are known from production installations. The different model systems show certain very important variations, which have improved the understanding of certain phenomena occurring with crude oils, particularly the water quality variations resulting from dispersion stability. This has also led to a proposed flow pattern for the dispersed phase that differs from the traditional plug-flow assumption. This assumption has been investigated numerically and compared to experimental results.

Chapter 2

Theory on gravity separator behaviour

This chapter will present the macroscopic properties studied in a model pilot-scale separator, and serve as background for the later results of varying nature. It lays out the basis of the thesis, by studying the outlet qualities as responses to the load to the pilot separator.

2.1 Introduction

Gravity separation in oil production can safely be regarded a "mature" process technology. The gravity separator vessel is a process component at virtually every installation that produces or treats oil in large scale. The process equipment is very simple: a large, mostly empty vessel in which a mixture of components is allowed to separate based on immiscibility and difference in density. A few internals may be present inside the vessel to improve a specific feature of the process, but it is generally desirable to minimize this and maximise the simplicity.

The gravity separator vessel is also known as "a process component partly designed by chance." The operation window has to be large, and the feed specifications are rarely known in full detail at any point in its lifetime. Not surprisingly, it sometimes fails to perform according to specifications, and at other times one may anticipate a change in upstream (or downstream) conditions and wish to perform modifications to alter the performance. If these modifications are of a mechanical nature, it is known as revamping.

The process supplier industry, "vendors", have performed pilot-scale work on gravity separators, probably for many decades. The main focus of pilot scale experiments is to test out the equipment in continuous operation where scale-up effects are minimised. The main problems associated are related to health hazards and cost — due to the large volumes involved it is desirable to operate at room temperature and atmospheric pressure, and the model oil thus has to be non-toxic and non-volatile. The classic choice has been

a paraffinic oil, close to kerosene in composition. These oils are known to separate very rapidly from water, and hence the limiting design parameter has been settling of the dispersed water drops. However, several oil fields have reported separation problems of a kind that does not appear to origin from incomplete settling.

A main part of this thesis has been a search for an oily model fluid that show the desired liquid/liquid separation features with water, and still could be utilised under atmospheric conditions. This chapter describes these features, and the separator performance under different feed conditions.

2.2 Theory of settling and separation under gravity

This section contains the basic relations governing gravity separation, with some newer relations from the literature.

2.2.1 Settling and flotation — force balances

The relative movement of macroscopically mixed, immiscible phases of different densities is traditionally described by force balances. Consider a case where two immiscible fluid phases are in contact along an interface A_I. As long as the fluids are immiscible, there will be an energy associated with the unit size of this interface, known as surface tension. The minimum energy state of the system is the state where this area is minimised. If the fluid phases have different density, the state of lowest energy in a gravity field will be when the lighter fluid is on top of the heavier one.

If this equilibrium system is exposed to mechanical mixing capable of disrupting the interfacial tension, the system will move to a state where the phases are mixed macroscopically, and one phase may exist as drops in the other. This is known as a dispersion, and is thermodynamically unstable. The drop phase is known as the dispersed phase, and the surrounding phase is known as the continuous phase.

Settling is the tendency of the heavier phase to separate from a lighter one, and creaming is the lighter separating from the heavier. These phenomena are described by the theory of flotation. Generally, three forces are acting on a droplet dispersed in a medium; buoyancy, viscous resistance and Brownian (thermally induced) motion. The thermally-induced motion is important only in the lower range of particle sizes $< 1\mu$m, and is usually disregarded for gravity separator applications. Along the vertical (y-) axis, the two other forces are described by equation (2.1) and (2.2) [3].

$$F_B = (\rho_d - \rho_c) g V_p = M g (1 - \frac{\rho_c}{\rho_d}) \tag{2.1}$$

$$F_D = C_D \frac{v_0^2}{2} \rho_c A_p \tag{2.2}$$

For single, rigid, spherical droplets in the laminar regime, Re$<$ 1, the experimental drag force is given by eq. (2.3) [3]

$$F_D = F_\mu = f\frac{dy}{dt} = 6\pi\mu_c\frac{d}{2}\frac{dy}{dt} \tag{2.3}$$

In the turbulent regime, the sphere drag coefficient shows a complex behaviour vs. Re. Two regimes can be identified; $10^3 < \mathrm{Re} < 2 \cdot 10^5$ and $\mathrm{Re} > 5 \cdot 10^5$ where the drag coefficient C_D is approximately constant; 0.44 and 0.20, respectively [3]. Settling in the non-linear drag range is much more complex and detail simulations are necessary, see [4].

Gravity separators are assumed to be operated under laminar conditions. The combination of equation (2.1) and (2.3) gives the sedimentation velocity $v_{St} = dy/dt$ in equation (2.4). This equation is generally known as Stoke's settling law.

$$v_{\mathrm{St}} = \frac{dy}{dt} = -\frac{2\left(\frac{d}{2}\right)^2(\rho_d - \rho_c)g}{9\mu} \tag{2.4}$$

A viscosity-based correction term compensating for internal flow in fluidic particles is given as eq. (2.5) [5].

$$v_{\mathrm{St,visc}} = \frac{\Delta\rho g d^2}{18\mu}\frac{\mu_c + \mu_d}{2/3\mu_c + \mu_d} \tag{2.5}$$

Kumar and Hartland [6] found an empirical expression for settling in concentrated batch samples, eq. (2.6) (for the laminar regime).

$$v_{\mathrm{KH}} = \frac{\Delta\rho g d^2}{18\mu}\frac{(1-\phi_d)^2}{1 + 4.56\phi_d} \tag{2.6}$$

2.2.2 Residence time and bulk velocities

The residence times in the different parts of a separator are traditionally set by the liquid inlet velocities and the liquid volumes [7]. These volumes are again given by the size of the separator and the liquid interface levels, which are adjusted by controlling the outlet valves. This is here referred to as the *plug flow-approximation*.

The residence volume of a horizontal cylinder part is given by equation (2.7).

$$V_R = 2Z\int_Y \sqrt{2Ry - y^2}\,dy \tag{2.7}$$

Solving between two levels y_1 and y_2 yields eq. (2.8).

$$V_R = Z\left[R^2\arccos\left(\frac{R-y}{R}\right) - R(R-y)\sin\left(\arccos\left(\frac{R-y}{R}\right)\right)\right]_{y_1}^{y_2} \tag{2.8}$$

And the residence time is given by dividing the residence volume with the fluid flow rates, equation (2.9).

$$t_R = \frac{V_R}{Q} \tag{2.9}$$

The superficial velocity is found similarly by dividing the flow rate with the wetted cross-section area $A_z = V_R/Z$. This assumes that the fluid flow is parallel to the cylinder axis.

Furthermore, the flow has to fulfil the equations of continuity-, momentum- and energy conservation. This, and the generality of the plug-flow approximation will be discussed more thoroughly in chapter 3.

2.2.3 Settling- and grade efficiency. Cut sizes.

Normally, a drop size distribution (DSD) enters the separator. This DSD contains a continuous range of drop sizes, which is commonly discretized into drop classes of different characteristic diameters d_i. Calculating specific vertical drop velocities from eq. (2.4) and solving these between two levels $Y = y_2 - y_1$ during the given residence time yields the grade efficiency, eq. (2.10) (following Hounslow [8]).

$$\eta_i = \frac{v_{\mathrm{St,i}} A_y \xi_Z}{Q} = \frac{v_{\mathrm{St,i}} Z_{\mathrm{sep}} 2\sqrt{2Ry_I - y_I^2}\xi_Z}{Q},\ \eta_i \leq 1 \tag{2.10}$$

As Hounslow's formulas are developed for a prism-shaped vessel, it is necessary to modify the equation for use on a cylindrical vessel, and the factor ξ_Z (eq. (2.11)) is introduced.

$$\xi_Z = \frac{\int_Y \sqrt{2Ry - y^2}\, dy}{(y_2 - y_1)\sqrt{2Ry_I - y_I^2}} \tag{2.11}$$

The numerator represents the area of the prism perpendicular to the flow (from the original framework), and the denominator represents the corresponding area in a cylinder. Note that y_1 or y_2 will correspond with y_I, depending on the which phase is the continuous one. If the initial normalised volume-based drop size distribution $V_N(d)$ is known, the overall efficiency is then given by (2.12).

$$\eta = \int_0^\infty V_N(d)\eta_i(d)\, dd \tag{2.12}$$

Various cut sizes can be found by solving eq. (2.10) for the particle diameter (from the Stoke's settling velocity or another settling equation) at the desired grade efficiency. Figure 2.1 shows the calculated grade efficiency for the water phase of a separator with R=0.315 m, Z_{sep}=2.3 m, ρ_w=1000 kg/m^3, ρ_o=795 kg/m^3, μ_w=1E-3 Pa s, μ_o=1.6E-3 Pa s, NIL=0.22 m, Q_w = 9 m^3/h.

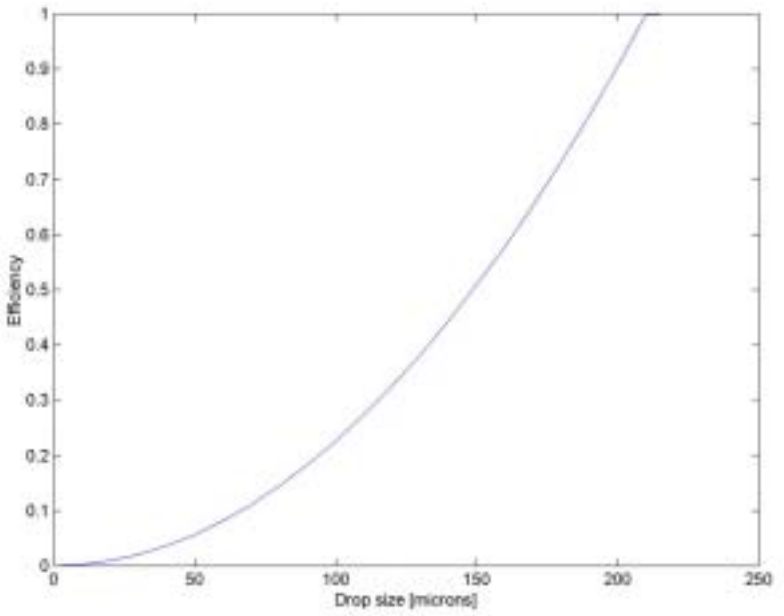

Figure 2.1: Sample grade efficiency calculation

2.2.4 Drop size distributions; turbulent break-up and coalescence

The drop size distribution entering the separator will be decisive for the overall efficiency, as shown in the previous section. It is therefore necessary to perform a short analysis of the existing theory describing the phenomena that concerns this.

The break-up of the dispersed phase is attributed to upstream turbulence as the phases flow through the upstream components. The basis for most of the existing theories around turbulent drop break-up comes from the work by Kolmogoroff [9] and Hinze [10], who developed and verified the equations for isotropic turbulent break-up in infinite dilution.

Consider a turbulent flow field in which a dilute dispersion flows. The end points of the diameter of a dispersed drop can be viewed as two points in space, where there may be a turbulent momentum energy related to a field-characteristic spectrum (2.13). The Weber number (2.15) is a dimensionless number that relates momentum energy to surface energy (2.14), and when this is larger than unity, momentum prevails over surface energy and further break-up may occur. When the Weber number is close to unity (depending on the surroundings), the energies balance; no further break-up occurs and the drops corresponding to this diameter (and below) will survive the field (2.16). This is known as the maximum surviving drop size. The dispersed phase will, neglecting coalescence, exist as a size distribution below this maximum size.

Assuming isotropic turbulence, the square turbulent fluctuation velocity over the space d is related to the turbulent energy dissipation (2.17), and the balancing energy level becomes (2.18). This is fortunate as the turbulent energy dissipation can be related to macroscopic parameters, for example a volume associated with a pressure drop (2.20). Equations (2.13) – (2.19) are from [11, 12], while eq. (2.20) is from [13].

$$E_k \propto \rho_c {v'}^2(d) d^3 \tag{2.13}$$
$$E_\sigma \propto \sigma d^2 \tag{2.14}$$
$$\mathrm{We} = \frac{E_k}{E_\sigma} \tag{2.15}$$
$$\mathrm{We}_{\mathrm{crit}} = C_1 \frac{\rho_c {v'}^2(d) d^3}{\sigma d^2} \tag{2.16}$$
$${v'}^2(r) = C_2 \epsilon^{2/3} r^{2/3} \tag{2.17}$$
$$\mathrm{We}_{\mathrm{crit}} = C_1' \frac{\rho_c \epsilon^{2/3} d_{\max}^{5/3}}{\sigma} = C_2' \tag{2.18}$$
$$d_{\max} = C_2' \left(\frac{\sigma}{\rho_c}\right)^{3/5} \epsilon^{-2/5} \tag{2.19}$$
$$\epsilon = \frac{Q \Delta P}{\rho V} \tag{2.20}$$

Some work has been performed on concentrated, stabilised emulsions (for example, [11]), which suggest that the above equations are valid up to a fraction of 0.015 with respect to the dispersed phase, and that $d_{\max}$ increases linearly with volume fraction above 0.15. Equations considering concentrated dispersions above volume fractions of 0.15 are usually on the form of eq. (2.21).

$$d = C_1(1 + C_2 \phi_d)\mathrm{We}^{-0.6} \tag{2.21}$$

Polderman [14] found that for the Draugen field, the inlet distribution $d_{\max}$ depended on choke valve pressure drop and dispersed phase concentration according to eq. (2.22).

$$d_{max} \propto \Delta P^{-3/5}(1 + 20\phi_d^2) \tag{2.22}$$

This equation has a form corresponding to (2.21), when the form of ϵ given in eq. (2.20) is used.

2.2.5 Dispersion layer theory

Hartland et al. [15, 16, 17, 18, 19] has developed a theory for batch liquid-liquid separation, referred here as the dispersion layer theory. The theory has the following assumptions:

1. The incoming fluid has a defined, pseudo-homogeneous continuity. Thus the incoming mixture consists of one defined continuous phase and one defined disperse phase. The total volume of drops entering the separator is equal to the incoming dispersed phase flow.

2. All of the dispersed phase (in drop form) has to be transported through the continuous phase layer and the interface in order to achieve separation. This process is divided into steps:

   (a) Transport through the continuous layer to the dispersion layer by settling

   (b) Transport through the dispersion layer by stack-wise removal of the interfacial drop layer by coalescence. The dispersion layer is considered a packed layer with a fixed drop concentration.

   (c) Transport through the interface by coalescence.

3. The settling through the continuous layer is hindered and described by equation (2.6).

4. The coalescence rate for a drop of diameter d_0 at the interface is either correlated from experiments or calculated by theory.

Following these assumptions, there will exist a point in time where the last drop settles at the top of the dispersion layer, the inflection point t_{*i} (where the dotted curve h_p meets h_s in figure 2.2). A mass (or rather a volume) balance is calculated from this point, describing the heights of the region boundaries (fixed in the xz-directions).

$$\frac{dy_c}{dt} = \Psi = \Psi_{*i} \left(\frac{y_*}{y_{*i}} \right)^p \tag{2.23}$$

The coalescence rate at the inflection point (the velocity with which the coalescing interface moves) is given by eq. (2.24), for a characteristic drop size d_0 with interfacial coalescence time t_0^c for a mono-layer.

$$\Psi_{*i} = \frac{2\phi_* d_0}{3t_0^c} \left(\frac{y_{*i}}{d_0} \right)^p \tag{2.24}$$

Figure 2.2 shows the measured dispersion growth/decay for a dispersion layer sample, together with fitted parameters and curves from the above model. See also appendix A.2 for details in the calculation and definitions of the various parameters in the figure.

Panoussopoulos [19] has studied several real- and model systems using this model, and reports values of ϕ_* ranging from 0.65 to 0.875 and p ranging from 0.23 to 0.68. The current lack of a theory predicting these variations is the major weakness of this model.

This theory is developed for batch tests, commonly known as bottle tests. In a continuous operation such as a horizontal separator, modifications of the model are necessary.

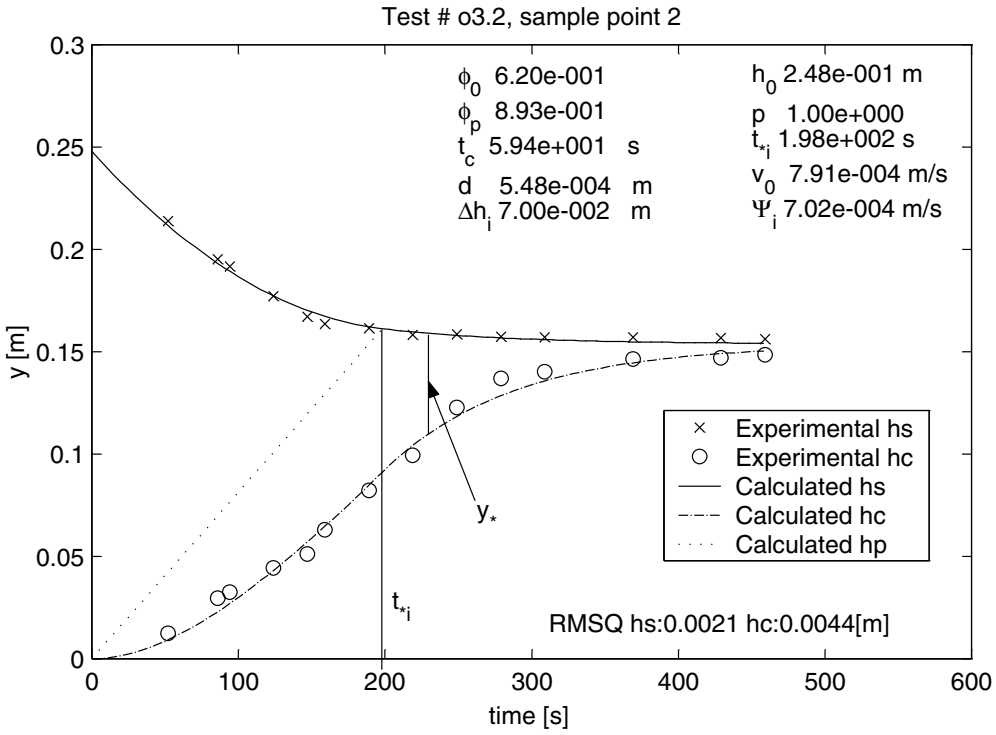

Figure 2.2: Sample batch dispersion decay calculation

Instead of looking at the process as time-dependent, it is here assumed that the process operates at steady state. Because of the low liquid velocities the momentum of the continuous liquid phase will be low, and gravity will dominate the separation section. The dispersion layer when fully developed can be assumed to have a constant height throughout this section [20], and Ψ will be constant. For complete separation, $\int_{A_I} \Psi dA_I$ must correspond to the incoming amount of dispersed phase, and t_0^c, Ψ_{*i}, and Ψ can be calculated if the height of the dispersion layer and the characteristic drop size d_0 is known. Furthermore, by knowing Ψ_{*i} and Ψ, the maximum capacity for a separator with given liquid levels and weir height can be calculated. In a continuous process, the dispersion layer is not free to expand and will be confined to the region between suction from the water outlet and the weir height. As the quality demand for downstream processing is more stringent on the water side than the oil side (see table 1.1), the dispersion layer will normally be forced to flow over the weir (flooding) if it exceeds this region.

Oil quality is normally reported as vol% water in oil, and if this value is high it may be caused by the above discussed phenomena. It will be shown that the dispersion layer volume is indeed proportional to the volume of incoming dispersed phase, and that the

separation performance therefore is a function of this parameter. As oil quality depends on water flow, the reported oil quality has to be transformed to a "water separation efficiency" parameter η_w when looking at oil qualities at high water cuts. This is defined by eq. (2.25).

$$\eta_w = \frac{Q_{w,\text{inlet}} - Q_{w,\text{oil outlet}}}{Q_{w,\text{inlet}}} \approx 1 - \frac{\phi_{w,\text{oil outlet}}(1 - \phi_{w,\text{inlet}})}{\phi_{w,\text{inlet}}(1 - \phi_{w,\text{oil outlet}})} \tag{2.25}$$

The consequences of the above will be further discussed in chapter 3.

2.2.6 SRTCA design theory

In recent years, Shell Research and Technology Center in Amsterdam (SRTCA) has published a new design philosophy ([21, 14]) based on extensive laboratory tests and field trials. The basis of this philosophy is close to that of Hartland (see above), and looks at the transport of the dispersed phase through an interface. The aim of this work has been to find guidelined for the design of vertical separators, and the dispersion layer behaviour has been correlated to the dynamic viscosity of crude oils. Hence, a prerequisite for this model is that the dispersed phase has to be appropriately destabilised (in order to make viscosity the only stabilising factor).

As mentioned, the theory is developed for vertical separators, with the oil flowing upward opposing the settling velocity of the dispersed water. This may explain the inclusion of the oil flow into the relations.

The main feature of the theory is the prediction of the dispersion layer thickness y_* as a function of total liquid flow rate Q_l and interface area A_I, eq. (2.26).

$$\begin{aligned} \frac{Q_l}{A_I} &= \frac{y_*}{\beta_1 + \beta_2 y_*} \\ y_* &= \frac{\beta_1 Q_l}{A_I - \beta_2 Q_l} \end{aligned} \tag{2.26}$$

Here β_1 and β_2 are constants depending on feed properties and operating conditions. These are determined by batch tests in the laboratory or in the field, where the decay of the dispersion band with time $-dy_*/dt$ is assumed linear to the flux, eq. (2.27).

$$-\frac{dy_*}{dt}\bigg|_{y_*} = \frac{Q_l}{A_i}\bigg|_{y_*} \tag{2.27}$$

Combining eqs. (2.26) and (2.27) yields the relationship (2.28), giving β_1 and β_2 from batch tests for a given system.

$$-\frac{dy_*}{dt} = \frac{y_*}{\beta_1 + \beta_2 y_*} \tag{2.28}$$

In comparison with the model shown in figure 2.2, equation 2.28 describes y_* as (y_s - y_c) both before and after the inflection point t_{*i}, and does not describe the packed layer (y_p-y_c) only. Neither does it describe the actual height as a function of time, but only the thickness of the non-separated layer (although the actual heights can readily be calculated by knowing the initial height of the dispersion). This facilitates the measurements as there is no need for isolating a dense layer with constant density, but removes some of the pedagogic features of the physical interpretations by Hartland *et al* [19].

Combined with experimental and field data, Polderman *et al* [21] have developed generalised design windows for destabilised crude oils, shown in figure 2.3. The design window for horizontal vessels (as opposed to vertical "tanks") is estimated from measurements on a vertical experimental set-up, and using a maximum dispersion thickness of y_*=0.4 m for horizontal vessels.

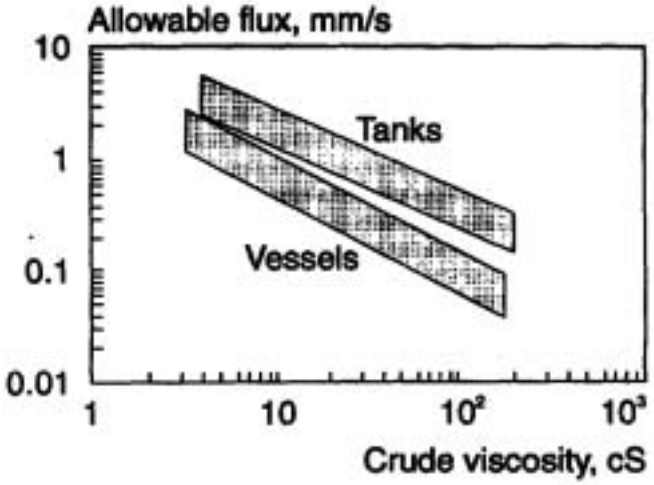

Figure 2.3: Generalised design window for dewatering vessels, from [21]

2.3 Experimental

The experiments in this chapter were performed on a pilot separator in a multiphase flow loop, located at the KPS lab in Trondheim, Norway, in the period 1997–1999. This is a low pressure-rig with high emphasis on flexibility, with separate pumps for oil and water and multiple possibilities for connecting various test instruments and -equipment. The pilot separator was made of a transparent plexiglas tube, making visual observations possible.

2.3.1 Equipment

Description of the pilot separator rig

The pilot model separator is mounted in a multiphase continuous flow loop, as sketched in figure 2.4 and 2.5. The loop consists of a feed separator with liquid volume 2.7 m^3, two positive displacement pumps, two shear valves, and control valves at the liquid outlets of the pilot separator. The pilot separator is shown in detail in figure 2.6, and geometric data are given in table 2.1.

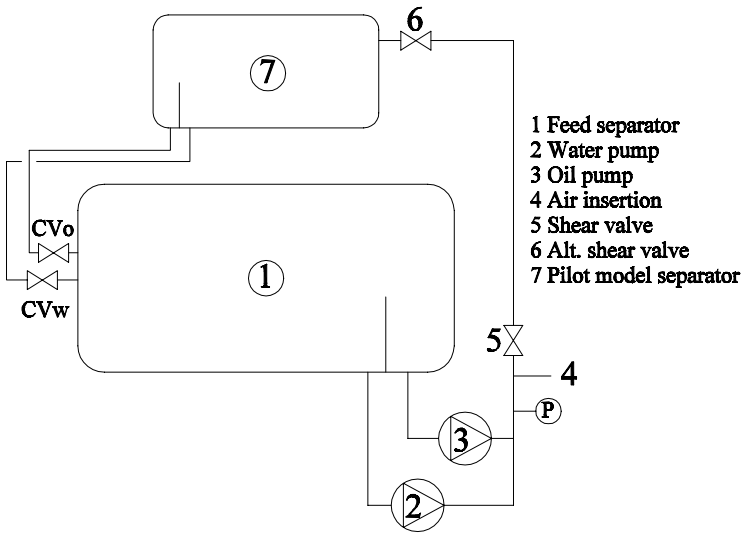

Figure 2.4: Multiphase flow loop with pilot separator

Instrumentation

Oil-in-water analyser from Deckma Hamburg GmbH, using scattering of IR-light to measure oil in water at ppm-level. Range: 0 – 1450 ppm.

Differential pressure cells manufactured by Fisher-Rosemount,

1. Water side: range 0–635 mm H_2O.
2. Oil side: range 0–0.2 bar

Flow meters Two flow meters were used for monitoring the feed rate; on the water feed side an electromagnetic flow meter from Endress + Hauser was used, type Discomag, range 0–30 m^3/h. On the oil feed side, a turbine meter of type Euromatic LFL/2 was used, range 2.2–55 m^3/h.

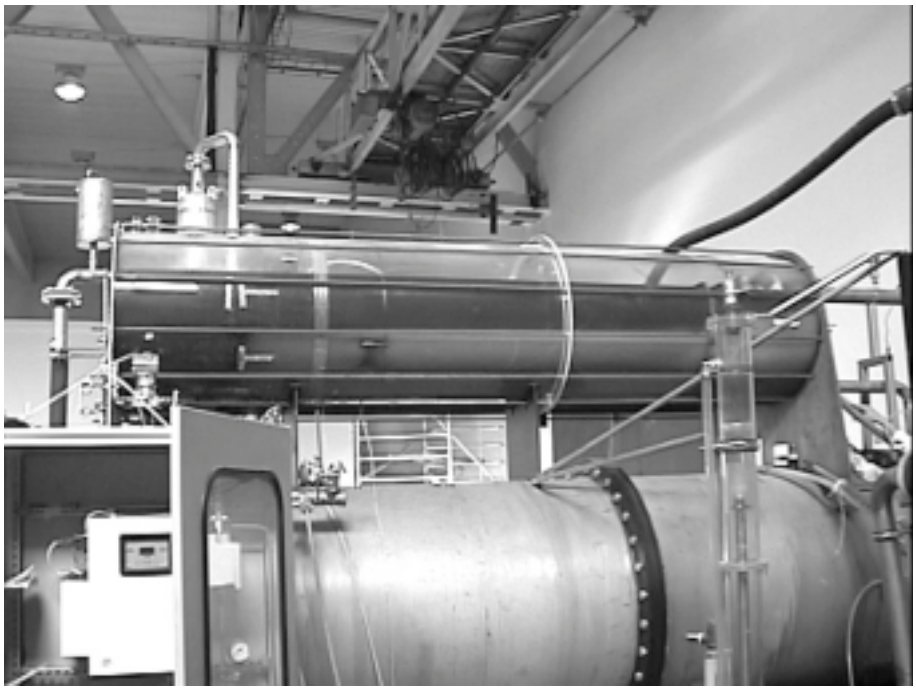

Figure 2.5: Picture of the pilot separator during an oil continuous run with fluid system 3. The dispersion band is clearly distinguishable as a gray layer between the transparent bulk liquid layers.Below the pilot model, the feed tank can be seen as well as the oil-in-water monitor. Flow direction is from right to left.

Pumps The feed pumps were positive displacement pumps from Ing. Per Gjerdrum A.S, max. diff. pressure 10 bar,

1. Oil side: Flow 1.5–34 m^3/h.
2. Water side: Flow 2.2 – 22 m^3/h.

Control valves on the pilot model liquid outlets, two butterfly-type control valves were used.

Data aquisition and process control Labview 5.0 from National Instruments.

Measuring cylinders For bottle tests and sampling, ⊘ 41.4 mm, V 250 mL

Shear valves For shearing the oil/water mixture a 2" ball valve were used, with manual pressure reading.

Item	y [mm]	z [mm]	Notes
Length		2800	
Diameter	630		
Inlet tube	490	0	O.D. 2”
Flow diffusers	450	400, 500	
Water outlet	0	2440	O.D. 1.5”
Oil outlet	0	2620	O.D. 1.5”
Gas outlet	0	2620	O.D. 1.5”
Weir	250	2530	
Sp (Sample point) 1	490	-500	Inlet tube
Sp2	240	2200	High dispersion layer
Sp3	200	2190	Middle dispersion layer
Sp4	160	2180	Low dispersion layer
Sp5	-120	2440	Water outlet
Sp6	-120	2620	Oil outlet
Z_1	0–300	350	Cross-section in the inlet zone
Z_2	0–300	450	Cross-section between flow diffusers
Z_3	0–300	550	Cross-section downstream flow diffusers
Z_4	0–300	1500	Cross-section 3/4 down the separation zone
Z_5	0–300	2600	Cross-section at the weir

Table 2.1: Geometric specification of pilot model separator

2.3.2 Fluid systems

The traditional fluid system for atmospheric, pilot scale separation experiments are air, Exxsol D-60 (or D-80), and saline water, usually tap water added 2.5–3 wt% NaCl. The Exxsol series is chosen because it is paraffinic and contains no additives, it hold reasonably tight specifications and poses little fire- or health hazard (all saturated hydrocarbon components, chain length C_9–C_{13}). Furthermore, the viscosity at ambient temperature is close to that of light/medium crude oils at (elevated) process temperatures, being slightly higher for the heavier D-80. And finally (and perhaps most important of all) they are transparent, making visual observations possible. These fluid systems have been used by the vendor industry for many years, and it is fair to say that most of the existing separation equipment installed has been tested with this model fluid system.

However, it has several serious differences from a usual crude, the most obvious being that the coalescence is very rapid for the oil continuous dispersion. Another major difference is the inversion point, which is in the region of WC 33%–38% (lower with increasing shear in the mixing point), as opposed to a normal WC 60%–80% for crude oils. It was therefore decided that it was necessary to create a model system that could simulate known aspects of crude oil behaviour more closely. Several attempts were made to create a fluid system that formed a dispersion layer while maintaining flow conditions

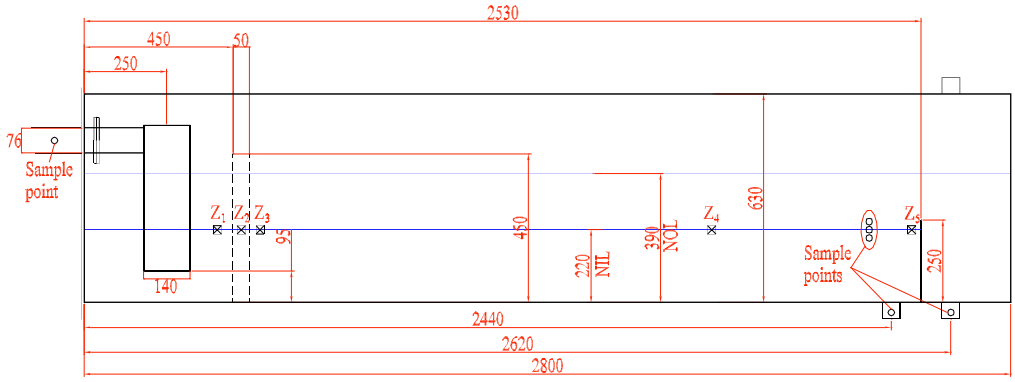

Figure 2.6: Sketch of pilot separator. Sample points at inlet, outlet and dispersion regions are shown, as well as points where the dispersion cross-sectional area was measured. All dimensions in mm. The sample probes have a diameter of 1/4"

as typically found in production systems, so that the separation mechanism was moved from the settling- to the coalescence controlled system. These attempts are listed in table 2.2, and the basis system with pure Exxsol D-60 as the oil phase is called *fluid system 1.*

There exists other model systems with various qualities (see for example Panoussopoulos [19], but these are unsuitable for pilot scale experiments either because of increased health/fire hazard or cost. In co-operation with Professor Sjöblom and Dr. Andresen at the Flucha programme, UiB (the University of Bergen), two other model systems were investigated in order to achieve the desired qualities. The first alteration was done with a synthetic agent, Berol-26 [22, 23]. This is a nonyl-phenolic ethoxylate compound, known to give very stable oil-continuous emulsions at high concentrations (>1000 ppm). The hypothesis was that this could be added in lower concentrations, and thereby give a controllable semi-stability desired for the tests. As will be shown in section 2.4, the stability to coalescence was changed for the water-continuous dispersion only, as the compound was added in small steps (30 ppm) up to 330 ppm. At this point, the addition was terminated to avoid complete stabilisation of the system. This system is called *fluid system 2.*

Fluid system 3 was also developed with UiB/Flucha, and consists of the addition of a particular crude oil, from Norsk Hydros Grane field. According to sources at Norsk Hydros research centre [24], a condensate with 1-10 vol% of a crude oil added exhibits separation characteristics very similar to the crude oil itself. Unfortunately, this will also remove an important feature of the model system; its transparency. The hypothesis this time was that Grane could be added in a much lower amount as it forms extremely stable oil continuous emulsions for a crude (there is little desire in having a model system exhibiting Grane characteristics, part from testing for the Grane field). Suitable condensate substrates in the required amounts were not discovered in the time span from test

planning to execution (it was necessary to remove light components in order to raise the ignition point), and Exxsol D-60 was used as substrate.

This system showed the desired stability behaviour for about a month, after which the stability fell dramatically (see section 2.4). These observations are supported by the UV-absorbance data (section 4.4.1). This is believed to be due to aggregation of the stabilising components in the paraffinic environment, according to Professor Kilpatrick [25]. The fluid system was used for different tests. Firstly for the "unloading" tests (see chapter 5) with an addition of 250 ppm Grane in the oil phase — this is refered to as batch 0. Secondly for tests referred here, with an addition of 500 ppm fresh Grane (as the stability from the first tests had disappeared) — this is referred to as batch 1. This second test series was of sufficient length to lose the stability of the second addition (which happened during two weeks of water continuous tests), and therefore these late test data is referred to as batch 3. The stability of this last batch is similar to using pure Exxsol D-60, corresponding to fluid system 1.[1]

Kathon FP 1.5 (a biocide) was added to all batches of fluid system 3, to prevent microbial growth.

Fluid system	Components	μ_o [cP]	Dispersion layer
1	Oil phase: Exxsol D-60. Water phase: Tap water, added 2.5 wt% NaCl. Gas phase: air (when present)	1.6	Only water continuous
2	As fluid system 1, added 330 ppm Berol-26	1.6	Only water continuous, water continuous dispersion more stable than for fluid system 1
3	As fluid system 1, added 750 ppm Grane crude oil	1.6	Both, oil continuous dispersion gradually disappeared after 1 month
Statfjord (light) crude		1.38	Oil continuous (unknown for water continuous), see chapter 6

Table 2.2: Overview of the different model fluids

2.3.3 Test matrixes and experimental results

The test matrixes for the various fluid systems listed above can be found in appendix B.1, with the measured experimental responses. The experimental data is divided into

[1]This manner of synthesising a model fluid system is a necessity from a cost/volume point of view as the 1.4 m^3 oil volume cannot be exchanged or discarded easily. Hence, quantitative results must be sacrified for a qualitative understanding of the different mechanisms that occur for different stabilities.

oil- and water continuous runs, for simplicity. For an explanation of the labelling of the experiments, please see the appendix.

2.3.4 Methods

Continuous pilot separator operation

An important assumption for the tests were that the steady-state approximation was valid. Figure 2.7 shows the variation in control valve position for an example run. The figure shows that the stability in flow rates were good, as could be expected from the positive displacement pumps, but the control valves show a large-scale fluctuation over the time span of 10 minutes which was selected as standard test time. This would increase the spread in phase quality data.

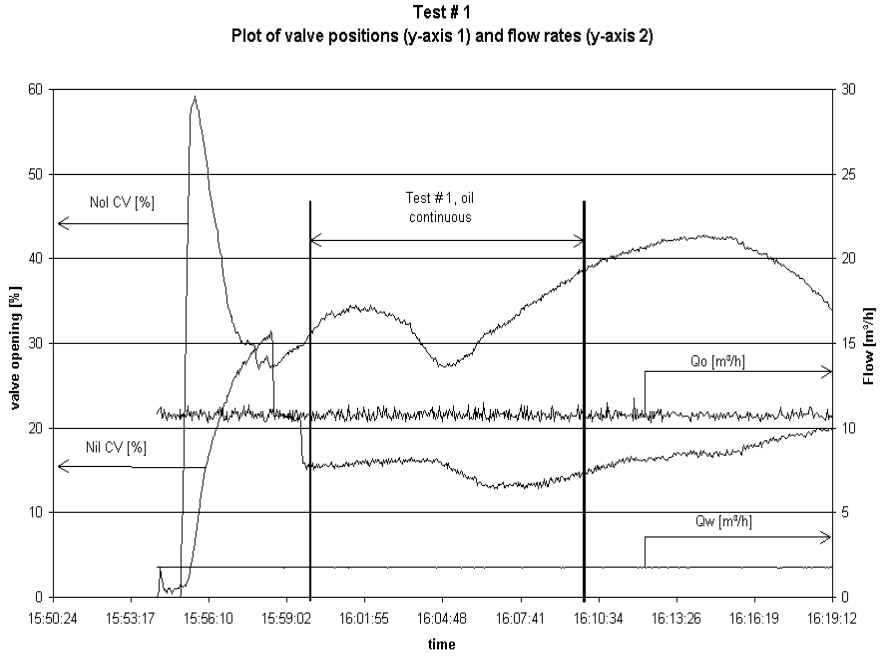

Figure 2.7: Example plot of outlet valve positions and flow rates for an oil continuous run.

These fluctuations were traced to instabilities in the output signals from the differential pressure transmitters used to control the levels. The reason for these fluctuations were never found, but after applying low-pass filters to the pressure transmitters, the spread in quality data was acceptable in comparison to the actual quality level, and no further action was taken to improve this. These filters were applied for the shown fluctuations in

figure 2.7. The outlet quality data were reported as "low" and "high"-values, as shown in appendix B.1, and the averaged values are shown in section 2.4.3.

Dispersion layer height measurements

The height and vertical position of the dispersion layer were recorded by reading the metric height along the wall of the pilot separator at five locations along the flow axis: Z_1 upstream the flow diffusers, Z_2 between the flow diffusers, Z_3 immediately downstream the flow diffusers, Z_4 at 3/4 of the length between the flow diffusers and the weir, and Z_5 immediately upstream the weir.

2.4 Results and discussion

2.4.1 Dispersion layer thickness

The dispersion layer thickness were measured for several oil- and water continuous tests with fluid system 3. As mentioned in section 2.3.2, the system lost much of its stability after one month of operation for oil continuous runs. When this occured, the dispersion layer was no longer present. The oil continuous data presented here are for the early tests, when the stability was in the desired range. Experimental values can be found in appendix B.1.1 and B.1.2.

Figure 2.8 shows the results for the oil continuous dispersion layer measurements for fluid system 3, batch 2, for the low choke pressure drop (ΔP=0.5 bar) at points Z_4 and Z_5[2]. Figure 2.9 shows a selection of these results, for experiments with a water cut below 0.3. At water cuts 0.3 and above, there was a tendency of water flowing over the weir and figure 2.9 shows a linear trend of increasing dispersion height with dispersed phase loading. This is well in correspondence with the theory presented in section 2.2.5, but differs from eq. (2.26) in that the thickness depends on the dispersed phase flow rather than total liquid flow. As mentioned in section 2.2.6, this may be attributed to the fact that references [21, 14] studied vertical separators (with the flow direction parallel to gravity), while this system was a horizontal separator.

The linear fits of the data is also shown in figure 2.9, and the slopes and intercepts are close for the two different observation points, which suggests that the thickness does not vary much throughout the settling/separation section of the separator (as defined earlier in figure 1.1.

Figure 2.10 and 2.11 show similar plots for the water continuous runs (for different pressure drops: ΔP=0.5 and 1.5 bar respectively). The general discussion from the oil continuous results in figure 2.9 is valid here as well. Additionally, the linear fit coefficients do not vary much between the two pressure drops. This suggests that the choke pressure drop is not determining for the dispersion layer thickness, which is well in accordance with the theory presented in sections 2.2.4 and 2.2.6: when the concentration of dispersed phase in the shear region (the valve) is high, the incoming drop size increase and the separator

[2]See table 2.1 and figure 2.6 for the placement of these points

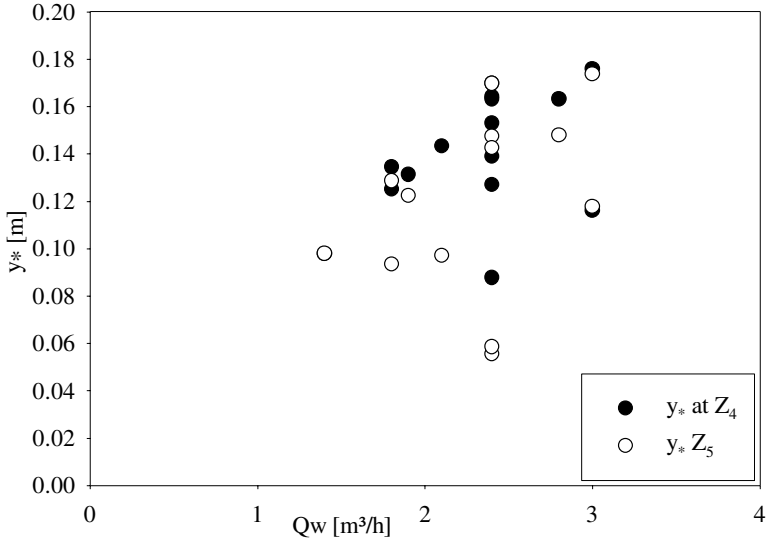

Figure 2.8: Dispersion heights at Z_4 and Z_5 (see figure 2.6) vs. Q_w (dispersed phase rate) for oil continuous tests with fluid system 3.

moves from a settling- to a coalescence-dominated operation mode. Although there is still a variation in continuous phase outlet quality (as will be shown below), the majority of the drops settles out and the main threat to separator function is the thickness of the dispersion layer, which in turn depends mainly on dispersed phase feed rate.

The slope is higher for oil- than for water continuous runs, suggesting a faster coalescence in the water continuous regime (corresponding to a larger Ψ in equation (2.23) for the water continuous regime, as more dispersion is removed for the same y_*). Also, the oil continuous intercept tends towards zero, suggesting that a dispersion layer will form for dispersed phase loadings tending towards zero. The water continuous intercept, on the other hand, suggests a clean interface near the end of the separator at $Q_o \approx 1.6$ m^3/h. This indicates that the coalescence rate upstream the flow diffuser is larger for the water continuous system than for the oil continuous system (where it is insignificant). The assumption that the dispersion layer thickness is constant throughout the separator is also better for the oil continuous- than for the water continuous system for low dispersed phase flow rates.

Multiplying the dispersion cross-sectional areas with the effective separation length Z=2 m and average volume fraction 0.85, and dividing by dispersed phase rate yields the average water residence time (needed for coalescence) within the dispersion layer. This is ca. 2 minutes in the oil continuous regime, independent of dispersed phase flow rate. The linearity of the plot suggests that the interfacial coalescence index p in equation (2.23) is close to 1 for both the oil- and water continuous system, but a larger spread in data would be desirable to increase the significance in this manner.

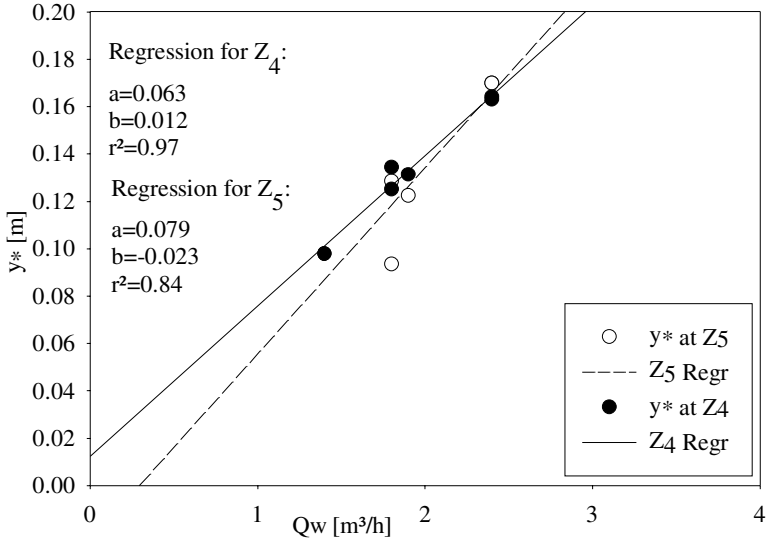

Figure 2.9: Dispersion heights at Z_4 and Z_5 (see figure 2.6) vs. Q_w (dispersed phase rate) for oil continuous tests with fluid System 3. Data for tests with WC<30% (complete separation) only.

The data were fitted to eq. (2.26) (substituting Q_l with dispersed phase flow rate) by non-linear fitting in Matlab, and this yielded parameters as shown in table 2.3 for oil continuous runs and table 2.4 for water continuous runs. For the oil continuous runs, the measured height at Z_4 correlated quite well with the model for all water cuts, but improved for the water cuts lower than WC 0.3. The measured height at Z_5 did not correlate well when including water cuts above 0.3, but the model was very well correlated when, in addition to removing the high water cuts, one additional point was removed (in figure 2.9, the point at (1.8, 0.094)). For the water continuous runs, the model correlated reasonably well with the experimental data. Removing two points for both fits, for Z_5 $(Q_o, y_*) =$ (3.2 0.05), (5, 0.19) and for Z_4 (3.2, 0.06), (5, 0.19) improved the correlation as shown in the table.

For oil continuous runs, the model is in better agreement with the experimental data for water cuts below 30%, which was expected because of the observed flow of dispersion over the weir for water cuts from 30% and above. It is however surprising that the height measurements at point Z_4 shows considerably better agreement than for Z_5 for the full watercut range. If this is the case, it suggests an acceleration of the dispersion layer between Z_4 and Z_5. Also, the parameter β_2 changes sign for the different types of continuous phase, being positive for oil- and negative for water continuous runs. As the interface area is one order of magnitude higher than the product $\beta_2 * Q_d$ (10^{-1} vs. 10^{-2}), this has an effect on the curvature of the model. The oil continuous model fit shows a weak negative curvature, while the water continuous one shows a weak positive curvature.

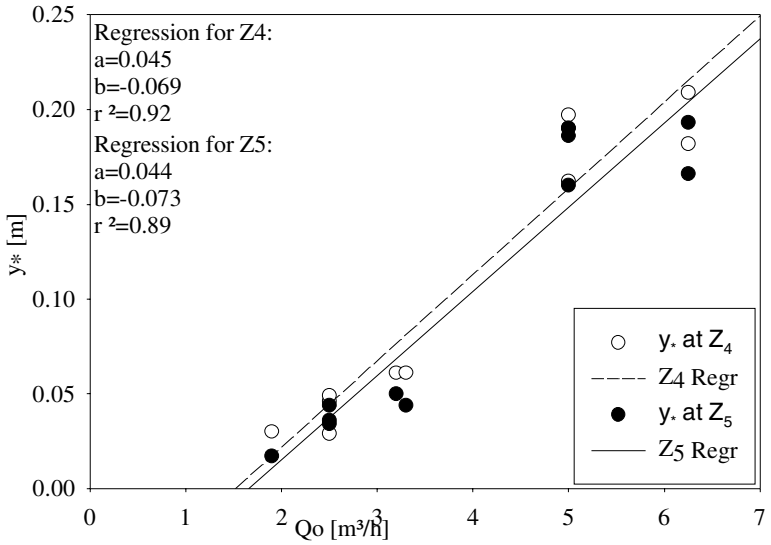

Figure 2.10: Dispersion heights vs. Q_o (dispersed phase rate) for water continuous tests with fluid system 3, ΔP=0.5 bar.

See also section 4.4.2 for bottle test treatments with this model.

It is also interesting that the SRTCA model, which was originally developed for viscosity-stabilised system only, can be applied to surface-stabilised systems such as the oil continuous system discussed here (fluid system 3 batch 1). This indicates that the dispersion thickness will affect the coalescence rate across the bulk liquid interface for a variety of stabilisation modes, and if this rate can be established with bench-scale tests, separator performance under coalescence-hindered operation can be predicted by these models.

2.4.2 Oil outlet quality

The oil outlet quality was sampled at the outlet and measured volumetrically. However, this method proved to be unsatisfactory as water often tended to creep along the wall of the outlet. Sampling thus would show pure oil when significant, visible contamination flowed through the outlet. Attempts were made to correlate control valve positions to the throughflow, but the variation in control valve position for a fixed rate was in the order of the expected position change for incomplete separation. Therefore, no good quantitative measure of water in oil is presented. Qualitatively it was straightforward to observe when visible amounts of water flowed over weir (down to visible drops) and also if the oil phase were "cloudy" with water drops from incomplete settling (this happened only during the oil continuous tests with $\Delta P = 5$ bar for fluid system 3 batch 1, which were discussed briefly in the beginning of section 2.4.1).

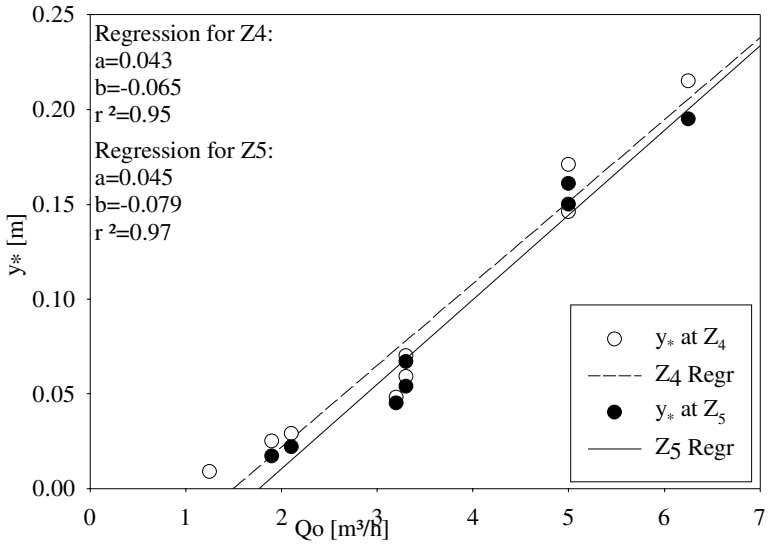

Figure 2.11: Dispersion heights vs. Q_o (dispersed phase rate) for water continuous tests with fluid system 3, ΔP=1.5 bar.

2.4.3 Water outlet quality

For oil continuous runs, the oiw (oil-in-water) content is an increasing function of choke pressure drop and water (disperse phase) flow rate. Figure 2.12 shows the oiw content for oil continuous runs with fluid system 3, batch 1, at constant $\Delta P = 0.5$ bar. The oil content at the water outlet increases with increasing water flow rate. There is no distinguishable effect of water cut (the water cut spans from 0.15 to 0.35), and the water quality is generally good (<120 ppm) for the given span in water flow rate. The spread in the data can be attributed to variations in the control system (see section 2.3.4). See table B.5 in the appendix for the actual values.

Attempts were made to perform tests at a pressure drop of 5 bar, but the system showed transient behaviour with increasing oiw content until the water quality was outside the range of the measuring device (>1400 ppm). Quality data were recorded between 5 and 15 minutes after the shear was initiated, and the resulting plot for an average between 10 and 15 minutes is shown in figure 2.13 (see also table B.5). The dispersion layer also disappeared after some time (between 15 and 30 minutes), and the oil phase became cloudy. The total oil volume in the loop is 1.4 m^3, and for a typical oil flow rate of 10 m^3/h, the mean residence time between each pass at the shear valve is 8.4 min. This suggests that the increase in shear ΔP from 0.5 to 5 bar initiates the creation of small droplets that do not settle within the given residence time in the flow loop/feed separator. The large surface formed by these drops may lead to the stabilising components being gradually depleted from the bulk phase solution, causing rapid coalescence in the

Fit vs.	y_* at Z_4		y_* at Z_5		
		WC< 0.3		WC< 0.3	WC< 0.3[a]
β_1 [h]	0.00493	0.00525	0.00342	0.00355	0.00447
β_2 [h/m]	0.0204	0.0211	0.0125	0.0102	0.0154
Correlation	0.927	0.973	0.670	0.880	0.984

[a]Point at Q_w=1.8, y_*=0.094 removed.

Table 2.3: Model fit parameters for the oil continuous dispersion height measurements with eq. (2.26), substituting Q_l with Q_w (dispersed phase flow).

Fit vs.	y_* at Z_4		y_* at Z_5	
		Mod. input[a]		Mod. input[a]
β_1 [h]	0.00175	0.00096	0.00178	0.00086
β_2 [h/m]	-0.0124	-0.0161	-0.0118	-0.0164
Correlation	0.839	0.977	0.825	0.977

[a]Modified input: removed points (Q_t, WC) = (12.5, 0.6) and (10.7, 0.7)

Table 2.4: Model fit parameters for the water continuous dispersion height measurements with eq. (2.26), substituting Q_l with Q_o (dispersed phase flow).

remaining dispersed fraction.

As mentioned, the oil continuous system lost its stability after approx. 1 month of operation. Figure 2.14 shows the results for this fluid system at different water cuts and pressure drops. The quality is poorer than for the stabilised system in figure 2.12 and shows a much stronger increase with increasing water rate. There is a clear increase in the oiw content for increasing choke pressure drop, and the trend vs. water flow rate is stronger for the higher pressure drop. Any dependence on water cut is still apparently absent. The values for the points labelled "Estimated values" are based on being partly inside the range of the measuring device — as the measuring device operated near the boundary at 1450 ppm, the variations in the reading gave values that were sometimes inside and sometimes outside the range of the device. Based on the time the meter was outside and inside the range, and much experience with the system, an estimate of the oiw content was given.

To investigate the role of coalescence in the tube between the shear valve and the separator, the shear point was moved to immediately upstream the separator (0.6 m as opposed to normally 20 m upstream). This was done for fluid system 3, batch 2, and the oiw content for the oil continuous regime is shown in figure 2.15.

Comparing figures 2.14 and 2.15, the oiw contents are very similar for the two different lengths of tube downstream the choke valve. Any variations are within the spread of the data. See also table B.8 in the appendix for the actual values.

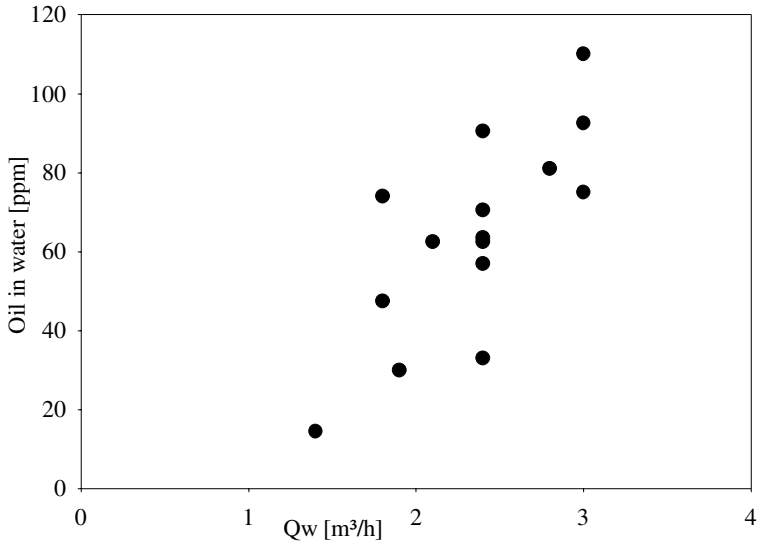

Figure 2.12: Water quality measurements for tests with fluid system 3, batch 1 (stable), ΔP=0.5 bar, oil continuous.

Data for batch 0 are also presented, for comparison with the above and for later reference, figure 2.16 shows the oiw content for different interface settings. The data are few and for a limited span in water cut and flow rates, and do not show the same increasing trend in oil content as in figure 2.12. This is probably due to the higher loading, which will give a larger spread in the data. Some points (above 300 ppm) are assumed to be caused by a partial drain of the dispersion band through the water outlet (the point near 2000 ppm is clearly caused by this). The background for these tests was to establish a reference for the "unloading" experiments (chapter 5) where one of the factors was to investigate how much the interface setting could be lowered for the particular device in question, and emphasis was also on the water continuous regime (it will be shown in chapter 5 that the effect of the device was very small in the oil continuous regime).

For water continuous runs, the oiw content is an increasing function of choke pressure drop and water flow rate, and a decreasing function of oil (disperse phase) fraction. The dependence of pressure drop and dispersed phase content is qualitatively in line with equations (2.21) and (2.22) — when the water cut increases, the concentration of dispersed phase in the choke valve (the break-up point) decreases, and the drops become smaller. As the phase quality measured is for the continuous phase, the measured qualities are expected to be dominated by settling mechanisms, and drop size will be determining. The dispersion layer thickness will still follow the coalescence mechanisms described in sections 2.2.5 and 2.2.6, as shown above in figures 2.10 and 2.11, and therefore the oil quality (assuming that the focus is on achieving a water quality treatable by hydrocyclones (table 1.1)) will be prone to the dispersion layer thickness relative to the available height

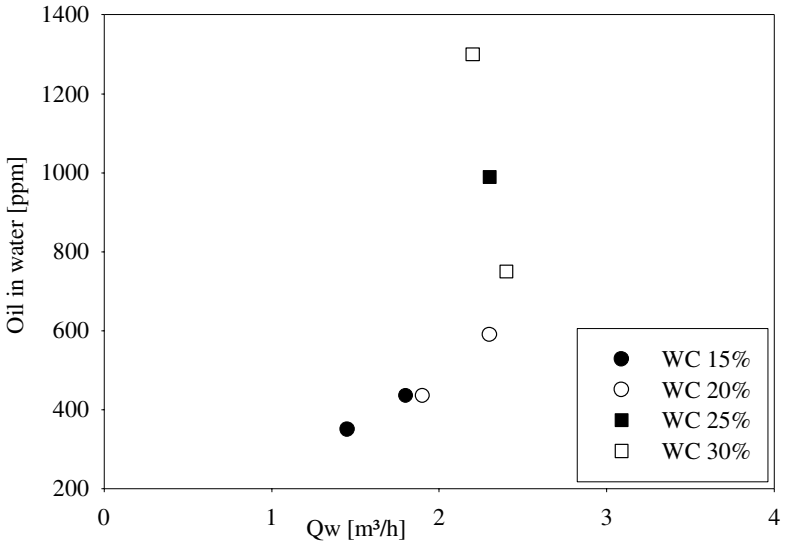

Figure 2.13: Water quality measurements for transient tests with fluid system 3, oil continuous, ΔP=5 bar, batch 1 (stable).

given by the interface setting and weir height.

Figure 2.17 shows the data measured for fluid system 3, water continuous runs. The curves are for constant pressure drop and water cut, and the increase in oil content is easily seen as a function of pressure drop, water cut and flow rate. There also appears to be a coupling between water flow rate and water cut as the oil content in the water outlet increases with decreasing oil fraction. This is readily understood when studying figure 2.1 and assuming a log-normal drop size distribution with a characteristic diameter following equation (2.21). As the volume of the smaller drops increase with increasing water cut (decreasing dispersed phase fraction) relative to the settling efficiency curve (which is fixed by the continuous phase flow rate[3] and the interface setting), the effect of flow rate will be greater for low dispersed phase fractions. The effect of pressure seems less dependent on the continuous phase flow rate. Note that the values for the higher flow rates at ΔP=1.5 bar and WC=0.8 was outside the range of the measuring device and had to be measured from volumetric samples (the low rate at WC 0.8 borders the maximum range) and are rough estimates.

Similarly to figure 2.16, the results for fluid system 3, batch 0 are presented for later reference in figure 2.18. Although the data are more limited than in figure 2.17, the same trends are distinguishable. Also, the quantitative values are similar to the ones in figure

[3]This assumes that the dispersed phase flow can be neglected, as assumed in the plug flow approximation. There will of course be a contribution from the dispersed phase to the average velocity, but as the dispersed phase settle rapidly and the concentrations in the outlet is at the level described here, the plug flow approximation is good.

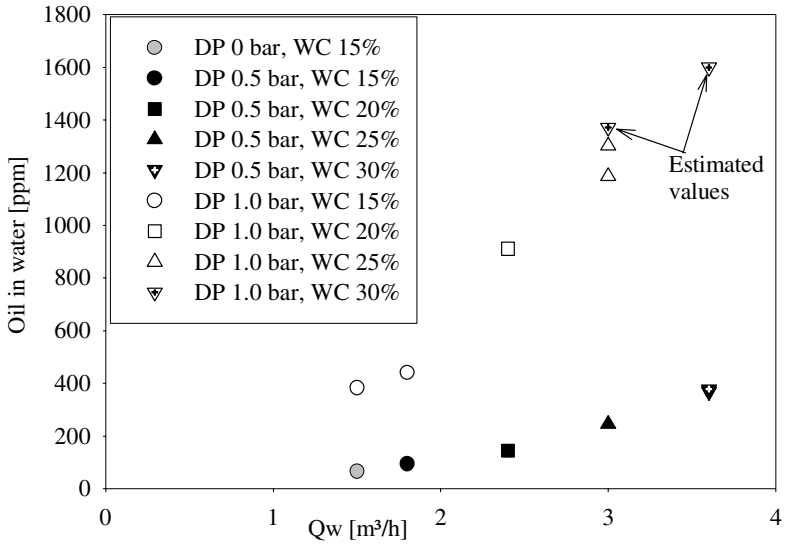

Figure 2.14: Water quality measurements for tests with fluid system 3, oil continuous, batch 2 (unstable).

2.17 for fluid system 3, batch 1, suggesting that the water continuous regime is unaffected by Grane concentration.

Tests were also done in the water continuous regime to investigate the effect of moving the shear point closer to the separator (0.6 m upstream the separator, as opposed to normally 20 m). These data are shown in figure 2.19. The same trends as in figure 2.17 are apparent, but the quality is significantly poorer, particularly for the higher water cuts. The levels of oiw content in the water outlet went outside the range of the measuring device already at the higher rate for WC 0.7, ΔP=0.5 bar. This suggests that upstream coalescence is important for the continuous phase quality as opposed for the earlier results, when oil was the continuous phase. Assuming that this is due to incomplete settling (following the earlier discussion), there is appreciable coalescence in the tube between the choke valve and the separator, particularly for the small end of the drop size distribution.

As the water quality depends on the dispersed phase concentration for water continuous runs, it can be assumed that the same applies for oil quality during oil continuous runs. This variation in continuous phase quality is, as previously discussed, attributed to the effect of variations in dispersed phase fraction in the high-turbulent zone (choke valve), combined with a settling (grade-) efficiency. However, the water (dispersed phase) quality is not visibly affected by concentration for oil continuous runs. This requires a closer discussion.

There are, to the author's knowledge, three different views regarding the origin of variations in dispersed phase quality (the water quality for oil continuous runs);

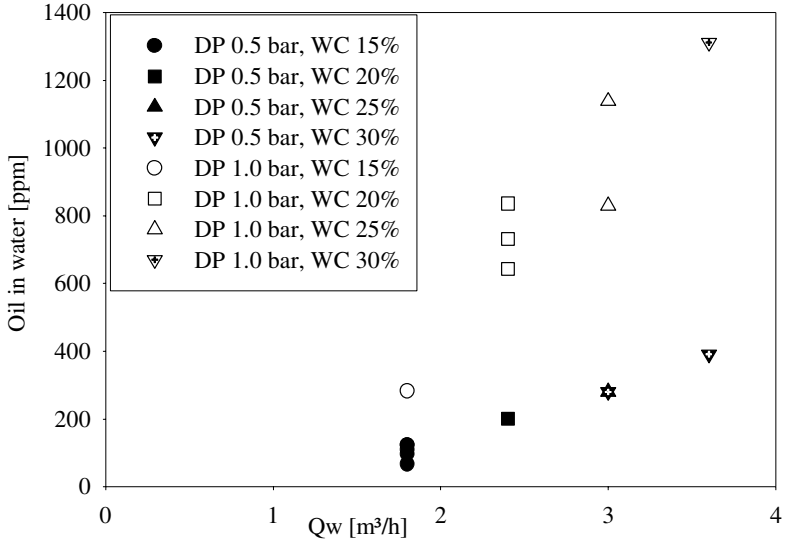

Figure 2.15: Water quality measurements for tests with fluid system 3, oil continuous, batch 2 (unstable). The shear point was moved to close upstream the separator.

1. The oil enters the water when water droplets coalesce with the water bulk phase, as a surge appears when the surface tension energy is released, creating a wave that may form a small oil drop in the wake from the water drop. This mechanism is shown in [26] for a secondary drop in the original continuous phase, but the same mechanism can form a droplet on the other side of the phase boundary as well.

2. The oil enters the water drops in the turbulent shear zone, as oil drops inside water drops (commonly named "complex-" or "double-" emulsions) [26, 27]. This has been observed experimentally here for the oil continuous system [22].

3. The phases are partly separated upstream the separator, and the water phase in the tube is contaminated by turbulent action (in the choke valve, within the tube or when entering the inlet) [28].

The variations in water quality is assumed to arise from settling mechanisms (as long as the dispersion layer is not pulled down to the water outlet hydrodynamically) due to the overall low level of contamination (less than 0.5% or 5000 ppm for all tests with fluid system 3). Several possible settling efficiency curve families due to variations in flow pattern will be discussed in chapter 3. However, as long as the pressure drop remains constant, figures 2.12, 2.14, and 2.15 suggest that the variation in water (dispersed phase) outlet concentration is mainly due to variations in water flow rate. When the continuous phase quality is monitored (figures 2.17 – 2.19), there is a clear effect of the dispersed phase fraction as well. Discussing this in terms of characteristic drop diameter suggests

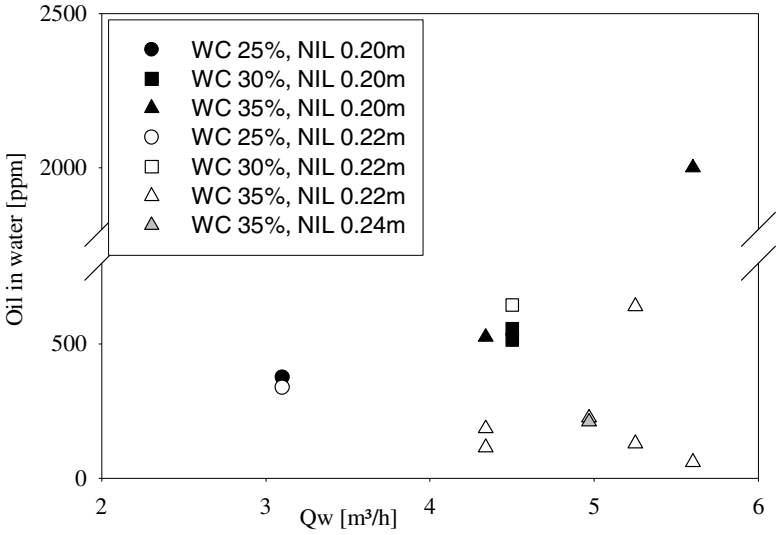

Figure 2.16: Water quality measurements for tests with fluid system 3, batch 0 (stable), ΔP=0.75 bar, oil continuous.

that equation (2.21) is valid for dispersed phase droplets, but the drop size of the dispersed phase is irrelevant for the subsequent dispersed phase effluent quality.

View 1 suggests that for oil continuous runs, oil-in-water droplets are related to the coalescence process (and hence the size of the water-in-oil drops), and one should be able to observe an effect of droplet size if this were the case. As the water quality is unaffected by dispersed phase fraction for oil continuous runs, this view is weakened.

View 3 is discarded, at least for fluid system 3 batch 1, as this system is unlikely to separate in the tube upstream the separator. Furthermore, all samples taken from the inlet tube for any model system have shown that the concentration in the sample is corresponding to the calculated dispersed phase fraction of the feed as shown in figure 2.20, and separation in the tube has never been observed (although reports from installations have shown corrosion marks in the bottom part of the inlet tube, suggesting a preseparation).

View 2 is the only that corresponds to the observations done here, and appears to be the better hypothesis for these systems.

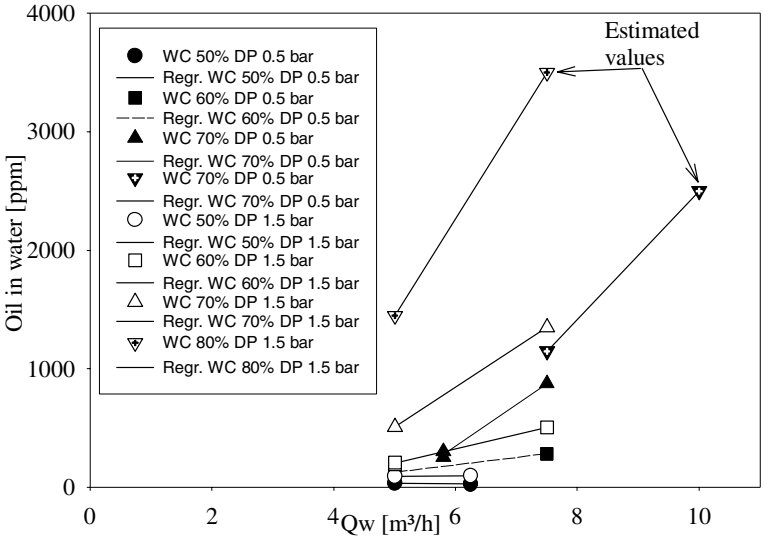

Figure 2.17: Water quality measurements for tests with fluid system 3, batch 1, water continuous.

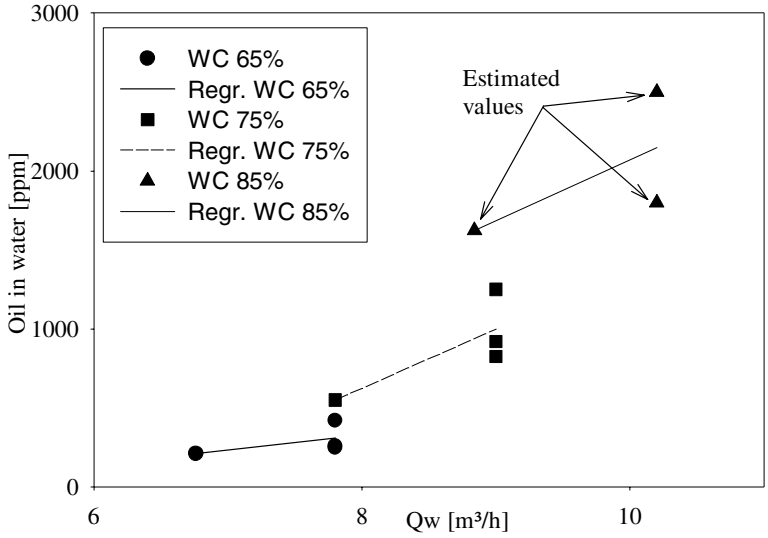

Figure 2.18: water quality measurements for tests with fluid system 3, batch 0, ΔP=0.75 bar, water continuous.

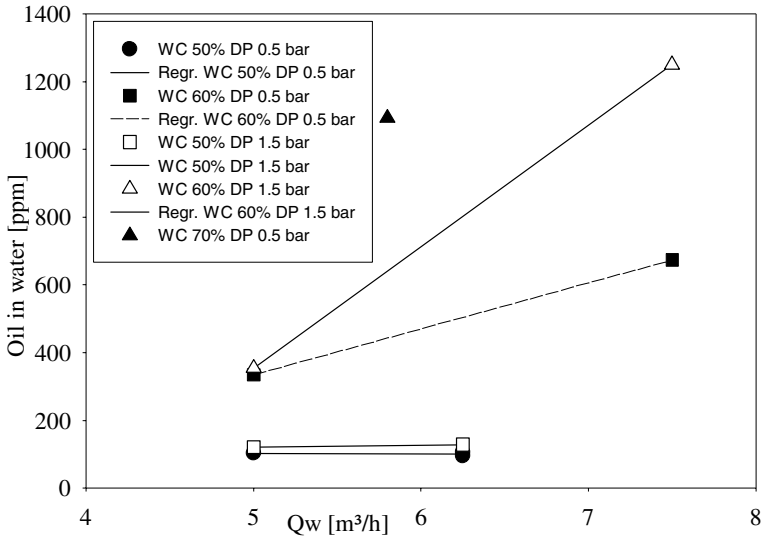

Figure 2.19: Water quality measurements for tests with fluid system 3, water continuous. The shear point was moved to close upstream the separator.

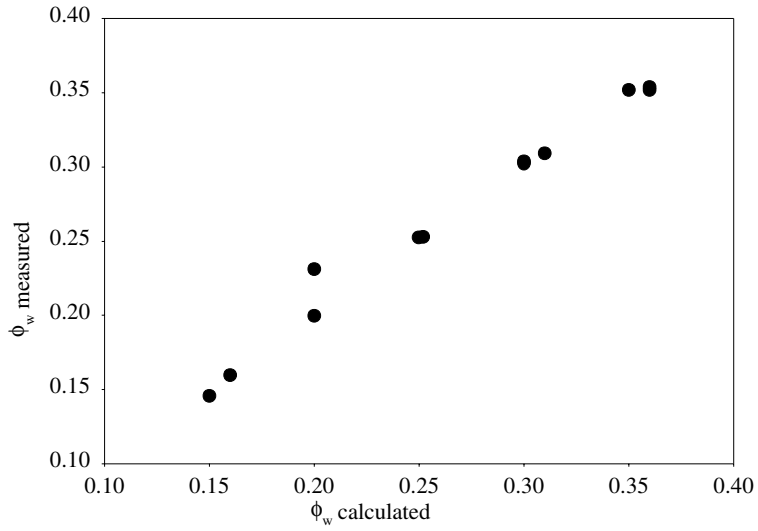

Figure 2.20: Inlet concentration sample vs. calculated value from flow rate measurements for fluid system 3 batch 1, $\Delta P = 0.5$ bar.

2.5 Conclusion

The water quality has been measured for several fluid systems and for both the oil- and water continuous regime. When water is the dispersed phase, the oil concentration at the water outlet increases with increasing pressure drop, increasing water rate and increasing coalescence rate. When water is the continuous phase, the oil concentration at the water outlet increases with increasing pressure drop, increasing water rate and decreasing dispersed phase [oil] concentration at the inlet. There is a coupling between the dispersed phase concentration and the water rate.

The dispersion layer height shows a near-linear increase in volume with dispersed phase fraction, and the coalescence rate is different for the different regimes of continuity. For fluid system 3, batch 1, oil continuous, the linear fit approaches zero for zero water rate, and all the water is transported through the dispersion layer. For the water continuous regime, the linear fit has a negative intercept and coalescence in the inlet region is appreciable. A model found in the literature [21] was fitted to the measured dispersion layer heights, with good results after an adjustment of the model, as will be further shown in chapter 4.

Chapter 3

Flow pattern analysis

3.1 Introduction

As discussed in section 2.2.2, the traditional view of the flow pattern in a gravity separator assumes rapid coalescence, meaning that the bulk of separation takes place in the inlet zone, and the mean velocity downstream the flow diffuser is in essence given by the inlet flow conditions and the wetted cross-sectional area of a phase.

This is a limiting case of the more general situation (as pointed out by Arntzen and Andresen [29]), which is that the separator behaviour are controlled by both settling and coalescence mechanisms. This can be illustrated by utilising the batch separation model by Hartland et al. [19], outlined in section 2.2.5. Assuming equal velocity in the water- and oil phase, the time axis in figure 2.2 can be converted to a z-axis (along the main flow direction) inside a separator. Focusing at the ZDLT (zero dispersion layer thickness) point (where the coalescing- and sedimenting heights meet), the following cases apply (see also figure 3.1):

1. If the ZDLT point is upstream the flow diffuser, there will be no dispersion layer in the separation section (between the flow diffuser and the weir) and the plug flow approximation is representative in both liquid bulk phases.

2. If the ZDLT point is between the flow diffuser and the weir, the dispersion will form a wedge. Given the shape of the coalescing curve, most of the dispersed phase separates early and the plug flow approximation is reasonable for both liquid phases.

3. If the ZDLT point where the sedimenting- and coalescing heights meet are "downstream the weir", the volume that "is located downstream the weir" will be transposed upstream the weir, causing an increased dispersion thickness here. As long as the kinetic energy is low[1], the dispersion layer thickness will be approximately constant throughout the separation section.

[1] A typical gravity separator has a mean velocity of either phase in the order of 0.05 m/s. Assuming a continuous phase density of ρ_c=800 kg/m^3 and a dispersion density of 900 kg/m^3, this kinetic energy

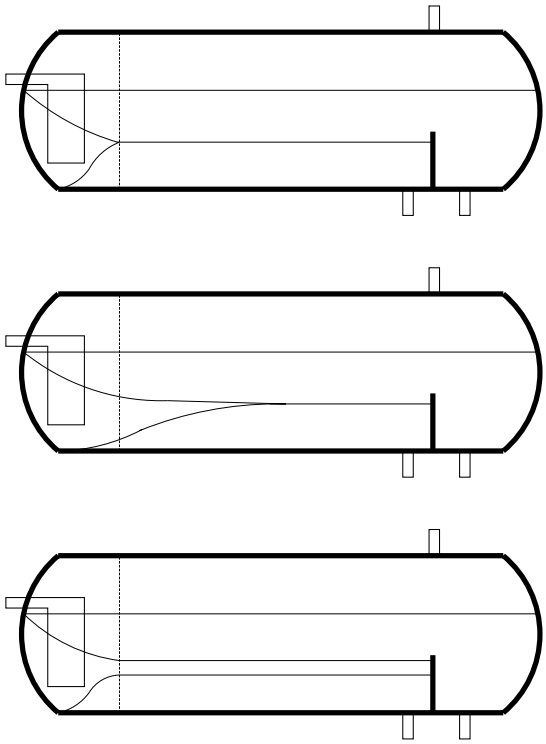

Figure 3.1: Sketch of three different dispersion layer formations in continuous systems. Top: rapid coalescence, no dispersion layer in separation section. Middle: somewhat slower coalescence, dispersion wedge formed. Bottom: full-grown dispersion layer extending from flow diffuser to weir, constant height.

In the batch model, the final interface will always occur at a height corresponding to the initial concentration of the phases. In a continuous process, this level is set based on criteria such as alarm levels and shutdown criteria. In addition, there is a danger of pulling dispersion down into the water outlet, causing excessive oil-in-water values here. As one of the critical criteria of the process is to achieve acceptable water quality, the dispersion layer is confined downwards by this event.

Above, it was assumed that the bulk phases moved with the same velocity, to readily transform time in the batch model to distance in a continuous model. This is rarely true. The bulk phase velocities will, for the case of rapid separation, move with velocities given by the bulk phase flow rate and wetted cross-sectional area (defined by the interface set points). There may also be a momentum exchange across the clean interface (with a no slip condition).

will (following Bernoulli's equation) not cause a larger increase in dispersion height than Δh=1 mm at the weir.

When a dispersion layer is formed, it is likely that the momentum exchange between the pure bulk phases will be reduced, as the viscosity of the intermittent dispersion is normally higher than any of the pure phases (due to non-Newtonian behaviour) [30]. And, if the dispersion layer extends throughout the separation section, it is probable that there will be little gross horizontal movement of the dispersion. The main pattern in the xz-plane will be rotational for this layer (due to no-slip conditions with respect to both bulk phases) and, consequently, the momentum interchange between the bulk oil- and water phases will be low.

3.2 Analytic

3.2.1 Alternative dispersed-phase flow pattern

Figure 2.9 showed the measured dispersion layer thickness at two points in the separation section for an oil continuous system. As discussed in section 2.4, the intercept of the linear trend is close to zero, implying that the coalescence is slow and a dispersion layer will exist in the separation section for all dispersed fractions. If the coalescence rate is constant in the z-direction (for the whole interface), this suggests that the water bulk phase will be fed mainly from the interface, and evenly throughout the separator (upstream the weir). Ideally, the mass flux through the interface can be assumed constant and independent of position at the interface, and there will then be a binary probability (0 or 1) that a drop will either follow or escape the dispersed phase interface flux. Due to the vessel geometry, for an oil continuous feed the vertical velocity will be lowest near the interface. The flow direction is parallel to gravity, and equation (2.10), in the extreme case that all of the dispersed phase coalesces evenly along the interface, is reduced to eq. 3.1.

$$\eta_i = \begin{cases} 1, & \frac{v_{\mathrm{St,i}} A_y}{Q} \geq 1 \\ 0, & \frac{v_{\mathrm{St,i}} A_y}{Q} < 1 \end{cases} \tag{3.1}$$

Regarding the bulk flow pattern of the separated dispersed phase in the separation section of the separator, the interface can be regarded as a second inlet. Assuming complete bulk separation (neglecting flow of dispersion above the weir) and assigning a fraction of the dispersed phase entering the separator to the "interface inlet", the grade efficiency can be assumed analytically to be a combination of eq. (3.1) and eq. (2.10). An analytical calculation of the case with a cylindric geometry and a real outlet becomes complex because the vessel shape gradually constricts the flow from the interface boundary, giving a higher downward velocity contribution when moving vertically through the (separated) dispersed bulk phase. The outlet location will also affect this contribution. This is therefore calculated by a numerical approach (see section 3.3.2 below). The overall efficiency is, depending on the drop size distribution, given by eq. (2.12).

3.2.2 Flow diffuser

The flow diffuser configuration used in the tests consists of a plate mounted vertically across the liquid section of the separator, with holes distributed evenly across the plate to allow the fluids to pass. The open fraction of the flow diffuser used was 0.18. The pressure drop across such a flow diffuser has been correlated to eq. (3.2) [31].

$$\frac{\Delta P}{\frac{1}{2}\rho v^2} = C\mathring{a}^{-e} \tag{3.2}$$

The coefficient $C = 1.246$ and the exponent $e = 2.16$ are valid for open fractions $0.05 \leq \mathring{a} \leq 0.22$ and velocities $0.01 \leq v \leq 2$ m/s perpendicular to the flow diffuser [31]. This equation is valid as long as the plate thickness is insignificant ($\Delta x_{\mathsf{plate}} \ll d_{\mathsf{hole}}$).

3.3 Numerical description

This section describes the basis for the numerical flow calculations performed. Two grids have been used: one representing the bulk water phase of a pilot gravity separator, and one representing the flow diffuser. The flow diffuser grid is used to calculate the velocity profile entering the separation section of the separator, while the bulk water phase grid is employed to calculate grade efficiencies for different boundary conditions. The emphasis of the calculations on the latter grid has been to examine the effect of release of water from the dispersion layer, as for oil continuous feed conditions in a gravity separator, on the grade efficiency.

3.3.1 Basic description of the models

All fluid simulations were performed with the commercially available Fluent 5.3, 3D finite volume double-precision solver. The features of this solver are described in detail in [32]. The problem at hand is to get a solution of the flow field in a given geometry as represented by a grid of finite cells, control volumes. The equations (conservation of mass and momentum) are then solved in each control volume, and the solution is fed into the neighboring cells. The equations of mass (3.3) and momentum (3.4) conservations on partial differential form, respectively, are given below ([33], [34]).

$$\frac{\partial \rho}{\partial t} + \nabla \cdot (\rho \mathbf{v}) = 0 \tag{3.3}$$

$$\rho \frac{D\mathbf{v}}{Dt} = \rho \mathbf{g} - \nabla P + \nabla \cdot \boldsymbol{\tau}_{ij} \tag{3.4}$$

All simulations performed have been for single-phase, incompressible newtonian conditions. Two viscous models have been employed — the laminar and the turbulent k-ϵ

model. These models are concerned with the last term of eq. (3.4). The laminar model assumes that the viscous forces dominate over the momentum forces, and that velocity irregularities in the flow field are dampened out quickly, and the stress tensor becomes $\boldsymbol{\tau}_{ij} = \mu \frac{dv_i}{dx_j}$[2] Turbulence models adresses the situation where momentum forces dominate the viscous forces, and velocity irregularities are present throughout the flow field. The k-ϵ-model is a two-equation model which is suitable for flows with isotropic turbulence, i.e. flows without rotation or strong interaction with solid obstructions, walls or the like. Turbulence is a large field of science, and no attempt will be made to elaborate further details here.

Finally, a word regarding the choice of single-phase modelling. Multi-phase models are available in various commercial solvers, but they are not very useful in the cases simulated here. Numeric solvers do not have good models for break-up and coalescence, mainly because these fields are not fully understood. Particularly, the coalescence modelling for fluids that contain surface active components are lacking. For example, the result of figures 2.8–2.11 cannot be modeled by the present solvers. Commercial fluid dynamics solvers with multi-phase capabilities may be applied with success where momentum/viscous forces are the dominating feature of the flow field, but are still lacking when coalescence- and break-up are dominating features of the flow field. Therefore, single-phase simulations of regions known to be dominated by one-phase behaviour have been performed here.

3.3.2 Alternative dispersed-phase flow pattern

The water phase separation zone-equivalent of the pilot model separator described in section 2.3.1 was simulated. Fluent 5.3 was used in the numerical simulations with unstructured tet-mesh (tetrahedral) cells because of difficulties in gridding the transition between the main body and the outlet of the water section. The single-processor solver was used for all cases except those with coupled interaction of discrete- and continuous phase, where the multi-processor-solver with two processors was used. Grid resolution was 29196 cells. An outline of the grid is shown in figure 3.2. Convergence criteria were that all residuals had decreased five orders of magnitude.

The end- ("flow diffuser-") and "interface inlet" were defined as velocity inlets with constant velocities as described in table 3.1. This corresponds to having a water feed component originating from the dispersion layer, with magnitude ϕ_I relative to the total water feed. The outlet was defined with an outflow condition.

First, The laminar viscous model was used, as the Reynolds number is in the vicinity of the transition point to turbulent flow for tubular flow (see table 3.1). Grade efficiencies were calculated by non-coupled Lagrangian particle tracking (see below).

The set for Q_w=5 m^3/h was also simulated with the turbulent k-ϵ-model. Here, the inlet boundary conditions for the turbulence model were calculated using the results from flow diffuser simulations (see section 3.3.3), for the input velocities shown in column v_{end}.

[2]Here, x_j represents any direction normal to the velocity v_i, and not the specified direction listed in the list of symbols.

Case	Q_w	ϕ_I	v_{end} *1E-3	v_I *1E-4	Re *1E3	k *1E-4	ϵ *1E-4
1	1	0	2.87	0.00	0.80		
2	1	0.2	2.29	0.37			
3	1	0.4	1.72	0.74			
4	1	0.6	1.15	1.11			
5	1	0.8	0.57	1.48			
6	1	1	0.00	1.85			
7	2	0	5.73	0.00	1.60		
8	2	0.2	4.59	0.74			
9	2	0.4	3.44	1.48			
10	2	0.6	2.29	2.22			
11	2	0.8	1.15	2.96			
12	2	1	0.00	3.70			
13	3	0	8.60	0.00	2.40		
14	3	0.2	6.88	1.11			
15	3	0.4	5.16	2.22			
16	3	0.6	3.44	3.33			
17	3	0.8	1.72	4.44			
18	3	1	0.00	5.55			
19	4	0	11.46	0.00	3.20		
20	4	0.2	9.17	1.48			
21	4	0.4	6.88	2.96			
22	4	0.6	4.59	4.44			
23	4	0.8	2.29	5.92			
24	4	1	0.00	7.40			
25	5	0	14.33	0.00	4.00	4.2	4.0
26	5	0.2	11.46	1.85		2.7	2.1
27	5	0.4	8.60	3.70		1.6	1.0
28	5	0.6	5.73	5.55		0.8	0.3
29	5	0.8	2.87	7.40		0.24	0.04
30	5	1	0.00	9.25			

Table 3.1: List of velocity boundary conditions for water phase simulations, applied on the inlet planes of the domain.

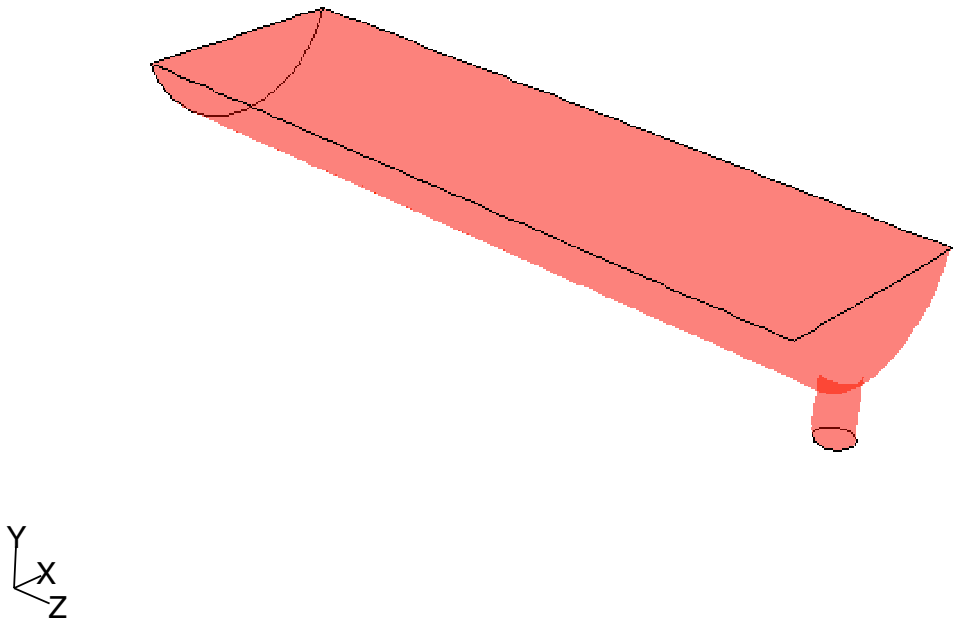

Figure 3.2: Outline of the pilot model water phase grid.

Both non-coupled and coupled Lagrangian particle tracking was performed and grade efficiencies were calculated.

Lagrangian particle tracking was performed for all cases, releasing a distribution of droplets from 0 to 250 μm in size bands of 10 μm from all cells at the end- and interface inlets, completing approx. 65500 droplet tracks for all cases. The input droplet size distribution parameters were set to $\bar{d}$=342 μm and n=3.26, as defined by the Rosin-Rammler distribution (see section 4.2.3). The kerosene mass flow input in the coupled Lagrangian tracking model was set to 1 volume% of the water flow. The wall- and end inlet boundary conditions were set to reflect droplets, the top inlet was set to trap droplets, and the outlet was set to let droplets escape. The droplets were then individually sorted by origin and fate, and grade efficiencies were calculated based on volume fractions of continuous phase released from each inlet. Table A.19 in the appendix shows an example for case 28 in table 3.1 with the laminar viscous model (this is also shown in figure 3.7).

The cases with Q_w=5 m^3/h were repeated with a more narrow droplet distribution to get a better resolution in the diameter range of interest. For the turbulent simulations of these cases, the "stochastic tracking" option was used. The turbulence is treated as average values in a control volume, and this option calculates the particle movement based on a stochastic treatment of the turbulent velocity fluctuations instead of using the averaged values. For each particle trajectory, 10 stochastic representations of the turbulent field were calculated.

The inlet boundary conditions had to be altered for the extreme cases in ϕ_I, as the solver had problems reaching a solution when an inlet had 0 inflow. The reason for this has not been studied in detail, but is assumed to rise from the formulation of the turbulence model. For these cases, the applicable zero-flow inlet was changed to a wall.

Finally, for the developed turbulent flow fields, the option "interaction with the continuous phase" was used. In uncoupled calculations, the flow regime is solved for the bulk phase, and the particles are then released from the appointed boundaries and follow the bulk flow solution (possibly modified by stochastic turbulence representation, as described above). In coupled calculations, the discrete phase is treated as real particles with bouyancy and drag. The resulting flow field solution will then depend on particle movement. This interaction were updated for every 10 steps of uncoupled calculations.

3.3.3 Flow diffuser

A typical case for a flow diffuser geometry was simulated. Fluent 5.3 was used in the numerical simulations with 31000 quad (prismatic) cells. The standard k-ϵ was used for modelling turbulence, as isotropic turbulence was expected. The inlet condition were water at 300 K, with a flat velocity profile of 0.05 m/s. The grid consisted of a symmetric section of the diffuser, containing 1/4 holes in each corner and one hole in the middle, with symmetry planes along the edges of the section (thus approximating an infinitely large diffuser). The hole size was 15mm x 25mm. The full repeating pattern in the xy-plane is a 58.4mm square, giving a total open fraction å=0.220. The plate thickness was 2 mm.The fluid section stretched 200 mm upstream the diffuser and 800 mm downstream the diffuser. Figure 3.3 shows the outline of the repeating structure of the grid, with symmetry planes in the xz- and yz-planes forming the prism, and with reference lines every 100mm in the z-direction.

Four cases with inlet velocities from cases 25–28 in table 3.1 were also solved, and values for k and ϵ were estimated from peak values found in plots of these values in the middle yz-plane. An example is shown in figure 3.4, for case 26 in table 3.1. Notice the peak at z=0.24 m, ranging from 2.1E-4 to 3.3E-4. The value of k used as an input in the end inlet boundary condition in this case was 2.7E-4, the average of the peak range.

Case 29 was also attempted, but would not converge because of a divergence in the turbulent viscosity ratio: as ϵ becomes very small, the turbulent viscosity ratio becomes large, and the solver fails to reach a solution because of a built-in relaxation term limiting this ratio to 1E5[3]. This was not regarded a major problem, and the values for k and ϵ were instead estimated from curve-fits based on v_{end}, using a 2nd-order polynominal for k and an exponential function for ϵ. These fits are given in appendix A.3.

[3]This relaxation term can be adjusted to allow the iteration process to continue, but this was not performed as it seemed unnecessary to continue the computation at these cases (which were assumed to be near the transition to the laminar regime).

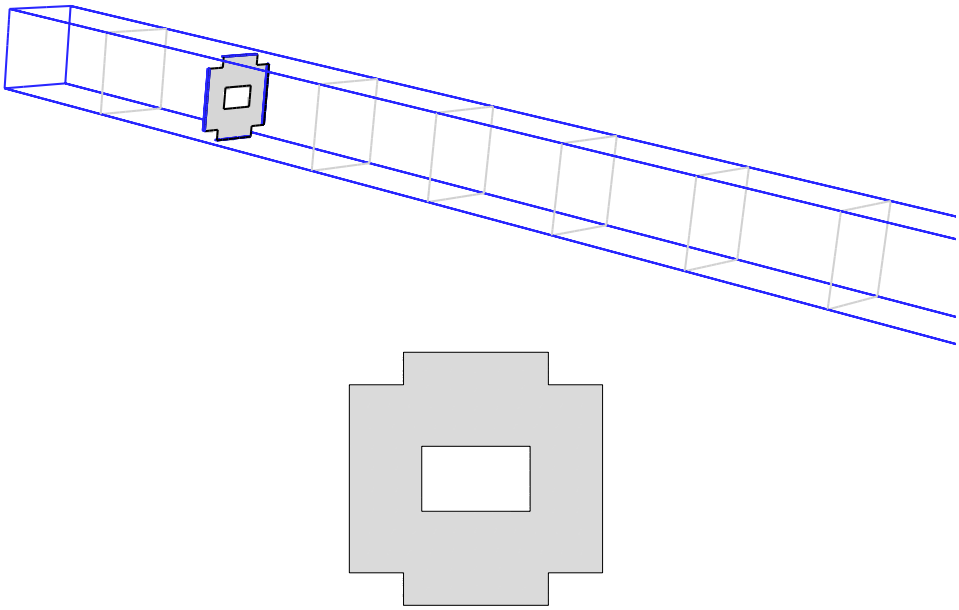

Figure 3.3: Top: outline of the flow diffuser grid, with reference lines every 10 cm in the z-direction, flow left to right. Bottom: magnification of the repetitional pattern forming the flow diffuser.

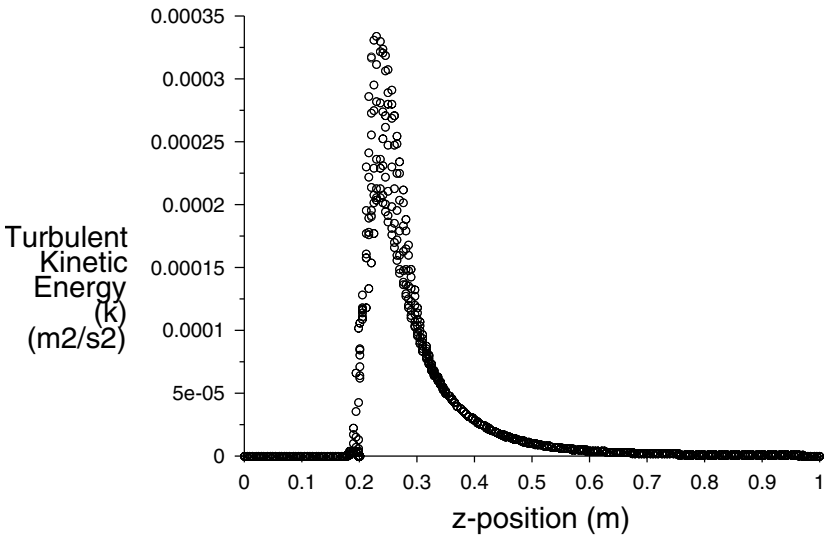

Figure 3.4: Example of estimation procedure for k and ϵ: plot of k in the middle yz-plane, for the geometry in figure 3.3.

3.4 Results and discussion

3.4.1 Alternative dispersed-phase flow pattern

Figure 3.5 shows the inlet velocity vectors for case 28, laminar in table 3.1, which is the chosen example for this section. The flow direction is from the left- and top plane, to the outlet (the bottom of the small cylinder at the bottom right). The reasons for choosing a laminar case as the example are several:

1. The laminar calculation is closer to the engineering approach described in section 2.2.3.

2. Due to the "trap particles" boundary condition at the interface, the efficiency calculation will perform as if the coalescence time is zero. For laminar solutions of the flow field, this is acceptable as a particle reaching the interface will rest there. For the turbulent calculation, the number of particles that are removed will be over-predicted as particles with very short contact times will count as trapped.

Case 28 routes 60% of the flow through the "interface inlet" (see section 3.3.2), and the respective inlet velocities are 5.7 mm/s from the "flow diffuser inlet" and 0.55 mm/s from the "interface inlet". The figure shows that the velocity along the interface is one order of magnitude higher than the set "interface inlet" velocity. The bulk of this velocity is the horizontal component from the "flow diffuser" inlet, and an effect from the outlet is seen in the last 25% of the length. Integrating the inlet velocities over the areas (0.0097 and 1.5 m^2, for the flow diffuser- and interface inlet, respectively) gives the total flow rate of 5.0 m^3/h.

Figure 3.6 shows the y-velocity in the centre yz-plane, together with the iso-surface of y-velocity = 5 mm/s. Looking at the development of the flow through the vertical centre plane of the separator, the y-velocity is below 1 mm/s throughout most of the separator, and rapidly increases in the vicinity of the outlet.

Table 3.2 shows the results from the Lagrangian discrete-phase tracking of kerosene droplets with a diameter range from 10 to 250 μm. For high fractions of water going through the interface (e.g. $\phi_I \geq 0.8$), eq. (3.1) dominates eq. (2.10), and the grade efficiency curves become steeper (see figure 3.7). For these cases, the size resolution of the drop size distribution will affect the results, as the change in efficiency occurs over a size range less than the 10 μm resolution of the input DSD. The cases with $\phi_I = 1$ suffer from this in particular. However, the grade efficiencies for the lower ϕ_I's are better represented. Figure 3.7 shows the calculated grade efficiencies for laminar cases with Q_w=5 m^3/h, and also the ideal grade efficiencies calculated with equations (2.10) and (3.1). The grade efficiencies calculated by equations (2.10) and (3.1), labelled "ideal" in the figure, are close to their numerically calculated equivalents.

The calculated cut sizes in table 3.2 are based on the assumption of a linear trend between the diameters where the grade efficiency traverses the applicable cut size probability (example: for Q_w=5 m^3/h, ϕ_I=0, $\eta_{20\mu m} = 0$ and $\eta_{30\mu m} = 0.098$. The resulting d_{05} is approximated to 25 μm.) Generally, for $\phi_I \neq 0$ the grade efficiencies at small diameters

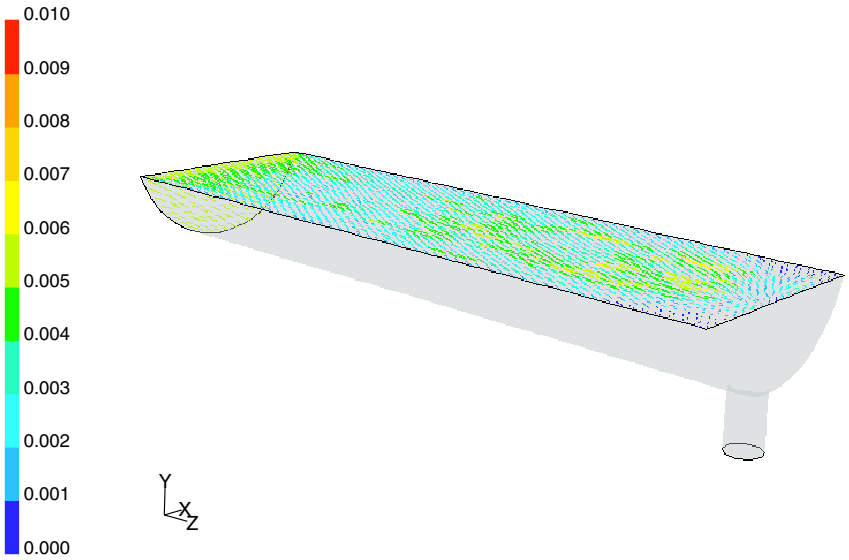

Figure 3.5: Inlet velocity vectors coloured by velocity magnitude [m/s] for case 28, table 3.1.

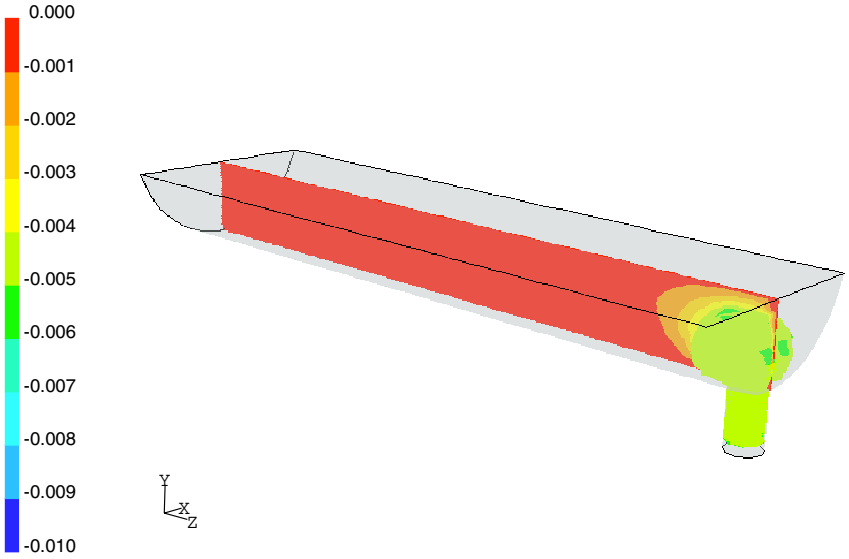

Figure 3.6: Contours of y-velocities [m/s] in centre yz-plane and iso-surface for $v = 5$ mm/s for case 28 in table 3.1, laminar calculation

ϕ_I	d_{05}	d_{50}	d_{95}	d_{05}	d_{50}	d_{95}	d_{05}	d_{50}	d_{95}
	Q_w=1 m^3/h.			Q_w=2 m^3/h.			Q_w=3 m^3/h.		
0	12	33	50	15	46	70	16	57	86
0.2	4	32	50	28	46	70	7	56	84
0.4	12	30	48	31	43	68	24	53	82
0.6	16	26	47	38	47	63	40	59	78
0.8	23	35	45	41	49	60	51	56	73
1	30	35	40	50	55	60	51	60	69
	Q_w=4 m^3/h.			Q_w=5 m^3/h.					
0	25	66	100	25	75	110			
0.2	17	64	98	23	72	109			
0.4	32	59	94	41	69	106			
0.6	47	54	90	52	68	101			
0.8	60	66	83	69	76	95			
1	70	75	80	79	84	90			

Table 3.2: Calculated cut sizes, water as dispersed phase: grade efficiencies, laminar cases. All diameters in μm.

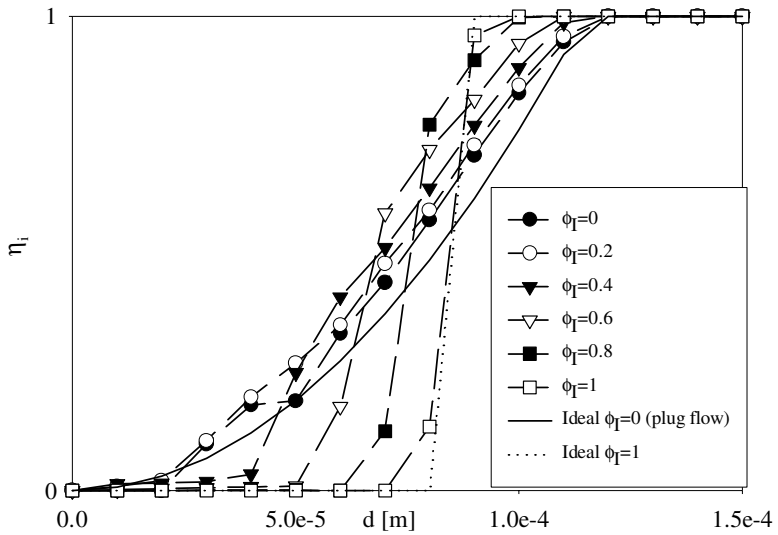

Figure 3.7: Grade efficiencies for simulated laminar cases with Q_w=5 m^3/h (case 25 – 30 in table 3.1). Ideal grade efficiency curves according to eq. (2.10) and (3.1) are also shown.

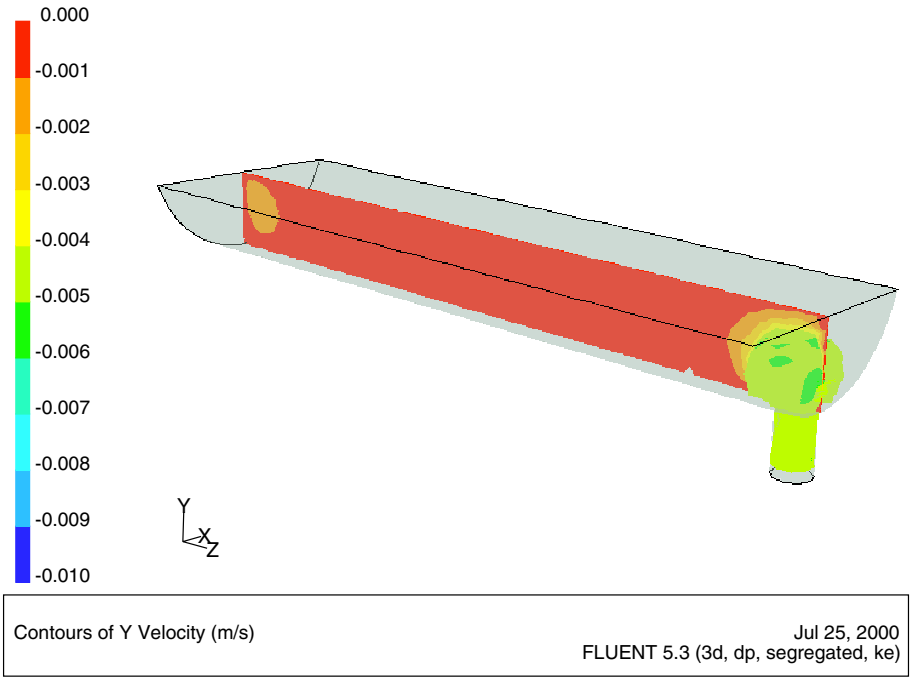

Figure 3.8: y-velocities in centre yz-plane and iso-surface for $v = 5$ mm/s for case 28 in table 3.1, turbulent calculation

is low, but not zero as opposed to for $\phi_I = 0$. Following the d_{05} columns for different ϕ_I's, there is a general trend of increasing diameter for increasing ϕ_I when $\phi_I \geq 0.2$, but d_{05} for $\phi_I = 0$ is often larger than for $\phi_I = 0.2$. Looking at figure 3.7, showing the results for Q_w=5 m^3/h, there are disturbances in the low diameter regime ($d \leq 40\mu$m). This is the reason for the mentioned deviation in the trend for d_{05} in table 3.2. The general trend of increasing d_{05} and decreasing d_{95}, or increasing slope in grade efficiency for increasing ϕ_I is the main result, and in accordance with the theory of section 3.2.1.

Figure 3.8 shows the y-velocity in the centre yz-plane, together with the iso-surface of y-velocity = 5 mm/s, for the uncoupled turbulent solution of case 28 in table 3.1, similar to the laminar solution in figure 3.6. Comparing the laminar and turbulent solution, there is a region near the top of the flow diffuser with a slightly higher y-velocity in the turbulent solution. Also, the effect of the outlet is slightly less for the turbulent solution. The reason for the difference near the flow diffuser is attributed to turbulent interaction between the entering flow from the two inlets, while the difference near the outlet arises from the decrease in range of viscous forces (due to the turbulence model).

The change from a laminar to a turbulent k-ϵ model had a large impact on the resulting grade efficiencies, as can be seen in figure 3.9. The uncoupled turbulent solution for ϕ_I=0

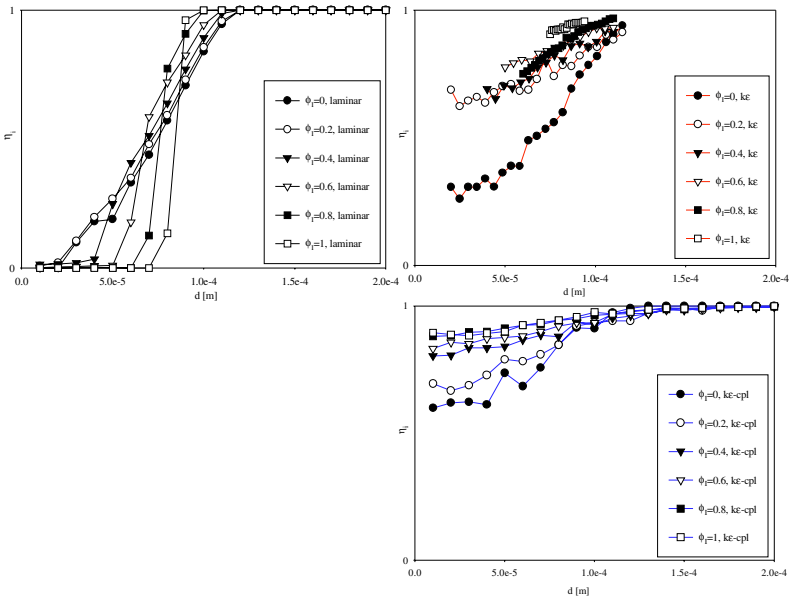

Figure 3.9: Comparison of grade efficiency calculations for cases 25–30 in table 3.1, for different viscous models. Top left: laminar flow solution (same as figure 3.7). Top right: k-ϵ turbulent solution, flow field solved independently of dispersed phase. Bottom left: k-ϵ turbulent solution, flow field solution dependent of dispersed phase.

shows a departure from the laminar solution at drop diameters below 50 μm as the turbulent field increases a particle's chance of reaching the interface, and zero contact time is the only requirement for removal. The trend vs. increasing ϕ_I is also completely different, as the increasing release of particles from the interface in a turbulent field will give an increasing probability for these particles to have a brief contact with the interface.

The coupled turbulent solutions showed an even larger departure from the laminar solutions. The grade efficiency curves for ϕ_I >0.4 are approaching efficiencies between 0.8 and 0.9 for very small diameters, and reach 0.95 in the vicinity of 100 μm. For ϕ_I of 0 and 0.2, the variation in efficiency with diameters are somewhat larger for diameters below 100 μm, but the efficiencies are still dramatically higher than for the laminar solutions, approaching 0.55 and 0.65 for ϕ_I 0 and 0.2, respectively.

These results are rather surprising as the turbulence level is very low (table 3.1. Naturally, the "coalescence model" problem of zero contact time at the interface will grossly over-predict the efficiency in actual systems with real contact times required for coalescence, but still there appears to be rather dramatic departures from ideal theory. Note also that the coupled solutions will depend on the drop size distribution which is not known for the secondary dispersions (as will appear in the water phase for oil continuous runs).

The results are also interesting in view of the results found in chapter 2 for the water quality in experiments with oil continuous, stabilised feed conditions. The observed improvement in water quality when going from an unstable- to a partly stabilised system is better explained by the grade efficiencies for the turbulent solutions as the secondary oil dispersion in the water phase is normally assumed to consist of very small drops. As the dependency on flow rate is weaker for the stabilised system compared to the destabilised system, one would expect that the grade efficiency curves should also be flatter for the stabilised system, which corresponds much better with the turbulent solutions.

As the diameters of separator vessels are very large, it is clear that the flow will be turbulent for the vast majority of applications. A typical primary separator in the North Sea have a diameter of 3m and a NIL setting of 0.75m, which gives a hydraulic diameter for the water phase of 0.96m, and a Re-number in the vicinity of 50000 (assuming ρ = 1000kg/m^3, μ_w = 1E-3kg/m,s and v=0.05m/s) which is clearly turbulent. It is unlikely that the large-scale turbulence is fully developed as typical separator lengths are seldom more than 15m, or approximately 5 diameters. Also, if the water enters mainly from the interface, the average velocity will be lower than 0.05 m/s for much of the available volume. However, the turbulent field will undoubtly affect separation because of the small size of the oil droplets here, and with a better understanding of the coalescence process and the possibility to incorporate this into flow field solvers, separator performance prediction by computed grade efficiencies will improve.

3.4.2 Flow diffuser

Figure 3.10 shows the velocity profile in the yz-plane over the middle of a hole, with a peak velocity slightly above 0.3 m/s, which is an acceleration of 6 times. The velocity is down to 0.05 m/s after 0.1 m. This acceleration creates a turbulent shear, resulting in a kinetic energy profile as shown in figure 3.11.

This energy will induce mixing in the xy-plane perpendicular to the main flow direction. The magnitude of the induced y-velocity is shown in figure 3.12, and in the zone where the kinetic turbulent energy is at its peak, there is an effective y-velocity of 0.01 m/s. From equation (2.4), this corresponds to the settling velocity of an oil drop (with density 800 kg/m^3) of 150 μm.

When the dispersion that is formed upstream the flow diffuser flows through this zone, the lower- and upper parts of the layer is subjected to these forces. Typical maximum drop sizes in the outlets of a gravity separator is $< 50\mu$m in the dispersed phase outlet and $< 200\mu$m in the continuous phase outlet [21]. Drops belonging to such size distributions will undoubtedly be affected by these velocities. As will be shown in section 5.4, taking action to remove this effect can have profound implications, in particular to the continuous phase quality.

The pressure drop over the plate was 45 Pa, as shown in figure 3.13. This is more than the calculated value 40.5 Pa from eq. (3.2), but this discrepancy is acceptable as the case is near the extreme of the model's validity. Some causes for this discrepancy may be:

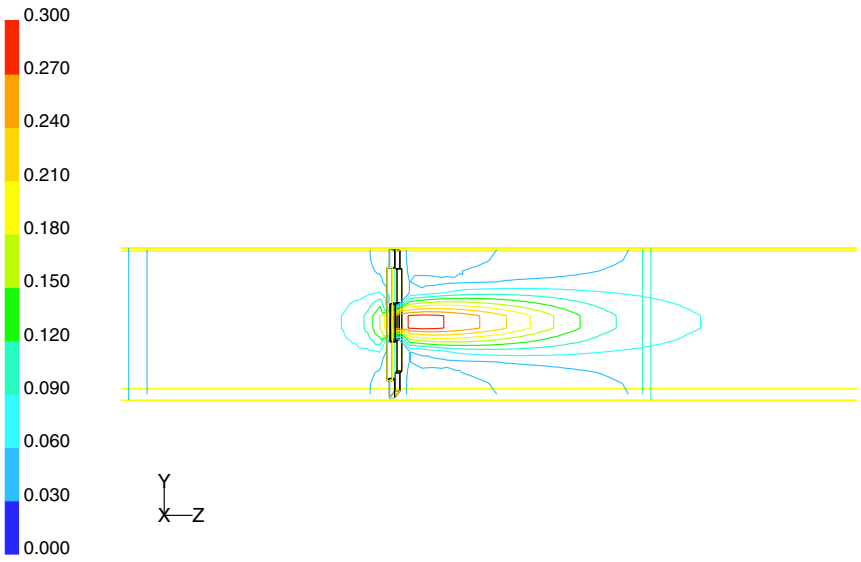

Figure 3.10: Velocity profile over flow diffuser hole, in the yz-plane. Contours colored by velocity magnitude [m/s].

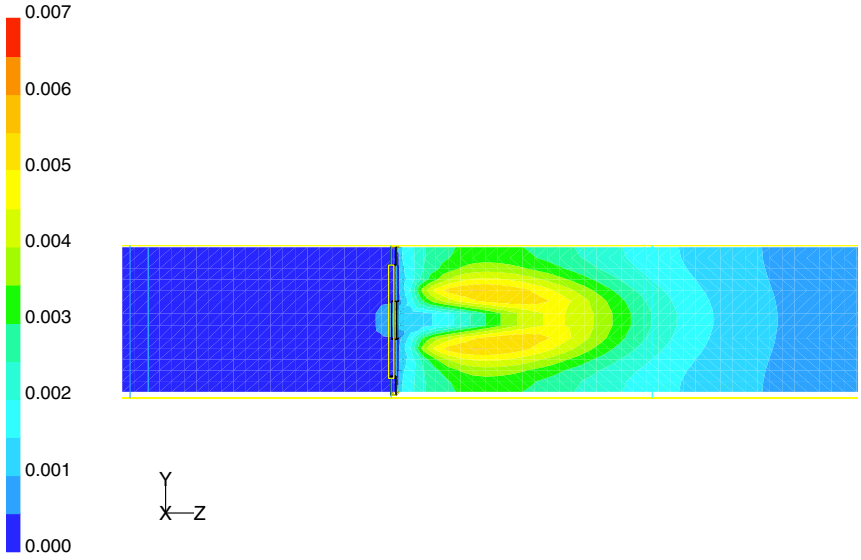

Figure 3.11: Turbulent kinetic energy profile over flow diffuser hole, in the yz-plane. Contours colored by k [m^2/s^2].

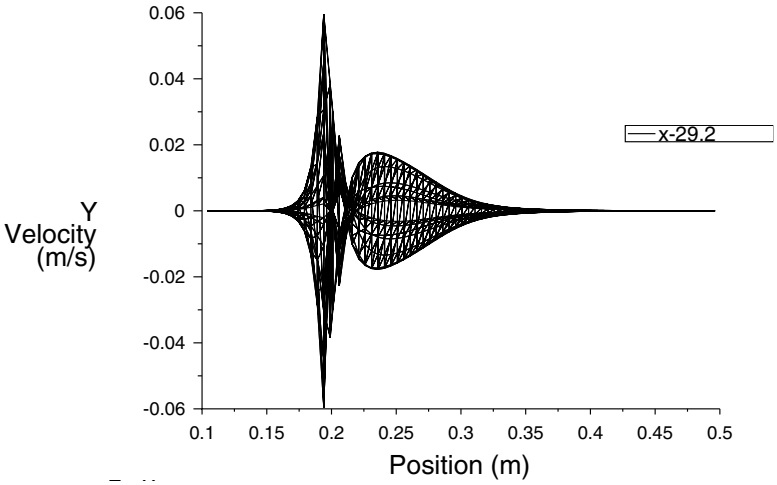

Figure 3.12: y-velocity profile over flow diffuser hole, in the yz-plane.

- The "symmetry" boundary condition, which has been known to affect the shape of the jet formed after the holes, and which may have been different in [31]
- Differences in the actual geometry of the hole
- Too coarse resolution of the grid (particularly near the walls of the hole)

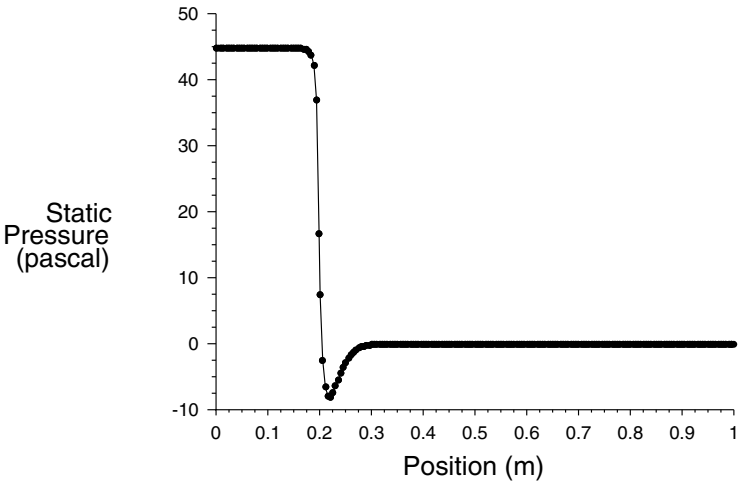

Figure 3.13: Pressure profile over flow diffuser hole, along centre line in the xy-plane.

3.5 Conclusion

An alternative model to the plug-flow approach has been presented, for the dispersed phase flow field. This approach directs part of the flow through the interface, as opposed to routing the bulk flow through the flow diffuser. The effect of this approach has been discussed in terms of grade efficiencies. Numerical simulations have been performed with both laminar- and turbulent models, and the effects have been discussed. These results will be further discussed in chapter 4.

The flow through the flow diffuser have been studied in detail, and it has been shown that in a region directly behind the diffuser, secondary flows are generated that may have an effect on the outlet quality. However, without the diffuser large secondary flows may very well be present and cause even larger effects on the outlet qualities. The effect of secondary flows induced by the flow diffuser will be discussed further in section 5.4.

Chapter 4

Detail mechanism studies

4.1 Introduction

The previous chapters have dealt with macro properties of the process, such as flow pattern and outlet qualities. This chapter will discuss three separate mechanisms that approaches different features of the system:

Coalescence profiles from bottle tests. It is highly desirable to be able to predict separator performance based on bench-scale experiments, for obvious reasons of simplicity and cost [15, 21]. In chapter 2 two bench-scale models for predicting the dispersion layer decay was referred: the dispersion layer model [19] and the SRTCA model[21]. One of these, the SRTCA model, has here been fitted to batch separation ("bottle tests") experimental data, and the results have been compared to pilot separator performance.

UV/vis absorbance model for concentration of stabilising components. In section 2.3.2 a model oil system with added Grane oil for increased stability regarding coalescence was introduced. The increased stability is believed to origin from surface-active components in the crude oil. The content of such components has been attempted correlated to UV/vis absorbance, and samples taken under various conditions have been studied.

Comparing measured droplet size distributions and calculated grade efficiencies with measured outlet qualities. The efficiencies obtained from classical- (laminar-) and empiric flow theory from earlier chapters can be used on experimentally obtained drop size distributions, and the resulting overall efficiency can be compared with the measured outlet qualities. As previously mentioned, much work has been done in co-operation with UiB, and dr. Andresen has kindly made his experimental DSD results available (see also [22]). This approach is the basis for conventional gravity separator design (with the exception that the droplet size distribution is not usually known), and it is interesting to investigate the validity of these assumptions.

The coalescence profiles and their connection with separator performance is at the core of the theory presented in section 2.2.5 and 2.2.6, while the use of measured droplet size distributions with calculated grade efficiencies follows the theory in section 2.2.3. As mentioned in the beginning of chapter 3, these two approaches represent the limiting behaviour of separator performance, and it is reason to believe that the former will dominate for increasing dispersed phase concentrations.

The study of concentration of stabilising components have been included for several reasons:

1. The stability of the model system vs. coalescence is assumed to be closely linked to the concentration of stabilising components in the continuous phase. As mentioned in section 2.3.2, the stability fell dramatically after a certain period of time. Also, it was noticed during bottle tests of samples from the dispersion layer that the color of the separated oil phase varied with sampling location, indicating a concentration gradient in the separator with regard to stabilising components which was unexpected.

2. The SRTCA model, used for modelling batch separation behaviour here, assumes that the dispersion is stabilised by viscosity only, which is clearly not the case. In view of item 1, a concentration gradient would have an impact on the coalescence and hence the interpretation of the results.

3. In light of the loss of stability, it was necessary to check whether the concentration changed gradually over time, or if the change was indeed sudden. This is crucial for the interpretation of the results in chapter 2 in terms of the comparability of the results for model system 3 batch 1.

4.2 Theory

This section will present the additional theory required to use the models described in chapter 2.

4.2.1 Coalescence profiles from bottle tests by the SRTCA model

The model described in section 2.2.6 is developed for batch separation tests known as bottle tests. Eq. (2.28) was solved by Maple with the condition $y_*\lfloor_{t=0} = Y_0$, the total height of the bottle test sample, and yielded equation (4.1).

$$y_*(t) = \exp \frac{-\mathsf{LambertW}\left(\frac{\beta_2}{\beta_1}\exp\frac{-t+Y_0\beta_2+\ln(Y_0)\beta_1}{\beta_1}\right)\beta_1 - t + Y_0\beta_2 + \ln(Y_0)\beta_1}{\beta_1} \tag{4.1}$$

The LambertW(x) function represents the principal branch of the omega function at x, defined as $\omega(x)\exp(\omega(x)) = x$, see [35]. The principal branch has an analytical value at x=0. The Taylor series of LambertW below exp(−1) is given by eq. (4.2) [36].

$$\mathsf{LambertW}(x) = \sum_{k=1}^{\infty} \left[\frac{(-k)^{k-1}}{k!} \right] x^k \tag{4.2}$$

Eq. (4.1) can then be solved numerically for given values of t and y_*.

4.2.2 UV/vis absorbance model for concentration of stabilising components

UV/vis-absorbance spectra were used to measure the concentration of added Grane crude oil in model system 3, to estimate the concentration of stabilising agents at different sample points in the separation process. The absorbance was measured for two wavelengths; 400 and 550 nm, and correlated to a linear concentration model (eq. (4.3)). Reference measurements for the linear models are shown in appendix B.2.

$$\phi_{\text{Grane}} = C_1 \alpha + C_2 \tag{4.3}$$

Based on calibration data, the model for finding the Grane concentration in a sample became eq. (4.4). The constants in the model are shown in table 4.1.

$$\phi_{\mathsf{Grane}} = \begin{cases} C_{1,400\text{ nm}} \alpha_{400\text{ nm}} + C_{2,400\text{ nm}} & \alpha_{400\text{ nm}} < 1 \\ C_{1,550\text{ nm}} \alpha_{550\text{ nm}} + C_{2,550\text{ nm}} & \alpha_{400\text{ nm}} \geq 1 \end{cases} \tag{4.4}$$

	400 nm	550 nm
C_1	1020.9	6716.5
C_2	-61.7	112.7

Table 4.1: Calibration constants for concentration model of Grane crude in Exxsol D-60 by UV-absorption

4.2.3 Drop size distributions

In order to describe the drop size distributions formed by the mechanisms described in section 2.2.4, a distribution function known as the Rosin-Rammler distribution was selected. This distribution is defined by eq. (4.5) [32].

$$\int_d^{\infty} V_N(d) = \exp\left[-\left(\frac{d}{\bar{d}} \right)^n \right] \tag{4.5}$$

As the volume size distribution is the relevant distribution with respect to separation and outlet qualities, the measured number size distribution had to be converted to a volume

size distribution. This was done by assuming that all particles were spherical, and that the characteristic diameter within a size band was the lower boundary of the band (a conservative approach with respect to separation quality). An example of normalised number- and volume size distribution for two reference cases are shown in figure 4.1. The volume size distribution will theoretically give the outlet quality when combined with the grade efficiency, see eq. (2.12).

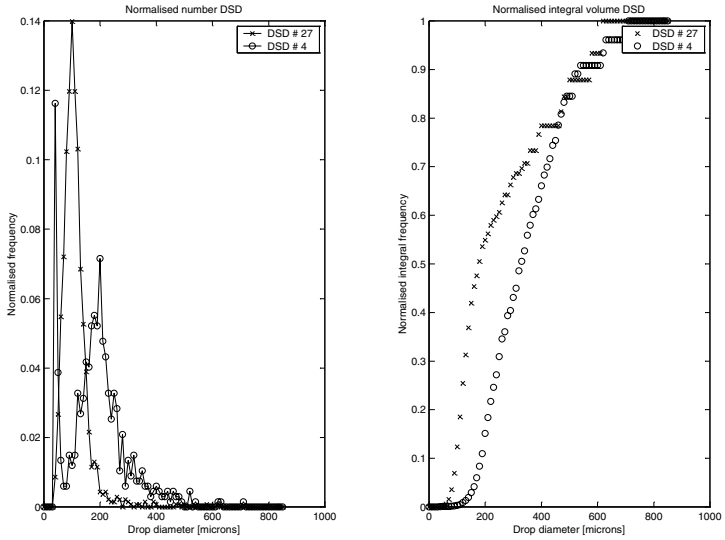

Figure 4.1: Measured DSD from inlet tube sample for two different water continuous cases, by Andresen [22]. Left: normalised number frequency distribution (as measured). Right: normalised volume integral distribution (assumed spherical particles). DSD # 4 is unstabilised, and DSD # 27 is stabilised with Berol 26. See table A.1 for details.

4.3 Experimental

4.3.1 Equipment

The pilot separator rig as described in section 2.3 was used for the tests. The water continuous reference DSDs shown in figure 4.1 were measured on fluid system 2 (stabilised with Berol-26, see [22]), while the water continuous separator performance data were measured on fluid system 3 batch 1 (see section 2.4).

4.3.2 UV measurements

As mentioned in section 2.3.2, several fluid systems were examined for the desired oil/-water separation characteristics. The fluid system showing the most interesting features was fluid system 3, with the addition of Grane crude from Norsk Hydro. This particular crude is known for its stability vs. oil/water separation, and was added in low concentrations (250-750 ppm) to the substrate model oil, Exxsol D-60.

During tests with this fluid system, it was noticed that the colour of the oil phase from the bottle tests varied with sample location. Oil phases from the different samples were therefore kept after settling was completed. These were later analysed for UV-absorbance at Statoil's research centre in Trondheim by dr. Kallevik, and the recorded spectra were modeled by a linear concentration model with absorbance at two wavelengths.

4.3.3 Methods

The pilot separator was operated as described in section 2.3, and the operating conditions for the various samples can be found in appendix B.1.

Dispersion sampling, bottle tests and model fitting

Samples from the centre of the inlet tube and at three heights in the dispersion layer (see figure 2.6 and table 2.1) were taken out in cylinders and set aside for settling, which was filmed with a digital video camera. The interface heights were measured from still frames as shown in figure 4.2 and fitted to the SRTCA model. Notice also the colour difference in the oil phase — the colour is very dark in the low dispersion layer sample, and gets lighter as the water concentration in the sample decreases. Evidence of drop growth in dispersion layer is also easily seen.

4.4 Results and discussion

4.4.1 UV/vis absorbance measurements

The full absorbance tables can be found in appendix B.2, tables B.25 – B.27, and the table for fluid system 3, batch 1 is shown in table 4.2. Sp1–Sp6 represents the sample points listed in table 2.1, repeated for convenience: Sp1=inlet sample, Sp2=high dispersion sample, Sp3=middle dispersion sample, Sp4=low dispersion sample, Sp6=oil outlet sample. These data showed a significant difference between the concentration of "Grane" in the dispersion layer samples (Sp2–Sp4) and from the inlet- and oil outlet samples (Sp1 and Sp6) for oil continuous runs in the early part of the period (batch 1). For the inlet/-outlet samples, the equivalent Grane-level ranged from 590 to 740 equivalent ppm Grane, and from 1170 to 6560 for the dispersion layer samples. For water continuous runs and for the later oil continuous runs (batch 2), the equivalent Grane-level ranged from 611 to 716 ppm, independent of sampling location. The lack of concentration differences for the water-continuous runs suggests that the added stabilising Grane components are more

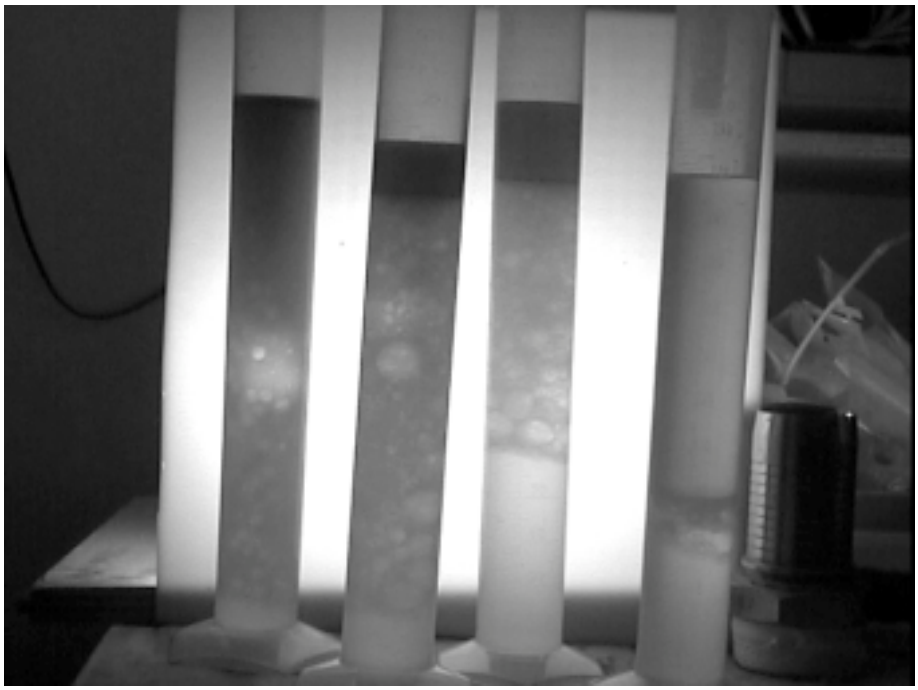

Figure 4.2: Example of bottle tests. From left to right: low- (Sp4), middle- (Sp3), and high (Sp2) dispersion layer sample, and inlet tube (Sp1) sample.

soluble in the oil- than in the water phase, and are situated near the interface mainly on the oil side. The stabilising effect will therefore be present only for the oil continuous runs.

Furthermore, samples were taken at different time intervals relative to start-up in case of depletion of stabilising components with time, but no such depletion was measured. The absorbance was also independent of inlet water cut. An increase in water cut will lead to a larger total interface which, if the concentration was insufficient, lead to a lower measaured concentration in the dispersion layer. As the concentration is independent of both time and water cut, the bulk solution appears to maintain a stable concentration of stabilising components. This is a necessary requirement for comparing with a one-through system (for exapmle real systems), and this suggests that the concentration gradient effect is not limited to this type of model system with a continuous, recycling flow-loop, but can be expected in any continuous operation with indigenous stabilising components.

The samples from the dispersion layer show a high water content, typically volume fractions of 0.8–0.9 (see appendix B.1). Using the measured dispersion layer heights from chapter 2, it is possible to estimate the water volume in the dense layer. Using an average of the measured thicknesses at Z_4 and Z_5 and projecting this over the separation section,

Test #	Sp1 [ppm] 400 [nm]	Sp4 [ppm] 550 [nm]	Sp3 [ppm] 550 [nm]	Sp2 [ppm] 550 [nm]	Sp6 [ppm] 400 [nm]
26	643		6561	3202	
27	634			5902	
28	615			5526	
1.1	589	3055	4257	3820	
24.1	620			4774	
CC	695		5217	1899	
1p		3028	3773	3377	
2p		2652	1651	1631	
3p	659	2081	1590	1187	616
3p3	740			2524	610
3p4	619	1550	1718	2369	620
4p	614	2094	1422	1167	605
6p	629	3538	2208	1993	
7p	644	2940	2309	1738	621

Table 4.2: UV absorbance values for fluid system 3 batch 1.

and using an estimated average water fraction of 0.83, the resulting average residence time for water within the layer is 153 s. This can be interpreted in terms of equation (2.27) as the time scale ($\beta_1 + \beta_2 y_*$) and will be compared with the results of the SRTCA model treatment of bottle test data below.

4.4.2 Coalescence profiles from bottle tests — SRTCA model treatment

Table 4.3 shows the non-linear fit of bottle tests results to the SRTCA model (see section 2.2.6) from Matlab, and figure 4.3 shows an example of the corresponding fit vs. the experimental data, for cases o3.1-Sp1, -Sp2, -Sp3, and -Sp4.

As can be seen from the table, parameter β_1 varies between 28.7 and 72.4 for the inlet samples, and between 117.8 and 371.0 for the dispersion samples. This excludes the dispersion samples o3.1l and o3.9l (more than 95% water) and the o3.6u (outlier, unusully high stabilisation). Furthermore, β_2 varies greatly, by 8 orders of magnitude. The values in table 4.3 can be compared to the values found from dispersion layer height measurements at the pilot separator, β_1 was 15 s and β_2 was 50 s/m (table 2.3), and also the estimated residence time for water within the dispersion layer of 153 s (section 4.4.1).

As mentioned, the variation in β_2 (found by the non-linear model fits) is very large and will affect the interpretation of the results. Assuming a dispersion thickness less than 1 m, the time scale $\beta_1 + \beta_2 y_*$ will be dominated by β_1 when $\beta_1 \gg \beta_2$. When this occurs for the dispersion layer samples (labelled Sp2, Sp3, and Sp4), β_1 spans from 123.3 s (case o3.1-Sp3) to 209.7 s (case o3.9-Sp2). The average water residence time in the dispersion

Sample	β_1 [s]	β_2 [s/mm]	$\sqrt{\overline{\Delta y_*^2}}$ [mm]	Sample	β_1 [s]	β_2 [s/mm]	$\sqrt{\overline{\Delta y_*^2}}$ [mm]
o3.1-Sp1	58.2	1.17E-08	2.3	o3.6-Sp1	32.1	2.24E-09	4.4
o3.1-Sp2	180.5	2.54E-01	15.4	o3.6-Sp2	*1052.4*	7.76E-08	9.0
o3.1-Sp3	123.3	3.21E-08	16.6	o3.6-Sp3	365.2	4.35E-01	24.5
o3.1-Sp4	*28.3*	3.58E-09	2.6	o3.7-Sp1	37.2	1.56E-09	7.5
o3.2-Sp1	51.8	7.52E-10	5.7	o3.7-Sp2	179.8	3.05E-07	14.1
o3.2-Sp2	120.6	1.42E-01	8.9	o3.7-Sp3	208.3	2.43E-01	26.7
o3.2-Sp3	182.8	2.12E-01	18.3	o3.7-Sp4	188.8	1.13E-07	19.5
o3.3-Sp1	55.8	3.19E-09	3.8	o3.8-Sp1	28.7	2.33E-09	6.4
o3.3-Sp2	220.0	2.53E-01	29.4	o3.8-Sp2	235.7	2.68E-01	18.8
o3.3-Sp3	196.7	2.26E-01	34.2	o3.8-Sp3	302.1	3.60E-01	25.4
o3.3-Sp4	371.0	3.98E-01	29.6	o3.8-Sp4	248.8	3.03E-01	23.7
o3.4-Sp1	72.3	2.21E-10	4.2	o3.9-Sp1	38.4	1.42E-09	7.0
o3.4-Sp2	128.6	1.86E-09	12.3	o3.9-Sp2	209.7	3.15E-09	10.8
o3.4-Sp3	188.4	2.08E-01	36.1	o3.9-Sp3	221.1	2.51E-01	32.8
o3.4-Sp4	245.3	2.98E-01	25.1	o3.9-Sp4	*43.4*	9.66E-09	14.4
o3.5-Sp1	72.4	2.36E-09	7.8	o3.10-Sp1	53.1	1.36E-09	9.2
o3.5-Sp2	318.9	3.41E-01	17.5	o3.10-Sp2	117.8	1.32E-01	8.9
o3.5-Sp3	135.7	1.80E-01	30.7	o3.10-Sp3	204.2	2.51E-01	13.1
o3.5-Sp4	123.1	1.39E-01	15.4	o3.10-Sp4	290.5	3.54E-01	9.5

Table 4.3: Results from bottle-test fitting to the SRTCA-model.

layer, 153 s, is comparable to these values.

When $\beta_2 y_*$ becomes significant compared to β_1, the time scale is less obvious from table 4.3. To circumvent this problem, the resulting water flux as calculated by eq. (2.26) has been calculated for two typical dispersion heights y_*= 0.1 and 0.2 m. This is shown in table 4.4.

Reviewing the results from chapter 2, the dispersion layer flux for y_*=0.1 and 0.2 m were approx. 1.5 and 3 m^3/h, respectively (see figure 2.9). Disregarding the values for o3.1-Sp4, o3.6-Sp2 and o3.9-Sp4, all the inlet samples show a modelled flux well above the calculated flux in the pilot separator, while the dispersion samples show a flux close to or below the calculated flux in the pilot separator. This was also expected from the UV/vis absorbance measurements — the stability is lower for the inlet samples than for the dispersion samples. More importantly, this suggests that the flux inside a separator with indigenous stabilising components cannot be estimated from an inlet sample directly (which shows the importancy of the prerequisite in [21] that the dispersion should only be stabilised by viscosity).

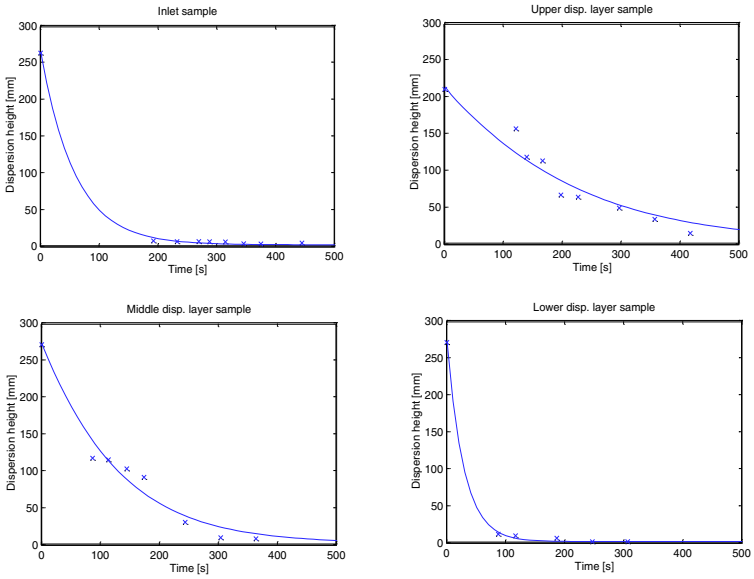

Figure 4.3: Model fit of the SRTCA model on case o3.1 from table 4.3. Top left: inlet sample (Sp1), top right: upper dispersion sample (Sp2), bottom left: middle dispersion sample (Sp3), bottom right: lower dispersion sample (Sp4).

4.4.3 Drop size distributions and grade efficiencies

As mentioned in the beginning of this chapter, work done in co-operation with dr. Andresen at UiB [22, 23] included droplet size distribution (DSD) measurements on the system, that has been made available here. These were performed on all the fluid systems described in section 2.3.2. This section shows the results from coupling these measured size distributions with grade efficiencies using the equations outlined in section 2.2.3, and comparing the calculated separator performance with the measured outlet quality results from section 2.4.3. This approach is, as previously mentioned, the basis of traditional separator design with respect to liquid-liquid separation and it will be shown that the validity of this approach is at best limited.

A problem in the DSD measurements was that the sampled droplets had a tendency to coalesce during the measurement, and hence the resulting size distribution would be less representative for the actual sample. In gravity separator tests, this is a typical problem as the stability needed for accurate DSD representation during sampling will normally lead to failure in separator performance, because of limited coalescence. In traditional separator design this is circumvented by applying a “rule of thumb” stating that the gravity separator should have a grade efficiency of 1 for droplets of 200 μm or bigger.

Sample	Q_w [m^3/h]		Sample	Q_w [m^3/h]	
	(y_*=100mm)	(y_*=200mm)		(y_*=100mm)	(y_*=200mm)
o3.1-Sp1	3.1	6.2	o3.6-Sp1	5.6	11.2
o3.1-Sp2	1.0	2.0	o3.6-Sp2	*0.2*	*0.3*
o3.1-Sp3	1.5	2.9	o3.6-Sp3	0.5	1.0
o3.1-Sp4	*6.4*	*12.7*	o3.7-Sp1	4.8	9.7
o3.2-Sp1	3.5	6.9	o3.7-Sp2	1.0	2.0
o3.2-Sp2	1.5	3.0	o3.7-Sp3	0.9	1.7
o3.2-Sp3	1.0	2.0	o3.7-Sp4	1.0	1.9
o3.3-Sp1	3.2	6.4	o3.8-Sp1	6.3	12.6
o3.3-Sp2	0.8	1.6	o3.8-Sp2	0.8	1.5
o3.3-Sp3	0.9	1.8	o3.8-Sp3	0.6	1.2
o3.3-Sp4	0.5	1.0	o3.8-Sp4	0.7	1.4
o3.4-Sp1	2.5	5.0	o3.9-Sp1	4.7	9.4
o3.4-Sp2	1.4	2.8	o3.9-Sp2	0.9	1.7
o3.4-Sp3	1.0	1.9	o3.9-Sp3	0.8	1.6
o3.4-Sp4	0.7	1.5	o3.9-Sp4	*4.2*	*8.3*
o3.5-Sp1	2.5	5.0	o3.10-Sp1	3.4	6.8
o3.5-Sp2	0.6	1.1	o3.10-Sp2	1.5	3.1
o3.5-Sp3	1.3	2.7	o3.10-Sp3	0.9	1.8
o3.5-Sp4	1.5	2.9	o3.10-Sp4	0.6	1.2

Table 4.4: Calculated water release from pilot separator interface, for two different dispersion heights.

Here, it was a dilemma of which DSDs to choose: the partly coalesced- that represented an unknown amount of the incoming dispersed phase or the stabilised- that represented a very different model fluid with regards to separation. It was decided to use all the measured DSDs indiscriminantly on all the ideally calculated grade efficiencies, and see whether the results would indicate which DSDs best represented the inlet conditions of the separator.

As the DSDs were obtained from several fluid systems and test cases, the flow rates (in particular), pressure drops and water cuts are different than for the experiments in chapter 2. Some of the DSDs are however obtained under similar conditions to some of the experiments in section 2.4.3. In particular, the drop size distributions measured on fluid system 2, water continuous were sufficiently stabilised to produce reliable size distributions [23], and should provide an acceptable starting point for calculating separator performance in water continuous runs.

The measured drop size distributions were multiplied by the calculated grade efficiencies for the water continuous runs, using the equations outlined in section 2.2.3. The results were then compared with the experimental values presented in section 2.4.3, comparing experimentally measured water outlet qualities with the quantity remaining after removal by the grade efficiency curve from the DSDs. The normalised DSDs were scaled

by the dispersed fraction at the inlet, to get a result comparable with experimental outlet qualities. Several of the obtained DSDs (both water- and oil continuous samples from tests with fluid system 1 and 2, see section 2.3.2 and [22]) were coupled with the water continuous grade efficiencies, for comparison.

The results are shown in appendix A.4 as m, mean over-predicted concentration (representing the degree to which the pilot separator performs vs. the predicted performance) and s, relative standard deviation in m ($s_i = \frac{\text{stddev}(m_i)}{m_i}$), a measure of the degree that m is representative for different feed conditions of Q_l and WC). As the DSDs were obtained from an earlier test series, the flow rates (in particular), pressure drops and water cuts are different than for the experiments in chapter 2. Some of the DSDs are however obtained under similar conditions to some of the experiments in chapter 2.

The results are not conclusive, as the calculated outlet qualities for a large variation in DSD feed specifications show similar m and s values. Table A.4 contains the values for experiments with WC 0.5, and the separator performs approx. 68 times better than expected (with respect to water outlet quality), using a stabilised DSD obtained under otherwise similar conditions (DSD #26 from table A.1). The results for DSD #26 coupled with calculated grade efficiencies for experiments from chapter 2 with WC=50% and ΔP=0.5 bar are shown in figure 4.4. As such, m(=68) represents the slope of the linear curve fit (not shown) of the +-series in figure 4.4. Using the same DSD (obtained for ΔP=0.5 bar) for the corresponding experiments at ΔP=1 bar gives an m-value of 6.5 (the slope of the $\circ$-series in figure 4.4). One would expect that the stabilised DSD #26 would give a slight over-prediction for ΔP=0.5 bar, but not as large as 68, and for the higher pressure drop an under-prediction would be expected. Similar values for WC 0.75 and 0.85 (compared to a DSD obtained at WC 0.8, #27) showed m-values of 146 and 89, respectively (table A.8). *All* the DSDs, coupled with the relevant grade efficiency, produce an over-prediction of the outlet quality (except DSD #3 in table A.3, but here the error is large. Also this DSD is not expected to represent the droplets in the applicable feed conditions).

This comparative method is as close to the classical design philosophy as can be achieved, with experimentally obtained DSDs and calculated ideal grade efficiencies, and it is interesting that the failure to predict the outlet quality is this large. In light of this, the quote mentioned in the introduction to chapter 2, " ... design by chance ... " comes to mind. The failure of this method is expected to arise from three effects that are believed to be important, and not included in the model:

1. The flow is not necessarily laminar, as was discussed in chapter 3. It is possible to obtain grade efficiencies for turbulent conditions, as was shown in the previous chapter, but it is not likely that the effects shown can explain the large discrepancy between the experimental- and predicted values. Also, the grade efficiencies obtained for turbulent flow has limited validity because of the insufficient coalescence modelling. This was therefore not done due to the extensive calculation scheme necessary and the limited chance of success.

2. Coalescence upstream the flow diffuser will be important as the convective forces are large here. As the flow field here is dependent on momentum, gravity and

coalescence it cannot be calculated satisfactorily. This was also discussed in chapter 3.

3. The method assumes that the drops are released homogeneously across the flow diffuser entrance to the separation section. This is probably not the case due to item 2 above, and will have a considerable impact on the grade efficiency.

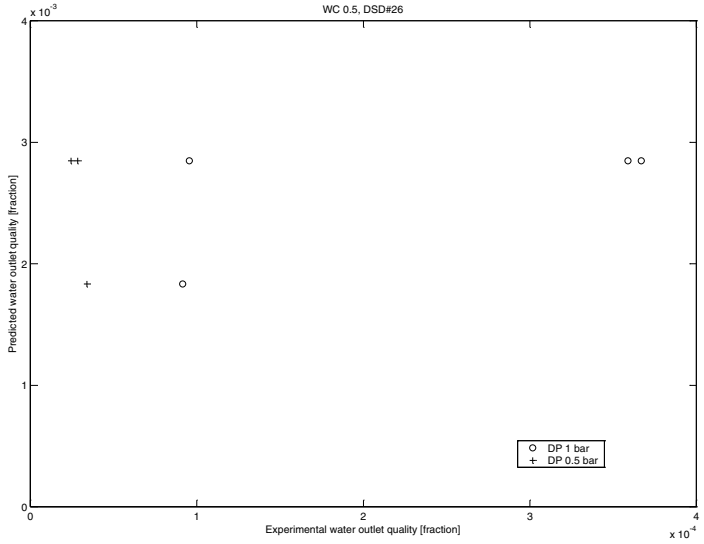

Figure 4.4: Example results for applying DSD # 26 on ideally calculated grade efficiencies for experiments with WC 0.5 (see appendix A.4), compared to experimental measurements

It was also attempted to use the DSDs obtained under oil continuous conditions and utilise these in a similar manner to predict the water outlet quality. This was not expected to yield very good results, as it would suggest that the water outlet quality was directly dependent on the oil continuous DSD, whereas the results in chapter 2 suggested that the mechanisms behind continuous phase quality and dispersed phase quality are different (see section 2.4.3). The results show that the s-values (indicating the relative error of the fit) are very high, typically 0.30–0.70, which was not surprising.

4.5 Conclusion

Microscale mechanisms have a profound effect on separator performance. In a fluid system partly stabilised by indigeneous components, as fluid system 3.1 in this thesis, there is an aggregation of these components in the dispersion layer as shown by UV/vis absorbance measurements. This results in a water release from the dispersion layer less than

predicted from inlet samples. The mass balance within the separator can thus not always be determined from such inlet samples.

The separation profile from bottle tests for samples obtained at different points in the separator, more specifically from the inlet and the dispersion layer, show different separation characteristics. The SRTCA model was utilised for these bottle tests, and the results show that the model fit of inlet sample bottle tests under-predicted the dispersion layer height for a given dispersed-phase rate, while the model fit of the dispersion samples slightly under-predicted the dispersion layer height. This is in good aggreement with the results for UV/vis absorbance, and also with the results in section 2.4.1.

Experimentally obtained DSDs were combined with ideal grade efficiencies and compared to outlet quality for water continuous cases. The calculated results showed poor aggreement with the experimental results, and furthermore no evidence was found to imply that the ideal grade efficiency is a good measure for separator performance. This is believed to be caused by effects that cannot be predicted sufficiently with the existing model framework, such as turbulent flow fields and the complex flow behaviour upstream the flow diffuser. For oil continuous results, the water quality showed no direct correlation with the oil continuous DSDs, which was expected from previous results.

Chapter 5

Mechanical alterations

5.1 Introduction

In gravity separator revamping, one can usually perform mechanical alterations based on better knowledge of the specific system separation characteristics than was possible at the time of the original design. At an offshore installation, revamping is economically limited to mechanical alterations that leaves the pressure vessel as intact as possible. This because of the size of the vessel. Hot work (welding/torching) may be allowed if critical to separator performance, but it is strongly desirable (because of safety regulations) to perform only cold work, which essentially means only insertions inside the vessel. Furthermore, time is critical as a modification of the separators normally means a stop in production and loss of money for the oil companies. As the components are put in place by manpower, the insertions have to be light and easy to assemble. There are also limitations in size due to man-holes being the only entrance available to the vessel.

The possible mechanical alterations are endless, and this chapter does not intend to discuss all such alterations and their effects. It rather looks upon three novel features that have been investigated, and discusses the effects found. These are presented as follows:

Cyclone liquid diffuser Various modifications to the KPS CCI inlet flow diffuser have been tested. The main focus has been on the location of the liquid exit of the cyclone, relative to the oil/water interface. It was found that the oil continuous dispersion layer thickness decreased when the liquid outlet was in the oil phase region.

Unloading An attempt was made to draw a water-rich stream from under the inlet (upstream the flow diffuser). This removal was to lower the average velocity in the water phase, and improved the water quality for water continuous runs.

Horizontal dispersion dividers At a lecture at Statoil's Research center by Prof. Hartland, an application of the models outlined in section 2.2.5 was presented: As the coalescence rate Ψ_i at the inflection point is dependent on the max. dispersion

layer thickness Δh_i to the pth power, a dissection of the separator into n narrow horizontal sections would increase the overall coalescence rate by $\frac{n}{n^p}$ (see section 5.4.1 and [19]).

Panoussopoulos shows a possible sketch of this concept, dividing the full height of the separator into locally reduced heights with slightly inclined plates. A variation over this idea was tested (as explained later), with unexpected results. Four horizontal plates were mounted in a rack with 15 mm distance between, covering the width of the separator at slightly lower-than-weir height, and extending almost 5/8 (1250mm/2030mm) of the distance between the flow diffuser and the weir (see section 5.4.2, figure 5.8). This resulted in a slight improvement of the dispersed phase quality, but also led to a build-up of dispersion layer near the weir.

5.2 Cyclone liquid diffuser

Inlets in gravity separators have traditionally had the function of stopping the incoming kinetic energy of the fluids from the inlet tube, and establish a quiescent flow ideal for settling and coalescence. The first inlets were therefore simple obstructions mounted at the end of the inlet tube, diverting the incoming multiphase flow into the end walls of the vessel. These are known as "momentum breakers" or "splash plates". It was necessary to let the fluids exit high into the gas-dominated zone of the separator, as the gas flow is normally larger than the liquid in terms of volume and exessive foaming would be the result of entering the fluids in the liquid zone. Foaming might however still be a problem as the kinetic energy of all three fluid phases (neglecting solids) is transformed into pressure loss and secondary velocity components in the same geometric zone.

Later developements have shown an improvement of the momentum breaker. Several vendors use inlets with vanes; the incoming fluid is diverted and guided by vanes, and the kinetic energy is transformed over a larger area and at more gentle conditions. These "vane type inlets" are generally superior to the momentum breaker in terms of foaming [14].

A different type of inlet altogheter is the cyclone type. It uses the inlet tube momentum to set up a spinning motion and thereby separate the fluids (normally the gas from the liquids). The kinetic energies are in this case transformed separately for the gas- and liquid phase, and the possibility of foaming is eliminated. This is the only current inlet class that allows the liquids to enter the liquid dominated section of the separator, and the design of the diffuser at the liquid outlet has been one of the main focuses of this thesis.

The impact of liquid diffuser outlet location was studied as part of a troubleshooting project at Statoil's Statfjord B installation. After installation of inlet cyclones, the platform reported problems regarding deteriorated oil quality. The inlet design had previously been tested in the test separator at Statfjord C, without these problems occuring. Samples drawn from the oil outlet showed that the water content separated after a few minutes, which suggested that a dispersion layer was formed that could not separate during the normal retention time within the separator. These effects, and others reported

from various installations will be discussed more closely in chapter 6.

For the test separator, the liquid diffuser outlet of the cyclones were situated near the interface level in the inlet zone; the NIL setting was 500 mm above BV (bottom of vessel), and the perforations in the liquid diffuser was from 280 to 620 mm above BV, or in the range of NIL. For the main inlet separator, the NIL setting was 820 mm above BV (bottom of vessel), and the perforations in the liquid diffuser was from 1220 to 820 mm above BV, or slightly above NIL. CFD single-phase simulations showed however that the liquid exiting the diffuser had a velocity component upward into the test separator, while it had a downward component in the inlet separator (see figure 5.1, [37]). As the incoming liquid was oil continuous at the time, with water cuts of typically 60%, this downward component could lead to the creation of large amount of dispersions as the incoming oil continuous fluids were released with a kinetic energy in the order of 10^5 Pa ($0.5\rho v^2$) (see also figure 6.2), into a predominantly water continuous liquid volume.

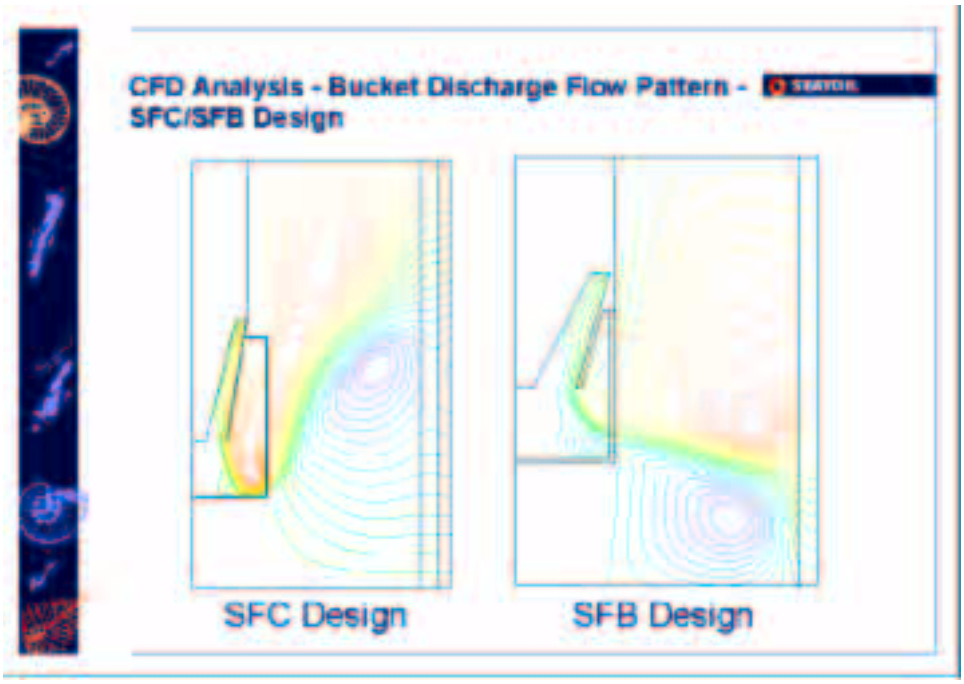

Figure 5.1: CFD simulations of liquid diffuser geometries, from [37] showing streamlines[2]on 2D axi-symmetrical simulations of two different CCI designs.

Tests were done in the pilot separator with fluid system 1 (paraffinic oil and saline water) with diffuser perforations above- and below NIL (figure 5.2), and also with various

[2]Streamlines presents the direction of the flow. Between any two streamlines the flow rate is equal — thus streamlines close to each other denotes a large velocity while streamlines far from each other denotes a small velocity.

blockage arrangements at the flow diffuser (figure 5.3). In order to produce a dispersion layer with this easy separable fluid system, very high liquid loadings had to be applied. Observations showed that when the perforations in the cyclone liquid diffuser was elevated to well above NIL, the dispersion layer was significantly thinner than when the liquid outlet was below/in the range of NIL.

5.2.1 Experimental

Different CCI liquid diffusers as well as flow diffuser blockage arrangements were tested. The different inlets tested are shown in table 5.1. Figure 5.2 shows the cyclone with the two liquid diffuser outlet heights (actually, the original cyclone was fitted into a box with two sets of outlet rows. These outlet rows of the external liquid diffuser is alternately blocked high and low to send the liquids to the water- and oil rich layers, respectively), and figure 5.3 shows the four different blockings of the flow diffuser. The test matrix in table 5.2 was followed during the first tests. Initially, lower flow rates were also studied, but the differences in performance were hard to identify from these results. Therefore, the rest of the configurations were only tested with these high flow rates. In reference to figure 5.1, inlet 7 corresponds to the inlet tested at the Statfjord C test separator, while inlet 8 corresponds to the inlet originally installed at the Statfjord B inlet separator.

Inlet config#	Description
1	"Cyclone 1", flow diffuser blocked - configuration 1
2	"Cyclone 1", flow diffuser blocked - configuration 2
3	"Cyclone 1", flow diffuser blocked - configuration 3
4	"Cyclone 1", flow diffuser blocked - configuration 4
5	"Cyclone 1", two lowest rows of liquid diffuser blocked, perforated plate not blocked
6	Reference, momentum breaker
7	"Cyclone 2", external liquid diffuser open in top
8	"Cyclone 2", external liquid diffuser open in bottom

Table 5.1: Inlet configurations for liquid outlet height tests

	Q_o [m^3/h]	Q_w [m^3/h]	Q_g [m^3/h]	WC
Case 2,1	16.2	10.8	27,0	0.40
Case 2,2	18.9	8.1	27.0	0.30
Case 2,3	10.8	16.2	27.0	0.60

Table 5.2: Test cases for liquid outlet height tests

Due to these high rates, the outlet qualities were very poor as the retention time in the vessel was low ($<$ 1 minute), and the qualities were measured by volumetric sampling into a measuring cylinder. This method has a volume fraction error of approx. $\pm$ 0.02, which is acceptable for the oil qualities, but inadequate for the water qualities.

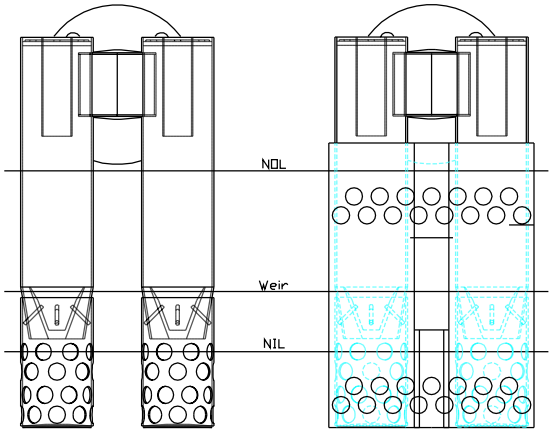

Figure 5.2: Inlet cyclone without (left, cyclone 1) and with (right, cyclone 2) external liquid diffuser.

5.2.2 Results and discussion

The results are presented as water in oil outlet (figure 5.4) and oil in water outlet (figure 5.5) for the different cases in table 5.1.

Oil outlet qualities

The oil qualities vary with inlet configuration and test case, and are discussed separately for each case below.

Case 2.1 (WC 0.4) displays a large variation in inlet configurations, where inlet config#7 (cyclone with external diffuser, liquid outlet high) is the best, followed by config#6 (reference momentum breaker) and 8 (external diffuser, liquid outlet low). The next group of performance consist of config#1, 3, and 4, variations in the flow diffuser blockings (see figure 5.3). Finally, inlet config#2 and 5 (flow diffuser blocked in the oil phase, and cyclone with halved liquid outlet area) shows very poor performance.

Case 2.2 (WC 0.3) was the most relevant case in the study, as this was the only oil continuous case in the set-up. Here, inlet config#3 and 7 showed the best performance, closely followed by config#6, 1 and 4 (in that order). Config#1 and 4 are very similar, the difference being that #4 has a row open at the bottom of the flow diffuser, to "allow for sand" to escape along the bottom.

Visual inspection of the tests showed that, for case 2,2, all inlet configurations gave a dispersion layer in the separation section except config#7 (which gave a clean oil/water interface). As this was the main problem to be solved, inlet configuration #7 was selected as a modification at the Statfjord B inlet separator.

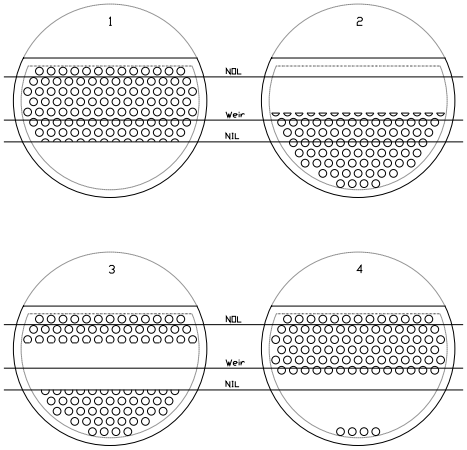

Figure 5.3: End view, flow diffuser blockage configurations

Looking at config#1–4 and the oil continuous case (2,2), config#2 is poorer than the other. This inlet configuration consists of a blocking of the oil phase across the flow diffuser, and shows that a marked increase of the dispersion layer is produced by forcing the liquid through the water dominated region low in the separator. Similarly, config#5 (double velocity from the cyclone, cyclone configuration 1) and config#8 (external diffuser, low liquid outlet) yields thick dispersion layers compared to the other configurations. These results support the assumption that for oil continuous inlet conditions, it is undesirable to let the liquids exit in a water dominated region. As inlet config#3 produced good results for case 2,2, there seems to be a dependency on the magnitude of mixing force.

Case 2.3 (WC 0.6) is not satisfyingly separated by any of the configurations, which suggests that this case is beyond the operational window of the separator (however, inlet config#8, cyclone with external liquid diffuser and low liquid outlet, shows the best perormance).

Water outlet qualities

The water qualities also shows variation with inlet configuration, and are discussed separately below.

Case 2.1 (WC 0.4) shows best performance for config#3 and #5.

Case 2.2 (WC 0.3) also shows best performance for config#3 and #5, while config#1, 2, and 8 are somewhat poorer than the rest.

Case 2.3 (WC 0.6) shows particularly poor performance for inlet config#1, 2, and 3.

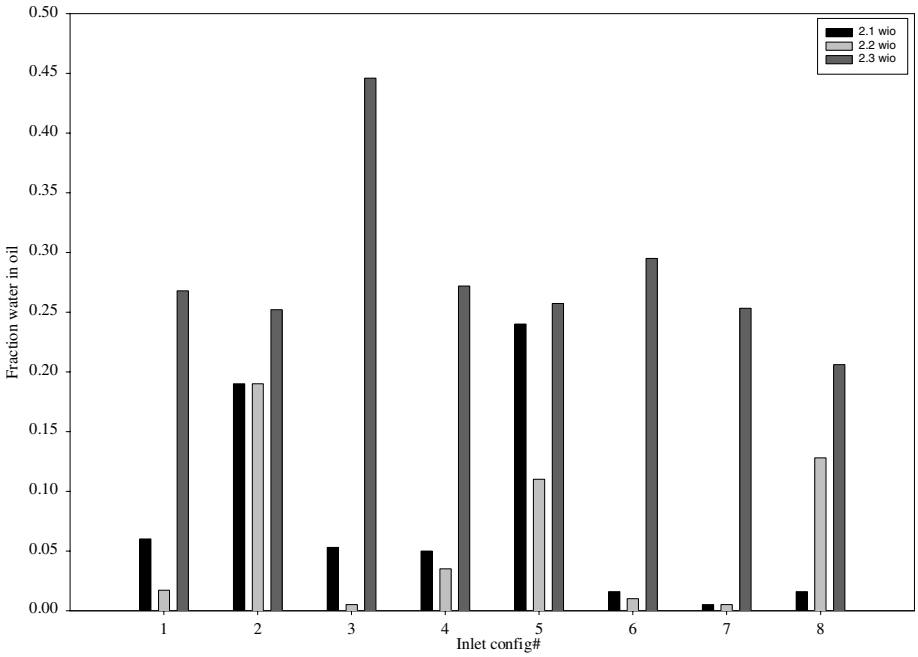

Figure 5.4: Inlet geomoetry test results, wio content at the oil outlet

In summary, config#5 (cyclone inlet configuration 1, halved liquid outlet area) yields the best overall performance.

The water quality results are difficult to interpret, as the results seem to vary rather arbitrarly. Bearing in mind the estimated error in volume fraction of ± 0.02, only two responses are actually significant. The further discussion of liquid outlet location with respect to water quality is therefore postponed to chapter 6.

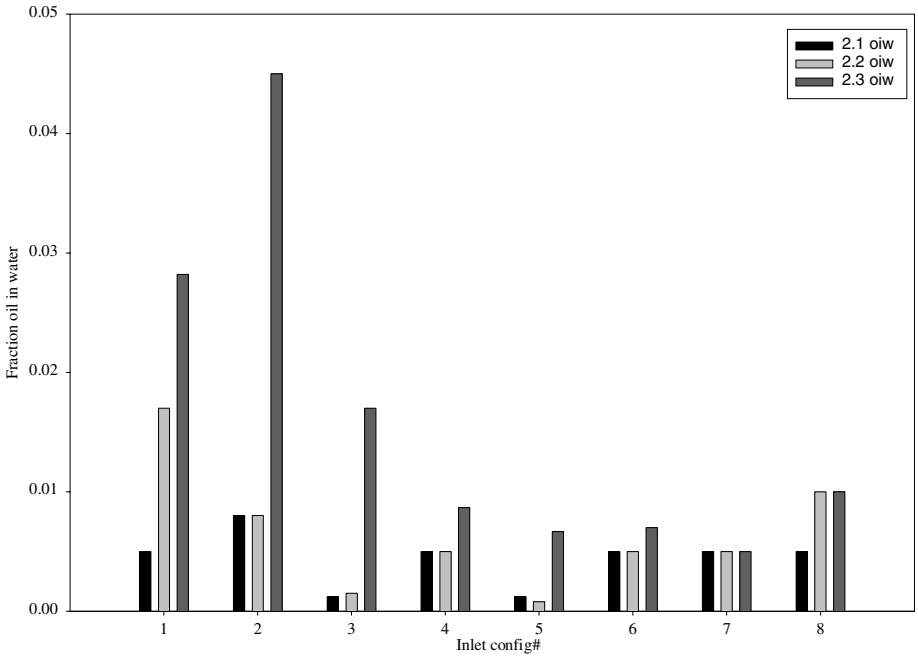

Figure 5.5: Inlet cyclone test results, oiw content at the water outlet

5.3 Unloading

The unloading concept is to remove a water-rich stream from the inlet zone, well below the inlet, in order to increase the retention time of the water phase. The inlet zone is defined as the region confined by the flow diffuser and the end wall, or in the case of a central inlet, between the flow diffusers. The tests were done in co-operation with Statoil a.s, and the objective of the tests was to investigate the possibility of increasing the water handling capacity at Statoils installation Statfjord.

The primary separators at Statfjord are of the central inlet type, and they all have a flange low down on the inlet section. Samples taken at the Statfjord B tests separator showed that in the region beneath the inlet, there was a water bulk phase with small amounts of oil. The idea was to remove a water-rich stream from this point and process it separately through a "pre-deoiler" cyclone, a cyclonic device that handles water continuous inlet conditions and produces a flow containing less than 1000 ppm oil in water, which is suitable for a standard de-oiler hydrocyclone. By removing part of the water from the separator, the water capacity was expected to increase and yield better productivity for the installation.

5.3.1 Theory

Following the theory presented in section 2.2, the outlet quality of a phase is heavily dependent on flow rate (eq. (2.10) and (2.12)). Under the assumption that coalescence is fast, removing a fraction of the incoming water feed ϕ_{qw} will change equation (2.10) to (5.1).

$$\eta_{i,w} = \frac{v_{St,i} A_{y,w} \xi_Z}{Q_w(1-\phi_{qw})} = \frac{v_{St,i} Z_{sep} 2\sqrt{2Ry_I - y_I^2}\xi_Z}{Q_{w,\text{ reduced}}},\ \eta_i \leq 1 \tag{5.1}$$

5.3.2 Experimental

The pilot separator rig was refitted with an extra outlet in the inlet zone beneath the inlet cyclone, as shown in figure 5.6. The flow through this outlet was controlled by a downstream pump and returned to the feed tank, to simulate process conditions. The primary objective was to test for tail-end conditions with a high water ratio in the feed, and water continuous conditions with Fluid System 1 were primarly tested. The pressure drop across the choke valve was kept constant at 0.75 bar. Otherwise the experimental setup was as described in section 2.3.

5.3.3 Results and discussion

The results are presented as water outlet quality for standard operation (without removing a partial flow below the inlet, same as figure 2.16) and while removing half of the incoming water, figure 5.7. All the cases are water continuous, for three different water cuts and

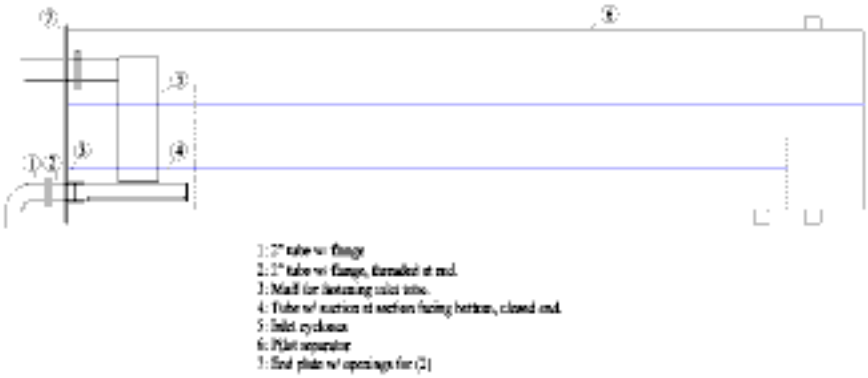

Figure 5.6: Side view of the pilot separator with added "unloading" outlet below the inlet cyclone

constant choke pressure drop 0.75 bar. Tests were also performed for 25% removal, but the trends were less clear for these cases.

Figure 5.7 shows that there is an improvement in water quality as a flow equal to half of the feed water flow is removed in the inlet section. The difference is dependent on the dispersed phase- (oil-) concentration, and increases with decreasing concentration. This is believed to be caused by the difference in the drop size distribution, because of the effect of concentration in the shear point (see section 2.2.4) — following eqs. (2.21) and (2.22), a decrease in dispersed phase fraction in the feed will cause the droplet size distribution to be shifted towards smaller diameters. A reduction in average water velocity will, as the grade efficiency curve is inversely proportional to the flow rate (eq. (2.10)), have a large impact on droplets in the range of 100-200 μm (see figure 2.1). As the improvement in water quality is larger for WC 85% than for WC 65%, this suggests that the small-diameter tail end for the DSD created at WC=65% and ΔP=0.75 bar is near 200 μm, while this is shifted towards smaller diameters at WC=85% and ΔP=0.75 bar.

The overall increase in water handling for the unloading alteration is, from figure 5.7, approximately 40% for a removal corresponding to 50% of the feed water rate, or an overall efficiency η=0.8, although this is more uncertain at removals lower than 50% of the feed water rate. The efficiency will obviously depend on the drop sizes entering the separator, but under the assumption that a separator is operated at water continuous conditions where the water quality is slightly too high for downstream specifications, this process alteration should have good chances in bringing the outlet quality down to the

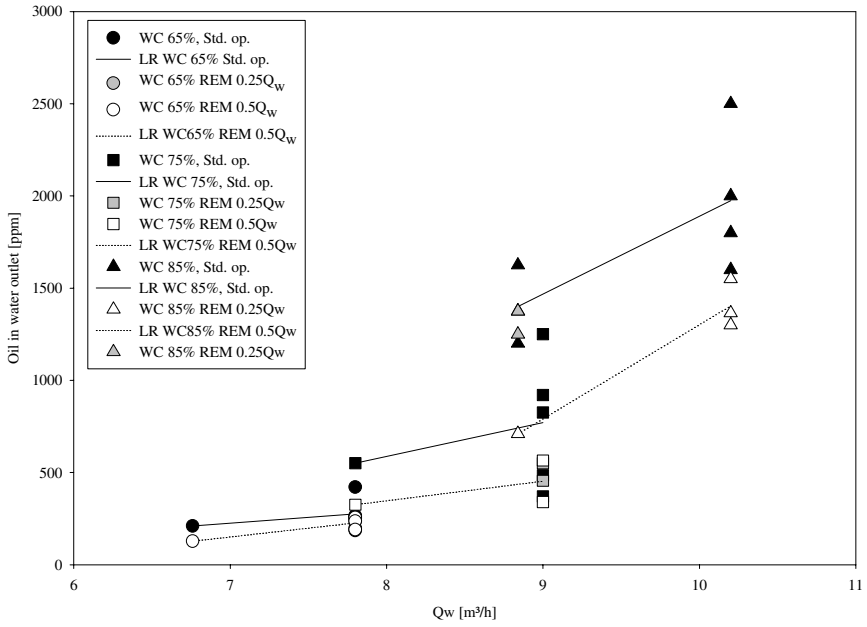

Figure 5.7: Results for the water quality during the Unloading tests

required level.

As discussed in chapters 3 and 4, the shape of the small-diameter tail end of the drop size distribution determines the outlet quality, and by reducing the average velocity the outlet quality is improved. Note that all the data for zero removal, WC 85% are estimated (as the values are outside the range of the measuring device, see section 2.4.3). The composition of the removed stream was also measured, and was found to vary between 94% and 99% water with typical values of 99%. This is well within the range of the planned post-processing device.

As the process change is only affecting the water quality, and likewise only the horizontal velocity in the water phase, it is best suited under water continuous inlet conditions which only occur at the tail production phase of an installation. In this phase of an installations' lifetime (which is gradually emerging currently on the Norwegian shelf), one will presumably see a dramatic deterioration in water quality as an increasing fraction of the produced wells change their continuous phase. As the inversion point for crude oils is generally in the vicinity of WC=70%–80%, the dispersed phase fraction after inversion is low (<30%) and the expected drop size distribution will be shifted towards very small diameters. The "unloading" process alteration will, at the space/weight cost of an extra post-processing cyclone package (and, depending on existing deoiler capacity, possibly including an increase of this as well), increase the lifetime of an installation significantly.

For oil continuous inlet conditions, the impact of this process change will also be dependent on the separability of the incoming liquids. As discussed in section 2.4.3 and chapter 3, the flow pattern in the dispersed phase will depend on the formation of a dispersion layer, and the amount of water entering from the interface relative to the coalescence upstream the flow diffuser. This process change will have larger impact for systems where the coalescence is rapid, and the majority of the water is released upstream the flow diffuser, i.e. in the zone below the inlet.

5.4 Horizontal dispersion dividers

As previously mentioned, this idea was presented by Prof. Hartland at a lecture at Statoil's Research Centre in Trondheim [38]. Following the theory presented in section 2.2.5, the decay rate of the dispersion volume is proportional to the coalescing area, and this can be artificially increased by a mechanical sub-division of the volume occupied by the dispersion into horizontal compartments. This will be briefly discussed in the theory section below. The mechanical consequences of the original idea; splitting the liquid separation volume into horizontal compartments with separate liquid outlets and control systems, however seemed unpractical. Also, ensuring an equal multiphase split to each compartment would be very difficult in practice, without applying mixing and consequently degrade separation.

Observations in the laboratory suggested that most of the dispersion had already collected upstream of the flow diffuser, and that it should be possible to section the volume occupied by the dispersion vertically by mechanical inserts downstream the flow diffuser. Such an arrangement was tested, by dividing half of the liquid separation length between the flow diffuser and weir into five horizontal compartments by inserting four plates covering the width of the separator. The fluids would then be allowed to come together prior to entering the zone of suction from the water outlet. To ensure that dispersion actually flowed through the plates, they were placed immediately downstream the flow diffusers where the flow is forced horizontally.

5.4.1 Theory

According to Hartland *et al.* [19, 17], the separation of a batch test will follow the model described in section 2.2.5. Following this, the coalescence rate across the coalescing interface, Ψ, is a function of the thickness of the packed dispersion layer $\frac{\Delta h}{\Delta h_p}$ in the power of p times the coalescence rate at maximum packed-layer-height, Ψ_i (eq. (2.23)). The total volume flux of dispersed phase is this rate times the coalescing area. Ψ_i is proportional to Δh^p (eq. (2.24)). Given a volume of packed layer, physically splitting this into n horizontal layers will give a coalescing rate $\Psi_{i,n}$ for each layer proportional to $\left(\frac{\Delta h}{n}\right)^p$, and the total for all n areas $\sum_n \Psi_{i,n} \propto n(\frac{\Delta h}{n})^p$. Comparing this with the original dispersed phase flux, the new flux should be $\frac{n}{n^p}$ times bigger.[3]

5.4.2 Experimental

Figure 5.8 shows a sketch of the pilot separator with the horizontal dispersion dividers. The requirements of the dividers were to force the dispersion to flow through them, and allowing the split dispersion to combine prior to approaching the weir and outlets. The length of 1250 mm is the standard length of steel plates from the supplier. The four plates were mounted together with nine bolts (eight along the edges and one in the centre),

[3] As $n > 1$ and $0 < p \leq 1$, the total dispersed-phase flux will always be greater when splitting the original height into lesser heights, and the difference will increase with decreasing p.

intermittent nuts providing the space of 15 mm. The stiffness of the 2 mm plates was expected to keep the plates horizontal, although some yield was noticed after mounting.

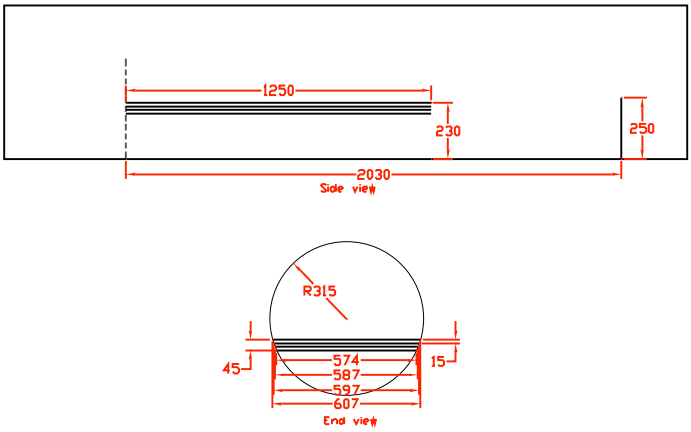

Figure 5.8: Detail sketch of horizontal dispersion dividers

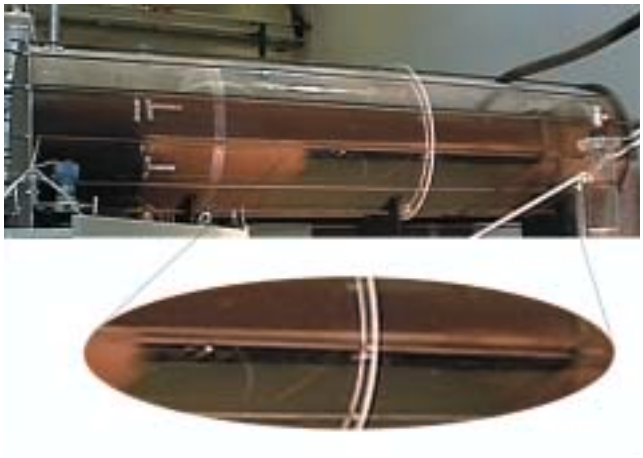

Figure 5.9: Picture of plates inside pilot separator

Otherwise, the same set-up as described in section 2.3 was used. The pressure drop across the choke valve was 0.5 bar.

5.4.3 Results and discussion

The horizontal dispersion dividers were tested on fluid system 3. Figures 5.10 and 5.11 shows the dispersion layer thickness at points Z_4[4] (slightly behind the exit of the plates) and point Z_5 (near the weir) for the oil- and water continuous regime, respectively. Data for tests with WC> 0.3 is removed in figure 5.10, for comparison with data in section 2.4.1.

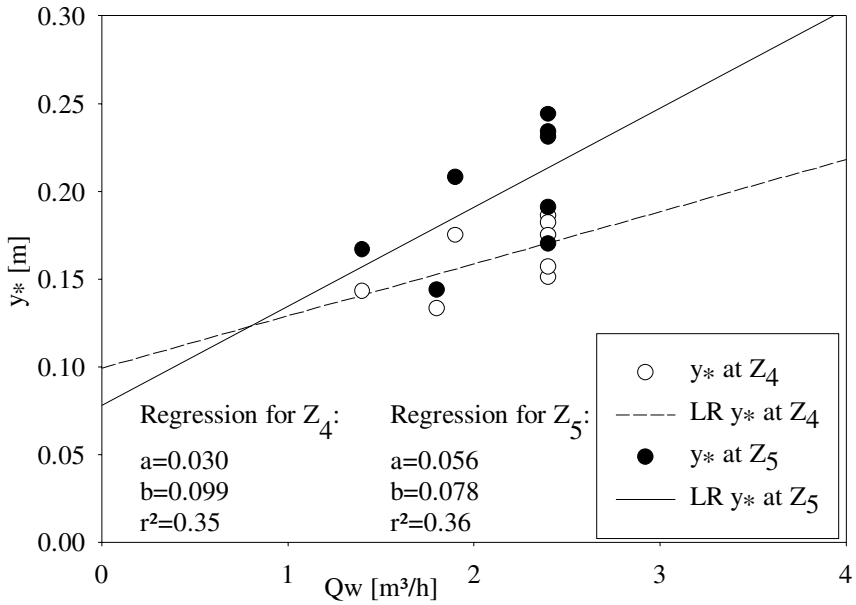

Figure 5.10: Dispersion height vs. Q_w (dispersed phase rate) for oil continuous tests with fluid system 3, batch 1, dispersion dividers.

Comparing to the narrow distribution of points found for the system without the dividers (figures 2.8 – 2.11), the spread is larger at both points, although the general rising trend is conserved vs. dispersed phase flow. Table 5.3 shows the linear fit coefficients for tests with and without dispersion dividers, for comparison. The oil continuous dispersion height measurements with dividers deviates from the results found in section 2.4.1, but also show a poor correlation with the linear fit. The water continuous dispersion height measurements with dividers have a larger spread than their counterparts from section 2.4.1, but are reasonably well represented by the linear fit, and the linear coefficients are close for the two systems.

The water outlet qualities are shown in figures 5.12 and 5.13, for the oil- and water continuous regime, respectively. Compared with the standard system without dividers (see figures 2.12 – 2.17), there is little difference for the oil continuous regime, although

[4]See section 2.3, table 2.1 and figure 2.6 for the location of these points.

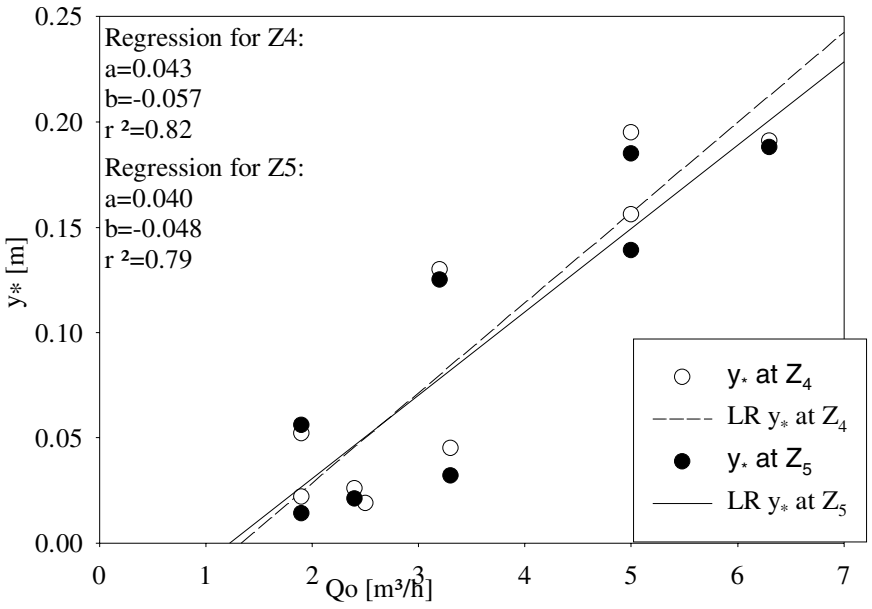

Figure 5.11: Dispersion height vs. Q_o (dispersed phase rate) for water continuous tests with fluid system 3, dispersion dividers.

the water qualities are somewhat improved. For the water continuous regime, however, the difference is noticeable. Comparing figure 5.13 and 2.17, the qualities with the diffuser plates are consistently better (note the different span of the ordinate axis — the series for ΔP=0.5 bar and WC=80% has a max value of $\sim$ 2500ppm, as opposed to 833 ppm for the divider series), and the same trends with regards to concentration and flow rates are seen.

The reason for these effects is better understood by looking at photographs for the system. Two factors are decisive for the effect of the dividers — the velocity through the flow diffusers and the distance between the end of the diffusers and the weir. Starting with the oil continuous system, figure 5.14 shows the case of (Q_l 9.6 m^3/h, WC 0.35, ΔP 0.5 bar) for both normal operation and with the horizontal dispersion dividers. For this oil continuous case, a "lump" of dispersion is formed downstream the dispersion dividers. As the horizontal kinetic energy formed through the flow diffuser cannot transport vertically to the bulk phases (the flow being confined by the dividers), gravity is unable to compress the dispersed phase and form a recirculation pattern in the full length of the separation section (between the flow diffuser and the weir). This recirculation is limited to the section downstream the dividers.

Although the coalescence might be increased because of the increased interface area, the dispersion height at point Z_5 has generally increased. As long as the formed "lump" is smaller than the weir height minus the area of suction from the outlet (for example, see

System	a (slope) [h/m^2]	b (intercept) [m]	r^2
Normal operation, oil continuous, measured at Z_4 (figure 2.9)	0.063	0.012	0.97
Normal operation, oil continuous, measured at Z_5 (figure 2.9)	0.079	-0.023	0.84
Dispersion dividers, oil continuous, measured at Z_4 (figure 5.10)	0.030	0.099	0.35
Dispersion dividers, oil continuous, measured at Z_5 (figure 5.10)	0.056	0.078	0.36
Normal operation, water continuous, measured at Z_4 (figure 2.10)	0.045	-0.069	0.92
Normal operation, water continuous, measured at Z_5 (figure 2.10)	0.044	-0.073	0.89
Dispersion dividers, water continuous, measured at Z_4 (figure 5.11)	0.043	-0.057	0.82
Dispersion dividers, water continuous, measured at Z_5 (figure 5.11)	0.040	-0.048	0.79

Table 5.3: Linear fit coefficients for dispersion layer height with and without dispersion dividers.

the iso-kinetic surface in figure 3.6) separation might be improved, but the sensitivity vs. dispersion volume has increased. As the dispersed phase fraction in the feed increases, this problem will grow, and the internal can therefore not be recommended. Dispersed phase (water) quality might be slightly improved, but the change is minimal.

This problem also occured for the water continuous runs, but here it was observed that the continuous (water) quality was significantly improved. A closer visual study revealed that the flow exiting the flow diffuser near the interface contained a significant amount of oil. In chapter 3 this was discussed, and the vertical flow component induced immediately downstream the flow diffuser was calculated. Figure 5.15 shows the case of (Q_l 9.6 m^3/h, WC 0.80, ΔP 0.5 bar) for both normal operation and with the horizontal dispersion dividers. The mixing downstream the flow diffuser is dampened, and the outlet quality is improved (compare figures 5.13 and 2.17 — the water phase is less cloudy when using the dispersion dividers). The length of the dividers can probably be reduced to 0.30 m, because of the results found in chapter 3 regarding the length of the y-velocity disturbance formed through the flow diffuser (see figure 3.12).

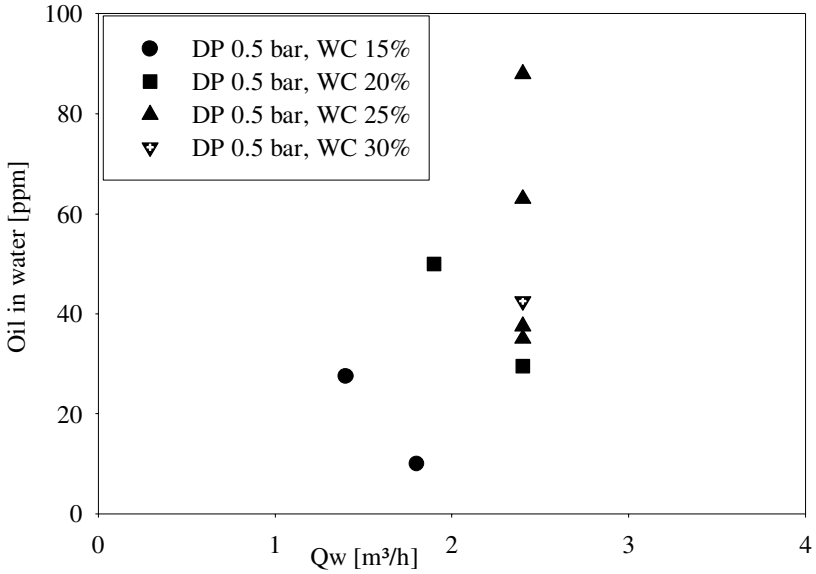

Figure 5.12: Water quality measurements for tests with fluid system 3, oil continuous, batch 1 (stable), dispersion dividers, ΔP=0.5 bar.

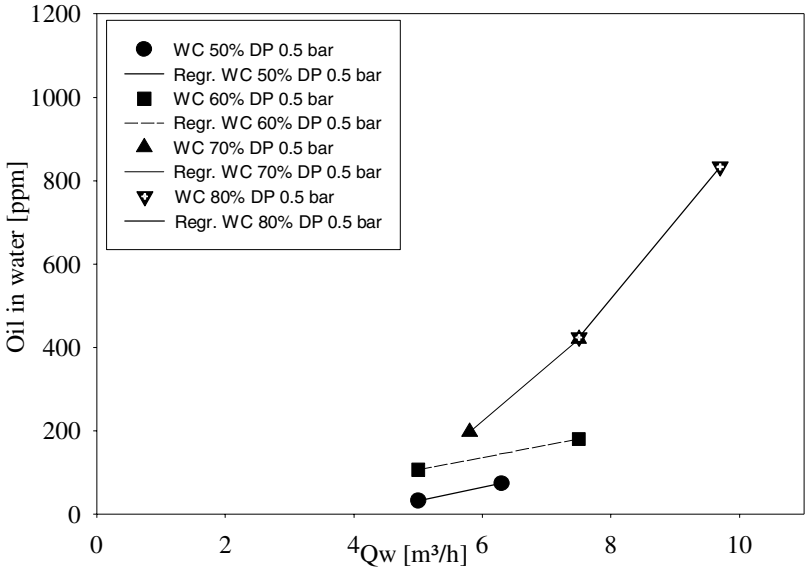

Figure 5.13: Water quality measurements for tests with fluid system 3, water continuous, dispersion dividers, ΔP=0.5 bar

Figure 5.14: Case: [Q_l 9.6 WC 0.35 ΔP 0.5]. Left: standard operation. Right: horizontal dispersion dividers, which can be seen in the right edge. Flow direction is from right to left.

Figure 5.15: Case: [Q_l 9.6 WC 0.80 ΔP 0.5]. Left: standard operation. Right: horizontal dispersion dividers. Flow direction is from right to left.

5.5 Conclusions

Three different mechanical alterations have been tested for pilot-scale gravity separation, and the effects on water quality and dispersion layer thickness have been measured. The entrance height of the liquid is important for cyclone-type inlets, the dispersion layer will increase unecessarily if the liquids exit in a phase region different than the continuous phase. This is believed to be due to mechanical mixing, and will therefore depend on the kinetic energy of the liquid exiting the cyclone.

It is possible to remove a water-rich flow from beneath the inlet, upstream the flow diffuser, which will reduce the average water velocity. This stream contains typically 95%–99% water, and is suitable for post-processing by a special hydrocyclone, known as a pre-deoiler. The effect of this alteration depends on the incoming drop sizes, and also the coalescence rate of the system, but will be ideal for very-high water cuts as typically found in tail production. The capacity increase is in the order of 40% regarding water flow rate for the removal of a flow sized to 50% of the feed water flow rate, giving an efficiency of approximately 0.8 for the process alteration under certain conditions.

"Dispersion dividers", a rack of horizontal plates filling the witdh of the separator, was tested, inspired by the work of Hartland and Panoussopoulos [19]. The purpose was to increase the area available for coalescence, and hence increase the separation. This effect, if present, was found to be over-shadowed by two other effects:

1. Due to the constraint on the dispersion flow, a "lump" was formed downstream the dividers during operation in the oil continuous regime. This increased the sensitivity towards fluctuations in level control, and also decreased the separator overall tolerance for dispersed phase.

2. For water continuous feeds, the water quality was significantly improved. This is believed to be due to a reduction of the vertical velocity component through the flow diffuser, and thereby reduced mixing.

Chapter 6

Field separator data analysis

6.1 Introduction

A successful revamp of an existing production separator involves the interpretation of the data available for the oil field, as finding the correct solution normally requires the asking of the correct problem. An oil producing facility is composed of a multitude of process equipment increasing the complexity of the problem solving process, feed data are often scarce and unreliable, and measurements are limited and costly.

This chapter contains an analysis of various test data made available by Statoil a.s, from the Gullfaks C and Statfjord C fields. The data consisted of outlet quality measurements for the 1st stage separators 20-VA01A and -B at Gullfaks C, and the test separator CD2014 at Statfjord C, together with feed conditions. These are all sites where the KPS CCI has been tested (in the test separator) and installed (in the production separator(s)). It is interesting to include the view from an oil producing installation, where the test schemes are at the mercy of daily profits. There is little control with the experimental parameters, and the resulting data are heavily scattered and very difficult to interpret.

Besides providing data as received from full-size producing systems, as opposed to the previously presented data from a controlled environment in a pilot-scale system, this chapter also discusses the effects of the liquid diffuser location (see section 5.2) with respect to water quality. This was not possible in the pilot-scale tests as the resolution for the water quality results was too poor to be decisive.

The work performed here is of an analytic nature. The data have been examined in a variety of ways, including residence time, non-dimensional groups, various local velocities etc. The focus has been to aid the development of the CCI, but the results presented in the previous chapters will be compared as appropriate. The presented results are believed to be the ones best representing the found effects, despite the fact that the results may seem ambiguous.

6.2 Description of the various inlets tested

The KPS CCI has undergone several design changes since the first installation tested at Gullfaks C test separator. In this text they are divided into three main categories or versions, as explained below. Sketches of the various liquid diffuser designs are shown in figure 6.1.

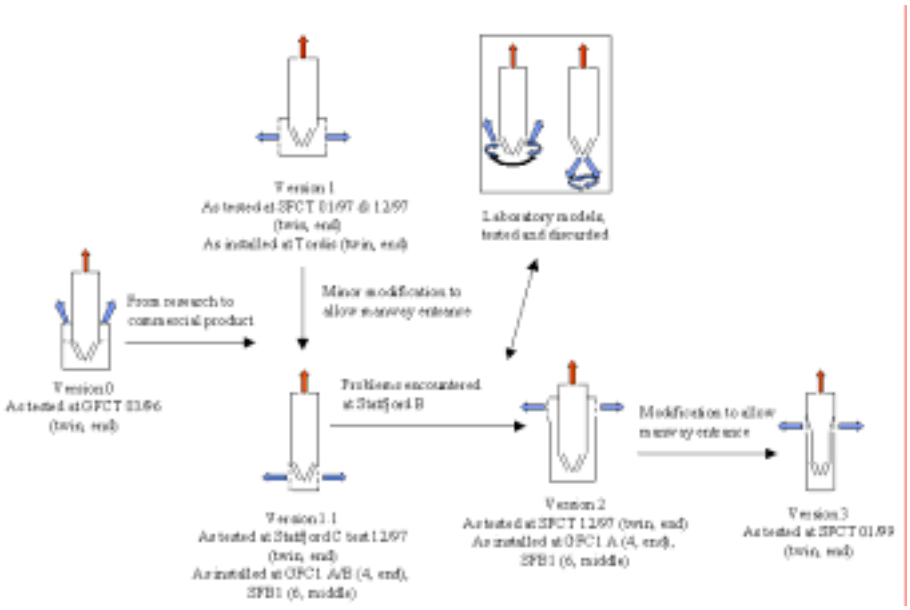

Figure 6.1: Design progress of the CCI

The first version had a liquid distributor directing the flow upwards, with vanes to remove the swirl component. This is called version 0. A problem with this diffuser design was that the liquid exiting the cyclone jets upward, and may break the gas/oil interface. Subsequently, for the Statfjord C test separator trials, a liquid diffuser was made designed to remove the tangential velocity component of the cyclone exit while directing the liquid outward perpendicularly to the cyclone centre axis. This has been installed on several installations, and is named version 1 and 1.1, the difference being dependent on the manway diameter and how large the liquid diffuser may be. The Tordis separator CCI got a liquid diffuser slightly larger than the cyclone body, as the manway diameter allowed this, to reduce the liquid velocity into the separator vessel.

After the Statfjord C test separator trials, the CCI version 1 was installed at the Statfjord B inlet separator, with unsatisfactory results with regards to oil quality. This initiated a research initiative to improve the liquid/liquid performance of the inlet. The result of this initiative was to raise the liquid diffuser outlet to above NIL, here named version 2.

Following the success of version 2 at Statfjord B, it was decided to use this liquid diffuser design as a standard. It was however desirable to simplify installing procedures, as the high liquid diffuser had to be wider than the cyclone body. Therefore a version 3, with two conical sections allowing the diameter of the liquid diffuser to coincide with the largest cyclone diameter. The current standard design alternates between version two and three, as determined by various requirements in the design.

Another feature that deserves attention is the sand drainage configuration. For versions 0, 1, and 2, there are openings in the bottom to allow the sand to exit and to allow drainage at shutdowns. In version three this drainage has been moved to the side of the diffuser, eliminating the small flow directed downwards in the inlet zone.

6.3 Results and Discussion

The results are split into water- and oil quality results. The tendency of water quality is explained fairly easily, while the oil quality seems much more complex in its behaviour. In addition, the different test series have to be compared in order to spot trends, as the magnitudes of the effects vary. Note that all flow rates, water cuts etc. are based on values at "actual" condition, not standard (STP) conditions.

6.3.1 Oil in water outlet

Figure 6.2 shows the water qualities vs. the calculated kinetic energy through the perforations in the liquid diffuser of the cyclone, for three test series at the Statfjord C test separator. The figure shows only CCI designs with liquid diffuser outlets near or below NIL. The oil content in the water outlet increases with increasing kinetic energy through the flow diffuser. This kinetic energy is only based on the liquid flow rate, mix density, and the open fraction of the liquid diffuser, and represents the mixing energy that enters near the interface/in the water dominated region upstream the flow diffuser. Note the difference between the two v1-runs, done with a one-year interval. This cannot be explained by the accessible material, and serves to illustrate the differences in separator performance caused by other factors, for example compositional changes in the fluids.

This energy is rather small (in the order of 10^3 Pa). Moving a little bit upstream, the kinetic energy at the bottom of the last conical section of the CCI where the tangential velocity is at its highest (this location is called "cyclone liquid outlet", and should not be confused with the "cyclone liquid diffuser outlet", through the perforations at the flow diffuser) is the region with highest turbulence in the whole separator, and hence represents the most probable zone of drop break-up in the separator. This kinetic energy is dominated by the tangential velocity, and therefore dependent on the gas feed rate as well as the liquid feed rate. The kinetic energy is calculated using the equations in appendix A. A plot of water quality vs. liquid outlet kinetic energy is shown in 6.3, for the three test series shown in figure 6.2 and two additional series with different liquid diffusers (see figure 6.1), with a high location (well above NIL) of the liquid diffuser outlet.

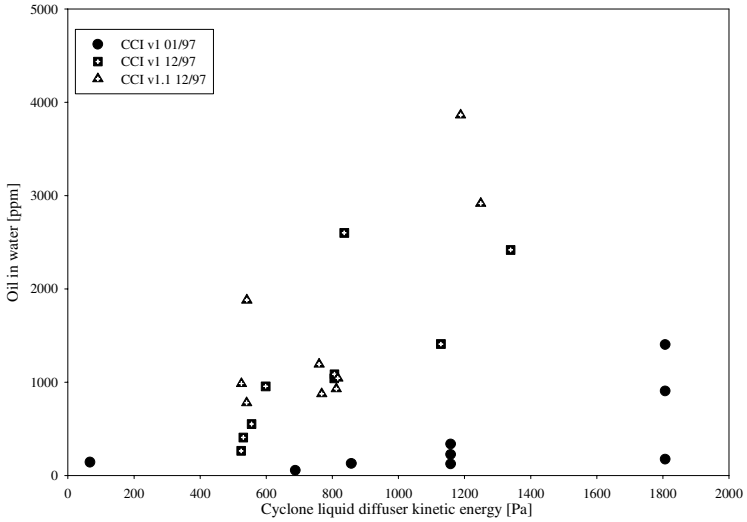

Figure 6.2: SFCT Oil in water vs. kinetic energy in the cyclone liquid diffuser outlet for low liquid diffuser versions (v1 and v1.1).

The patterns for CCI's with a low liquid diffuser outlet is similar to those in figure 6.2, but the CCI's with a high liquid diffuser outlet shows a very different pattern, and the water quality seems to be little affected by magnitudes of the kinetic energy as high as 8E4 Pa. In view of the discussion regarding mechanisms for dispersion phase outlet qualities (chapter 2, page 29) it is probable that the poor water quality observed for inlet types v1 and v1.1 is not due to turbulent break-up in the high-velocity zone, but rather to mixing of the bulk phases immediately downstream the CCI. The difference in performance for inlet types v2 and v3 can probably be attributed to the difference in drainage configuration, as the v2 has a drainage hole in the bottom of the diffuser, while v3 has a horizontally directed drainage. This will lead to somewhat poorer performance for the v2.

Plotting high liquid diffuser versions vs. water plug velocity instead, figure 6.4, gives a better view of the mechanisms present. There is a general increasing trend for oil-in-water content as the water plug velocity increases, consistent with the behaviour in section 2.4. The trend for CCI v3 is similar to the trend for a momentum breaker, which releases the liquid in the gas phase (and avoids any mixing near the bulk water phase). It should be noted that the qualities for high liquid diffusers are generally good, which makes them more exposed to stochastic variations. The momentum breaker performs very well with respect to water quality, but one should still bear in mind the thicker dispersion layer that was formed in the pilot separator tests (figure 5.4), and also that this inlet type is highly prone to foaming.

Similar tests to the ones shown for the Statfjord C test separator was performed at Gullfaks C. At Gullfaks C, there are two production separators in parallel, the A- and

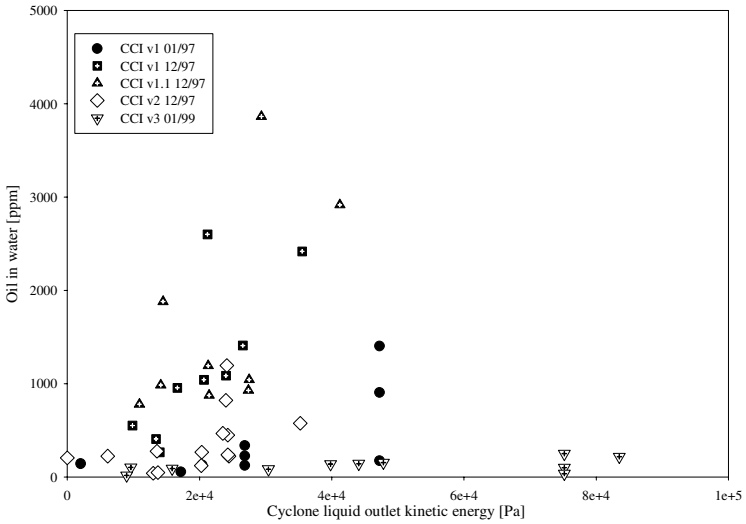

Figure 6.3: SFCT Oil in water vs. kinetic energy in the cyclone liquid outlet.

B-train, and the A-train is equipped with a CCI v2-type, while the B-train has a CCI v1-type. This makes a very interesting set-up for the types of studies presented here. Figure 6.5 shows water quality for these two production separators vs. kinetic energy through the perforations in the cyclone liquid diffuser, similar to figure 6.2. The B-train values, with a low liquid diffuser (v1), show an increasing tendency vs. kinetic energy. Note that the y-axis has a span one decade less than for the SFCT-data. The A-train (v2) is much less affected by the kinetic energy.

As the water quality for the A-train is better than 200 ppm for all the tests available, the stochastic nature of the data has made it impossible to find any trends for water plug velocity (or any other parameter), and is not further discussed.

The amount and types of chemical additives during the tests have varied. However, this is not accounted for when looking at water quality. This is done partly because the working mechanism of the different chemicals used is not fully known, and because (as all tests are oil continuous) it was expected that chemicals should not adversely affect the water quality. The condition for this is of course that the chemicals do not change the interfacial coalescence, but rather the drop-drop coalescence (which has less effect on water quality). If the interfacial coalescence was changed the water quality would be affected due to the different flow patterns induced, as discussed in chapter 3.

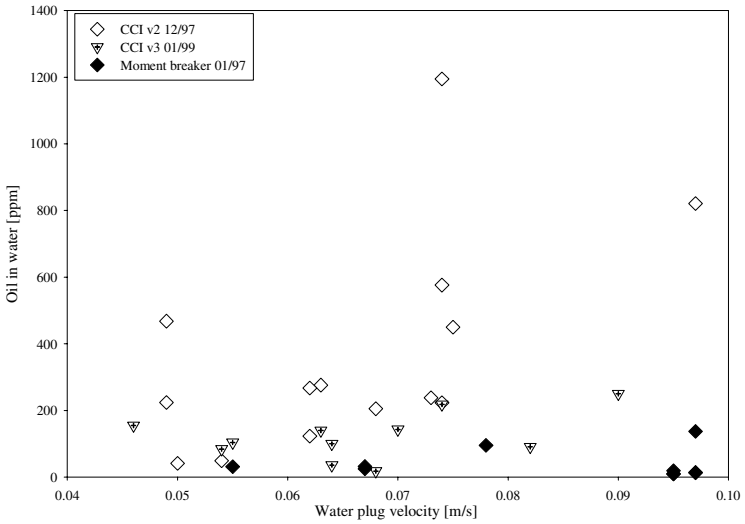

Figure 6.4: SFCT Oil in water vs. water plug velocity for high liquid diffuser versions, and moment breaker.

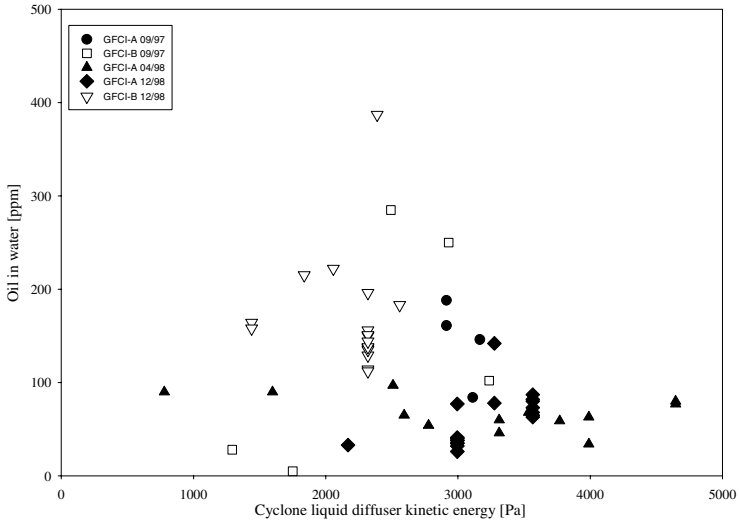

Figure 6.5: GFCI oil in water vs. kinetic energy in the cyclone liquid diffuser outlet

6.3.2 Water in oil outlet

The results for water in oil outlet are presented as separator performance, "water separation efficiency" $\frac{Qw_{\text{water outlet}}}{Qw_{\text{feed}}}$, rather than oil quality. The separator performance with, for example, 5% water in the oil outlet is very different for the same liquid feed rate and water cuts of 30% and 60%, and the effect of water cut can then only be shown by plotting this directly. In chapter 2 it was shown that the continuous phase quality depended primarily on dispersed phase fraction (e.g. water cut for oil continuous operation) and continuous phase [oil] flow rate (or plug velocity), and hence it is desirable to use the performance parameter instead of the raw outlet quality. The relationship between these sets is governed by incoming water cut, as explained in section 2.2.5.

As opposed to water quality, oil quality will generally be affected by chemical additions for oil continuous inlet conditions. The following plots are not discriminating different chemicals and amounts/effects, as little data was available both on the type of chemicals used and the effects of these. When appropriate, the possible effect of chemical addition is included as a suggestion for explaining discrepancies.

Figure 6.6 shows water separation efficiency for tests at the Statfjord C test separator vs. liquid flowrate. The four points below 70% efficiency has later been attributed to an unusually high asphaltene content: during field trials, the flow rate is controlled by varying the well combination going to the separator, and for these four points one specific well with high asphaltene content was used to reach the desired feed rate and water cut. These points therefore represents an anomaly, and should not be given specific weight. For the other points, the efficiency starts to decrease around 350 m^3/h, but some points show good performance up to 550 m^3/h. The momentum breaker series is also shown, and compared with the CCI v1 trials performed in the same period, it performs rather poorly.

Figure 6.7 shows the water separation efficiency vs. water cut for the same points as shown in figure 6.6. The point below WC 35% is at a very low flow rate. The points at high efficiency at ca. WC 42% are with coalescence-enhancing chemicals. Still ignoring the four points below 70% efficiency, there is an improvement in efficiency as the water cut increases above 50%.

Figure 6.8 shows the water separation efficiency vs. the kinetic energy in the narrowest diameter of the CCI, the cyclone liquid outlet. The performance is generally good up to 3.7E4 Pa, where it starts to decline. Also, the afore mentioned asphaltene-stabilised points are exposed to a very high kinetic energy (and turbulent shear), higher than 7E4 Pa, which can expected to further worsen the effect of stabilisation with regards to separation as the presumely stabilised droplets are exposed to shear.

The trials at the Statfjord C test separator did not show large differences with respect to oil quality for the different inlet diffusers, but the water qualities were, as mentioned above, improved. Also, the operators claimed that the production separator "behaved more robustly" after raising the liquid outlet of the flow diffusers, meaning that the daily separator operation was less sensitive to changes in feed condition.

Figure 6.9 shows the water separation efficiency vs. the total liquid feed rate for the Gullfaks C trials. The performance data for the B-train starts to decline near 800 m^3/h,

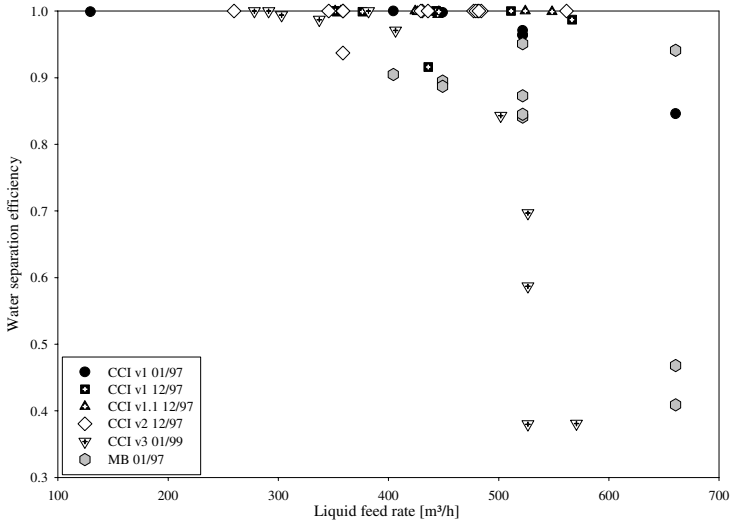

Figure 6.6: SFCT water separation efficiency vs. total liquid flowrate.

while the A-train performs well up to 1100 m^3/h. As mentioned above, the A-train is equipped with a CCI with a high liquid diffuser outlet, while the B-train is equipped with a low liquid diffuser outlet (figure 6.1).

Figure 6.10 shows the water separation efficiency vs. water cut. The data for the B-train declines for water cuts below 40%, while the A-train seems unaffected by water cut.

Figure 6.11 shows the 3D-plot of water separation efficiency vs. water cut and liquid feed rate, from two different angles. For the B-train, water cut seems to have a stronger effect than the liquid flow rate with respect to water separation efficiency, while little new insight is gathered for the A-train.

6.4 Overall discussion

The difference between the two groups of CCIs with different liquid diffuser outlet heights is most pronounced for water quality, where the group with low outlets (v1 and v1.1) shows poorer performance than the group with high outlets (v2 and v3). Furthermore, the water quality depends on the kinetic energy in the liquid diffuser outlet for v1 and v1.1, while this is not visible in the same degree for v2 and v3. This has been shown for both the installations Statfjord C and Gullfaks C.

As the oil quality depends both on water cut and flow rate, these results are more difficult to interpret. On an installation, one does not have full control over these parameters but have to produce the existing wells in various combinations. This is particularly true for the tests at Gullfaks C shown here, as these are performed on the production sepa-

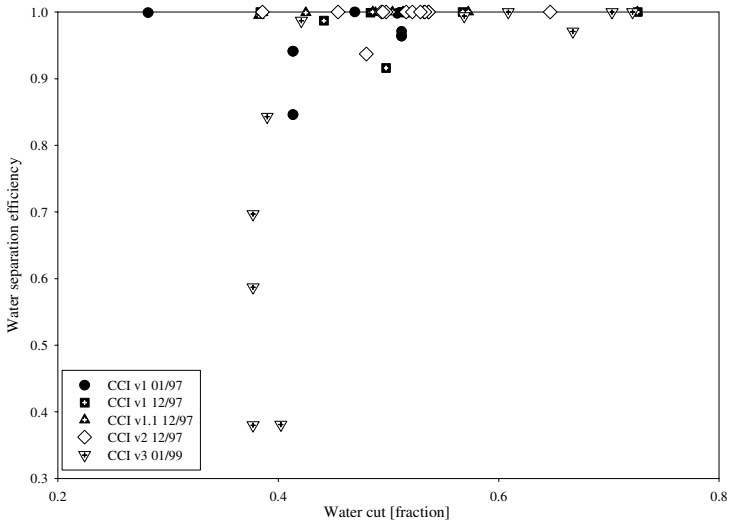

Figure 6.7: SFCT Water separation efficiency vs. water cut.

rators (and not on the test separator, which were used at Statfjord C). Any separation efficiency below 0.9 can generally be expected to be caused by dispersion flowing over the weir, as the choke pressure drop does not vary much within a tests series and the required amount of water flowing over weir in order to have such low performance cannot readily be explained by incomplete settling. There is a decrease in performance as the separator liquid feed increases, which is expected. For the Gullfaks C production separators this decrease appears earlier for the B-train equipped with a CCI v1.1-type inlet than for the A-train equipped with a CCI v2-type inlet. This is attributed to formation of excess dispersion for the v1 and v1.1-types, as was discussed in section 5.2 for pilot separator tests.

The separators seem to perform poorer at lower water cuts when equipped with CCI v1 or v1.1. This is not fully understood, and the results for separators equipped with CCI v2 or v3 does not show the same pattern. It might be that as the water cut increases, the incoming feed cannot produce excess dispersion as the water concentration is too high, and that the incoming water droplets coalesce faster than the ones created by mixing due to the smaller size. The droplets created by the relatively low kinetic energy out of the cyclone liquid diffuser will be very large (several millimeters) and it is known that coalescence rate decreases with increasing drop size [19]. This is however only speculative.

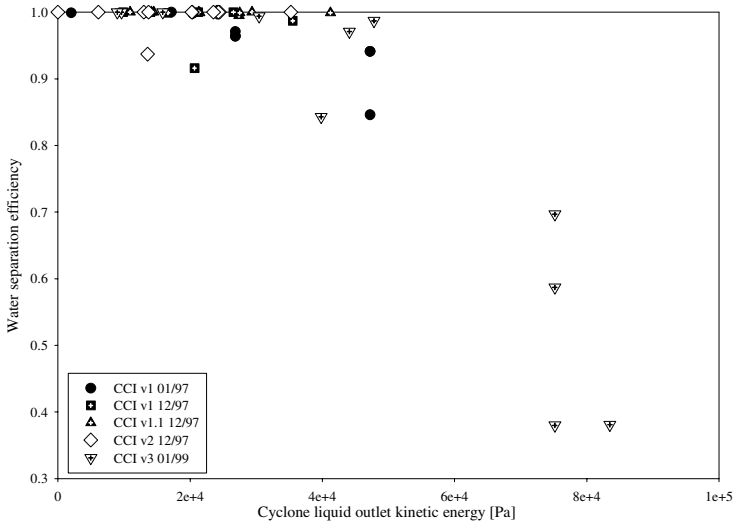

Figure 6.8: SFCT water separation efficiency vs. liquid outlet momentum.

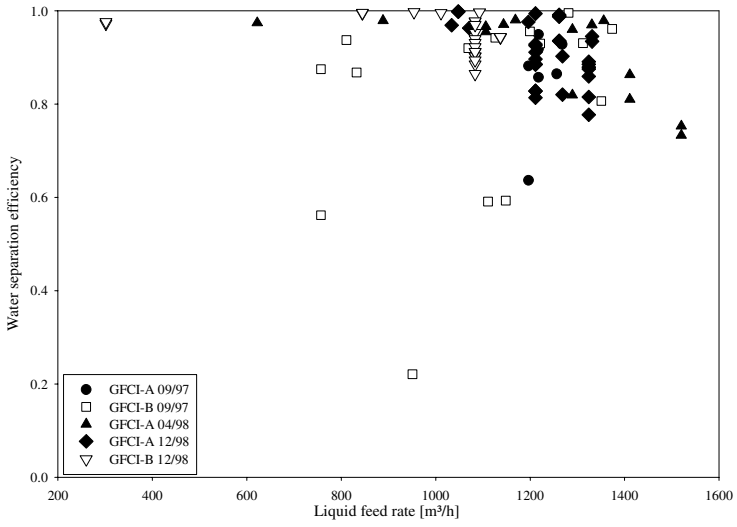

Figure 6.9: GFCI water separation efficiency vs. total liquid flowrate.

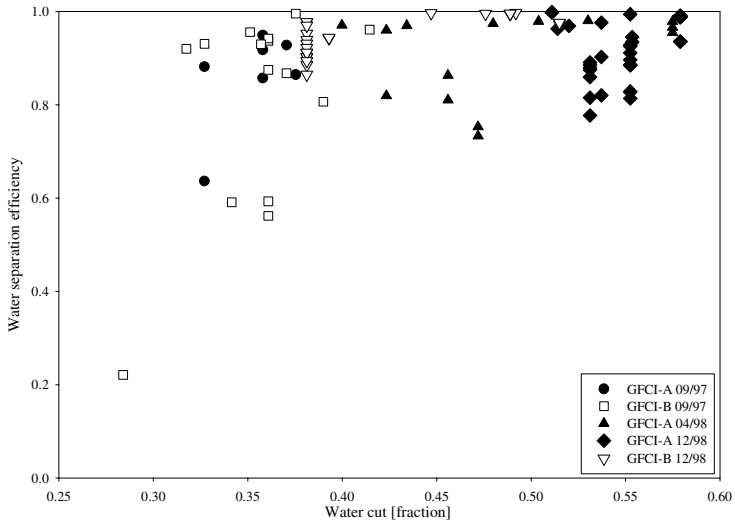

Figure 6.10: GFCI water separation efficiency vs. water cut.

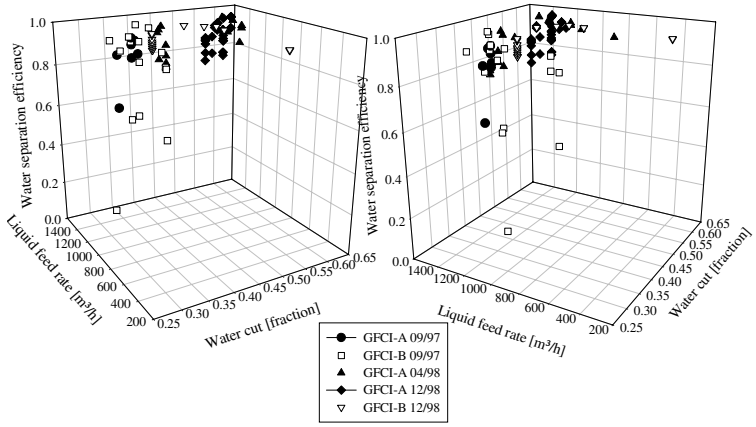

Figure 6.11: GFCI water separation efficiency vs. total liquid flowrate and water cut.

6.5 Conclusion

A data body consisting of test results from full-scale separators in operation at the Statoil operated fields Gullfaks and Statfjord have been reviewed. The focus of the tests have been to investigate the liquid qualities resulting from inlet design changes, particularly for the KPS Compact Cyclone Inlet. It has been found that the water (e.g. dispersed phase) quality was improved when the liquid outlet of the cyclone was raised to the oil phase (above NIL) as opposed to when it was below, or in the vicincity of NIL. The oil quality results were less certain, but the CCI types with a low liquid diffuser outlet appeared to experience instabilities in the quality at lower rates than the types with higher liquid diffuser outlets. The reason for these improvements is believed to be that the release of an oil continuous flow into a water-dominated region causes unnecessary mixing of the two liquid phases, and that this causes the creation of more dispersion, and also more oil drops into the water phase.

Chapter 7

Overall discussion and conclusion

Several features of a gravity separator has been reviewed, and a variety of experimental results have been presented and discussed. In chapter 2, separator data for an "empty" gravity separator, with only a cyclonic inlet and a flow diffuser as internals, were presented for different fluid systems. The data showed that in particular five variables were determining for the system;

The dispersed phase flow rate determined the thickness of the dispersion layer as this layer increased in thickness with increasing dispersed phase flow rate. The relationship was close to linear within the limited range investigated. A literature model [21] was compared with the data, and with a modification this gave good agreement with the results. The modification in question was to exchange the total flow rate with the dispersed flow rate, which is an essential one from a mechanistic point of view.

In order for the outlet qualities to be unaffected by the thickness of this layer, the layer must stay within two height criteria:

1. The top of the layer must stay below the weir height, or the dispersed layer will flood the weir and deteriorate the oil quality.
2. The bottom of the layer must stay above the suction zone from the water outlet, or some of the layer will be drawn through the outlet and pollute the water phase.

The pressure drop in the shear point was determining for both the dispersed- and continuous phase quality, as both decreased with increasing pressure drop.

The dispersed phase fraction in the shear point was determining for the continuous phase quality, which is believed to rise from a concentration effect here. It showed no effect regarding the dispersed phase quality.

The position of the shear point relative to the separator had an impact on separator performance, as the continuous phase quality showed a degradation when the shear point was moved closer to the separator.

The composition of the continuous phase (e.g. the oil phase) with respect to stabilising components affected both the continuous phase quality (by increasing the thickness of the dispersion layer) and the dispersed phase quality. For the model oil used, the addition of stabilising components determined the very existence of a dispersion layer at low- to moderate feed rates. Also, when the dispersion layer was present the dispersed phase quality was significantly improved.

It is interesting that some variables affect both liquid outlet qualities, while some only affect one. The conditions in- and placement of the shear zone (as represented by a valve) affects the outlet qualities differently — the magnitude of the pressure drop affects both, while the concentration and placement only affects the continuous phase. This suggests that the dispersed phase quality is affected only by the initial turbulence, while the continuous phase is affected by downstream coalescence and turbulent energy absorbtion (due to concentration effects). The thickness of the dispersion layer may affect either or both phases depending on the manner of control and the criteria to be met downstream — as the downstream criteria are usually more stringent on the water side, the dispersion layer will normally affect the oil quality.

However, the most surprising finding during these tests was that the dispersed phase outlet quality improved when the composition of the oil phase was partly stabilised and a dispersion layer was formed. This led to a hypothesis that the flow- and mass transfer patterns inside the separator was affected by the dispersion layer, and that the grade efficiency for the dispersed phase would depend on the stability vs. interfacial coalescence. This hypothesis was elaborated in chapter 3, using computational fluid dynamics (CFD) with discrete-phase tracking to calculate grade efficiencies for various hypothetical mass transfer patterns in the dispersed phase. It was found that the grade efficiency would indeed be affected by this variation in mass-transfer pattern. The mass-transfer patterns would also be affected by turbulence. Unfortunately, due to limitations in the CFD-code and uncertainties in the coalescence kinetics, the results regarding the impact of turbulence should be viewed with scepticism.

In chapter 4, bench-scale tests of samples were analysed and modeled with the same [SRTCA-] model used for the dispersion layer thickness in chapter 2. The agreement between the pilot-scale and bench-scale tests were acceptable in view of the uncertainties in both methods. The oil phase from some of the bottle tests were analysed by UV/vis-absorbance as it was noticed that the colour of the oil samples varied. It was found that the dispersion layer samples contained 2–10 times the amount of stabilising component found in the feed and oil outlet, for oil continuous feed conditions. For water continuous conditions the amounts found in the dispersion layer was similar to the amounts found in the inlet and oil outlet. This suggests that the stabilising components are more soluble in the oil- than the water phase, and aggregates near the water drops as the dispersion layer coalesces. Also, the dispersion layer thickness model, when used for predicting the overall coalescence rate in the separator, performed better when based on dispersion layer

samples than on inlet samples. This implies that bottle tests on feed samples for systems with indigeneous stabilising components will over-predict the overall coalescence rate.

Also, experimentally measured drop size distributions from the inlet tube were used with calculated grade efficiencies to obtain total efficiencies, and these were compared with the experimentally found outlet qualities. The agreements were poor as the calculated total efficiency was much lower than the experimentally obtained, often by more than a magnitude. This was attributed mainly to effects upstream the flow diffuser which is difficult to quantify and non-existent in the efficiency model.

Chapter 5 presented three mechanical alterations compared to the results obtained chapter 2, all of which in theory should improve the separator performance. "Horizontal dispersion dividers", a variant over a method suggested by Hartland and Panoussopoulos [19] involving the segregation of the separator into several compartments to increase the interface area and hence promote coalescence, instead altered the flow pattern inside the separator and forced the dispersion to distribute unevenly in the separation section. This gave undesirable results near the weir as the thickness here quickly reached the conditions 1 and/or 2 presented above. However, the results also showed an improvement of the continuous phase quality (for water continuous runs) as long as condition 2 was avoided. This was believed to arise from the dampening of the flow disturbance created by the flow diffuser, which was discussed in chapter 3. It is therefore anticipated that a modified design, where the dividers are much shorter and the dispersion layer is allowed to distribute over a larger part of the separation section, can be helpful in cases where the dispersed phase quality is poor and the dispersion layer thickness does not provide the main threath to the outlet qualities.

Another mehcanical alteration, the "unloading" principle where the water phase retention time is increased due to the removal of a fraction of water near the inlet, showed promising results. For water continuous cases, the performance was significantly improved. As producing installations reach the tail end of their production profile, it is foreseen that the water quality will deteriorate heavily, and this type of modification can potentially increase the lifetime of a field at the cost of installing a minor separate post-processing package.

The third alteration tested, the variation in liquid outlet diffuser height for a cyclonic inlet, showed that the preferential liquid diffuser outlet height was into the zone where the feed continuous phase could diffuse into its own bulk phase. When it was forced into the feed dispersed phase's bulk phase, excess dispersion was formed, and also the dispersed phase was suspected to deteriorate. The latter was further shown in chapter 6 where data from operating fields were presented. The main difference between the pilot-scale and the full-scale results were that the pilot-scale results were clearer on the excess formation of dispersed phase and the deterioration of the oil quality, while the full-scale results showed a clearer effect on the dispersed phase quality, and more ambiguiety regarding the continuous phase results. The combination of these results however shows the importance of proper liquid outlet design for cyclonic inlet devices.

Bibliography

[1] G. C. Broussard, Neil Meldrum, and M. S. Choi. Case history: Design, implementation, and results of separator retrofits. *Journal of Petroleum Technology*, 8:702–707, 1994.

[2] American Petroleum Institute. *API specification 12J: Specification for Oil and Gas Separators*, 7 edition, October 1., 1989.

[3] C. J. Geankoplis. *Transport processes and unit operations*. Allyn and Bacon, Inc, Massachusetts, USA, second edition, 1983.

[4] R. Mei. Effect of turbulence on the particle settling velocity in the nonlinear drag range. *Int. J. Multiphase Flow*, 20(2):273–284, 1994.

[5] Graham Davies. What's wrong with primary separators? In *IBC: Production Separation Systems*, 1996.

[6] Arun Kumar and Stanley Hartland. Gravity settling in liquid/liquid dispersions. *Can. J. Chem. Eng.*, 63(June):368–376, 1985.

[7] Ernst W. M. Hansen, Harald K. Celius, and Bjørn Hafskjold. Fluid flow and separation mechanisms in offshore separation equipment. In *International symposium on Two-phase Flow Modelling and Experimentation*, page 16, Rome, Italy, 1995.

[8] M. J. Hounslow. *Particle Rate Processes*. The University of Sheffield, Sheffield, 1999.

[9] A. N. Kolmogoroff. *Dokl. Acad. Nauk, S.S.S.R.* (N.S.), 66, 1949.

[10] J. O. Hinze. Fundamentals of the hydrodynamic mechanism of splitting in dispersion processes. *AIChE J.*, 1(3), 1955.

[11] M. Zerfa and B. W. Brooks. Prediction of vinyl chloride drop sizes in stabilised liquid-liquid agitated dispersion. *Chem.Eng.Sci*, 51(12):3223–3233, 1996.

[12] J. T. Davies. *Turbulence Phenomena*. Academic Press, London, 1972.

[13] Herman Kolderup. Hydrocyclones: drop breakup and coalescence. Report OR 221907.00.02.90, SINTEF Applied Chemistry, September 07., 1990. Open.

[14] H. G. Polderman, F. A. Hartog, W. A. I. Knaepen, and J. S. Bouma. Dehydration field tests on Draugen. In *SPE Annual Technical Conference and Exhibition*, volume 48993, page 19, New Orleans, Louisiana, USA, 1998. Society of Petroleum Engineers.

[15] S. A. K. Jeelani and Stanley Hartland. Prediction of steady state dispersion height from batch settling data. *J. AIChE*, 31(5):711–720, 1985.

[16] Stanley Hartland. Separation of liquid-liquid dispersions. Technical report, Swiss Federal Institute of Technology Zurich ETHZ, September 1997.

[17] S. A. K. Jeelani, Konstantin Panoussopoulos, and Stanley Hartland. Effect of turbulence on the separation of liquid-liquid dispersions in batch settlers of different geometries. *Ind. Eng. Chem. Res.*, 38:493–501, 1999.

[18] Stanley Hartland and S. A. K. Jeelani. Effect of dispersion height on separation of oil/water dispersions. Technical report, Swiss Federal Institute of Technology Zurich ETHZ, May 1999.

[19] Konstantin Panoussopoulos. *Separation of Crude Oil-Water Emulsions: Experimental Techniques and Models.* Dr. techn., Swiss Federal Institute of Technology Zurich ETHZ, 1998.

[20] S. A. K. Jeelani and Stanley Hartland. The continuous separation of liquid/liquid dispersion. *Chemical Engineering Science*, 48(2):239–254, 1993.

[21] H. G. Polderman, J. S. Bouma, and H. van der Poel. Design rules for dehydration tanks and separator vessels. In *SPE Annual Technical Conference and Exhibition*, volume 38816, pages 669–674, San Antonio, Texas, USA, 1997. Society of Petroleum Engineers.

[22] Per Arild Kjølseth Andresen. *Determination of Droplet Size Distributions of Emulsions in Model Gravity Separators. Correlation to Emulsion Stability and Separator System Characteristics.* Dr. scient, University of Bergen, 1999.

[23] Per Arild Kjølseth Andresen, Richard Arntzen, and Johan Sjöblom. Stability of model emulsions and determination of droplet size distributions in a gravity separator with different inlet characteristics. *Colloids and Surfaces*, 170, September 2000.

[24] Per Gramme. Personal communication. Meeting at Norsk Hydro's Research Centre, Porsgrunn, October 1998.

[25] Peter K. Kilpatrick. Personal communication. Lecture at Statoil Research Centre, Trondheim, May 1999.

[26] Nissim Garti and Axel Benichou. Double emulsions for controlled-release applications — progress and trends. In Johan Sjöblom, editor, *Emulsion encyclopedia.* Marcel Dekker inc., New York, USA, in press (Feb. 2001).

[27] Per Gramme. Developments in the separator design/methods. In *Developments in Production Separation Systems*. ibc, June 1995.

[28] Rune Gammelsæter. KPS inlet cyclones for Åsgard B Midgard inlet separator, 20VA201 and Smørbukk oil inlet separator, 20VA401. Technical Report 03-0100, Flow Dynamics as, 2000.

[29] Richard Arntzen and Per Arild Kjølseth Andresen. Three-phase wellstream gravity separation. In Johan Sjöblom, editor, *Emulsion encyclopedia*. Marcel Dekker inc., New York, USA, in press (Feb. 2001).

[30] Kenneth J. Lissant. *Demulsification : industrial applications*, volume 13 of *Surfactant Science Series*. Marcel Dekker, Inc., New York, 1983.

[31] Harald Laux and Bodil Hop. CFD verifisering av oppgraderingsarbeider for Tordis innløpsseparator. Technical Report STF24 F96569, SINTEF, 1996.

[32] Fluent user guide, 1999.

[33] Frank M. White. *Fluid Mechanics*. McGraw-Hill, Inc., New York, third edition, 1994.

[34] Frank M. White. *Viscous fluid flow*. McGraw-Hill, Inc., New York, second edition, 1991.

[35] Darren Redfern. The Maple Handbook, Maple V Release 4, 1996.

[36] Keith Briggs. W-ology or some exactly solvable growth models. http://epidem13.plantsci.cam.ac.uk/∼kbriggs/W-ology.html, Nov. 1999.

[37] Arne Myrvang Gulbraar and Jan Høydal. Latest experiences from adopting the G-Sep CCI (Compact Cyclone Inlet) to Statfjord B Separators. In *IBC: Production Separation Systems*, 1998.

[38] Stanley Hartland. Personal communication. Lecture at Statoil Research Centre, Trondheim, December 1998.

Appendix A

Calculations

A.1 Inlet cyclone calculations

The KPS compact cyclone inlet (CCI) is an inlet device for gravity separators, aiming at separating gas from liquid thus eliminating foaming. The key of the device is the patented gas blockage arrangement inside the bottom cone, creating a physical blockage for the gas flow. When the swirling liquid is spinned up through the second conical section, the pressure at the top of the gas blockage is increased relative to the reference point outside the cyclone. The gas is then forced to be contained within the diameter of the gas blockage, and exits through the vortex finder at the top of the cyclone body.

The critical steps in the design of a CCI is:

1. Calculating the tangential velocity inside the cyclone from the inlet pipe
2. Calculating the velocity profile inside the cyclone (or rather the transition between solid body rotation and free vortex rotation)
3. Calculating the pressures at the different critical positions inside the cyclone.

Axial velocities and momentums are calculated traditionally according to Bernoulli (A.1), following a streamline between point 1 and 2.

$$P_1 + \rho_1 g h_1 + 1/2 \rho_1 u_1^2 = P_1 + \rho_2 g h_2 + 1/2 \rho_2 u_2^2 \tag{A.1}$$

Tangential velocities are calculated ideally by conservation of rotational velocity, described by eq. (A.2).

$$c_{\theta R_1} R_1 = \mathsf{Constant} = c_{\theta R_2} R_2 \tag{A.2}$$

However, this does not apply for a cyclonic device where there are turbulent losses. Instead, the relation between the velocity at radii R_1 and R_2 is given by eq. (A.3).

$$\frac{c_{\theta R_1}}{c_{\theta R_2}} = \left(\frac{R_2}{R_1}\right)^n \tag{A.3}$$

When guiding the flow tangentially into the cyclone there will be an energy loss due to non-ideal behaviour. This is modelled as a constant function of the liquid flow squared, eq. (A.4).

$$c_\theta^2 = K_i c_{\theta,\,\mathrm{id}}^2 \tag{A.4}$$

In fully developed multiphase flows, the gas phase moves faster than the liquid phase, and a slip factor α_{slip} is used to calculate the mixture velocity (A.5). This factor is set to 0.7.

$$u_{\mathrm{mix}} = \frac{Q_l + Q_g \alpha_{\mathrm{slip}}}{A} \tag{A.5}$$

$$\alpha_{\mathrm{slip}} = \frac{u_l}{u_g} \tag{A.6}$$

The transition from the inlet with area bh to the cyclone body with radii R_1 is then calculated by eq. (A.7), following an area-weighted streamline.

$$\begin{aligned} c_{\theta 1} &= \frac{Q_l + \alpha_{\mathrm{slip}} Q_g}{bh} \left(\frac{\sqrt{0.5\rho_l[R_1^2 + (R_1 - b)^2]}}{\sqrt{0.5\rho_l[R_2^2 + R_1^2]}}\right)^n \sqrt{K_i} \\ &= \frac{Q_l + \alpha_{\mathrm{slip}} Q_g}{bh} \left(\frac{R_1^2 + (R_1 - b)^2}{R_2^2 + R_1^2}\right)^{0.5n} \sqrt{K_i} \end{aligned} \tag{A.7}$$

Here, R_2 is the cup outer diameter, representing the inner boundary for the flow.

A.2 Dispersion layer calculations

The equations are taken from Panoussopoulos [19] and are shown for reference purpose only. The equation for coalescence height h_c:

$$h_c = \begin{cases} V_{hp} t - V_{hp} \frac{\Delta h_i}{\Psi_i}(1 - \exp(-\frac{\Psi_i t}{\Delta h_i})), & t < t_i \\ \frac{\phi_0 - \phi_p}{1 - \phi_p} H_0 + \frac{v_0 t_i}{2} \frac{\phi_p}{1 - \phi_p} + 1/2 \Psi_i t_i, & t = t_i \\ \phi_0 H_0 - \phi_p \Delta h_i \exp(-\Psi_i \frac{t - t_i}{\phi_p \Delta h_i}), & t > t_i \end{cases} \tag{A.8}$$

The equation for sedimentation height h_s:

$$h_s = \begin{cases} H_0 - v_0 t + (v_0 - \Psi_i \frac{1-\phi_p}{\phi_p}) \frac{t^2}{2t}, & t < t_i \\ h_p, & t \geq t_i \end{cases} \tag{A.9}$$

The equation for the packed-layer height h_p:

$$h_p = \begin{cases} h_{c0} + tV, & t < t_i \\ H_0 - (v_0 + \Psi_i \frac{1-\phi_p}{\phi_p}) \frac{t_i}{2}, & t = t_i \\ \phi_0 H_0 + (1-\phi_p) \Delta h_i \exp(-\Psi_i \frac{t-t_i}{\phi_p \Delta h_i}), & t > t_i \end{cases} \tag{A.10}$$

The equation for the velocity of the packed layer V after $t = t_i$:

$$V = \frac{H_0}{t_i} - \frac{1}{2}(v_0 + \Psi_i \frac{1-\phi_p}{\phi_p}) \tag{A.11}$$

The equation for coalescence rate at t_i, Ψ_i:

$$\Psi_i = \frac{2\phi_p d}{3\tau} \left(\frac{\Delta h_i}{d} \right)^p \tag{A.12}$$

The equation for the thickness of the packed layer at t_i, Δh_i:

$$\Delta h_i = \frac{3\tau[2H_0(1-\phi_0) - v_0 t_i]}{2(1-\phi_p)(3\tau + t_i)} \tag{A.13}$$

The equation for the convergence criteria for t_i:

$$\begin{aligned} H_0 \frac{\phi_p - \phi_0}{1-\phi_p} &= -Vt_i + V \frac{\Delta h_i}{\Psi_i} \left(1 - \exp\left[-\Psi_i \frac{t_i}{\Delta h_i} \right] \right) \\ &+ \frac{t_i v_0}{2} \frac{\phi_p}{1-\phi_p} + \Psi_i \frac{t_i}{2} \end{aligned} \tag{A.14}$$

A.3 Curve-fits of k and ϵ

The inlet parameters k and ϵ were fitted to v_{end} for case 29 based on the values for cases 25–28 in table 3.1. These fits are given below:

$$k = 0.0183 v_{\mathsf{end}}^2 + 0.0292 v_{\mathsf{end}}^2 \quad , R^2 = 0.9995 \tag{A.15}$$

$$\epsilon = 0.0023 v_{\mathsf{end}}^{2.809} \quad , R^2 = 0.9993 \tag{A.16}$$

A.4 DSD vs. grade efficiency treatment

The following section contains treatment of the measured droplets from experiments performed under the FLUCHA program by Dr. Andresen [22], from which the raw data has been applied directly. They have also been fitted to the Rosin-Rammler distribution, for later use in the Fluent CFD package (see chapter 3). Table A.1 contains the summary of measurements on fluid systems 1 and 2 (as shown in the column "C_{Be26}", representing the concentration of the added surfactant. Items in **bold face** suggest similar conditions for the applicable conditions under which the DSDs and the experimental values were obtained.

Table A.2 shows the correlation between the experimentally obtained water quality for water continuous cases, and the different combinations of ideal grade efficiency curves for these cases and the measured DSDs from table A.1.

Table A.3 shows a statistical analysis of the various combinations between the obtained experimental values for water quality during water continuous runs. The column labeled "m" is the multiplier between the measured- and calculated outlet quality, defined as $1/n \sum_n \frac{\text{calc. outletvalue}}{\text{expm. outletvalue}}$. Here it is assumed that the measured DSD represent the full dispersed phase fraction. The "s"-column shows the relative standard deviation across a series for this m-value, an estimate of the error in "m" and thereby the consistence for a series. Tables A.4–A.8 show the same calculations for separate water cuts.

The DSDs were compared with the water quality for the oil continuous cases in a similar manner (however, no discretisation of water cut was performed). This is shown in tables A.9–A.11.

Table A.12 contains the Rosin-Rammler parameters for DSDs measured on fluid system 3. These have also been coupled with ideal grade efficiencies and compared to the water outlet quality. Table A.14 shows the results for calculations discretised on experimental set-up and pressure drop, and tables A.15 – A.18 for calculations additionally discretised on water cut.

#	WC	Q_l	ΔP	Probe placement	C_{Be26}	d_{50}	Coales-cence	Rosin-Rammler parameters	
								d_m	n
1	0.16	18	7	inlet	0	47	yes	46	1.51
2	0.25	18	7	inlet	0	57	yes	38	0.79
3	0.5	18	7	inlet	0	275	yes	266	2.39
4	0.83	18	7	inlet	0	212	yes	201	1.93
5	0.83	18	7	cyclone D	0	227	yes	185	1.36
6	0.83	18	7	cyclone D	0	229	yes	226	2.10
7	0.83	18	7	inlet	0	207	yes	177	1.44
12	0.25	18	7	inlet	330	78	yes	77	1.22
13	0.16	12	3	inlet	330	59	yes	50	1.04
14	0.16	18	7	cyclone D	330	48	yes	39	1.13
15	0.25	18	3	inlet	330	86	yes	91	1.62
16	0.5	12	7	inlet	330	124	no	128	4.89
17	0.83	18	3	inlet	330	95	no	96	2.11
18	0.83	12	3	inlet	330	102	no	103	2.59
19	0.5	12	3	inlet	330	122	no	126	4.89
20	0.16	18	7	cyclone B	330	63	yes	58	1.12
21	0.25	12	3	inlet	330	66	yes	64	1.12
22	0.25	12	7	inlet	330	58	yes	54	1.46
23	0.16	18	7	cyclone F	330	49	yes	43	1.05
24	0.16	12	7	inlet	330	41	yes	37	1.24
25	0.83	12	7	inlet	330	121	no	122	2.17
26	0.5	12	0.5	inlet	330	206	yes	233	1.37
27	0.83	12	0.5	inlet	330	106	no	109	1.91
28	0.83	18	7	inlet	330	82	no	84	2.67
29	0.5	18	7	inlet	330	101	no	101	2.28
30	0.5	18	3	inlet	330	99	no	97	2.62
31	0.16	18	7	inlet	330	46	yes	41	1.19
32	0.16	18	3	inlet	330	70	yes	67	1.28
33	0.16	12	0.5	inlet	330	68	yes	59	1.07
34	0.25	12	0.5	inlet	330	87	yes	77	1.07

Table A.1: Drop size measurements from Andresen, with Rosin-Rammler distribution fit, for fluid system 1 and 2

DSD#	ΔP=1 bar	ΔP=0.5 bar	ΔP=0.75 bar Unloading
1	0.89	0.93	0.80
2	0.81	0.93	0.77
3	0.42	0.80	0.67
4	0.51	0.85	0.69
5	0.54	0.86	0.69
6	0.49	0.84	0.68
7	0.53	0.86	0.68
12	0.70	0.90	0.71
13	0.81	0.92	0.75
14	0.86	0.93	0.78
15	0.78	0.91	0.73
16	0.65	0.89	0.67
17	0.88	0.92	0.76
18	0.84	0.92	0.74
19	0.67	0.89	0.67
20	0.83	0.92	0.75
21	0.81	0.92	0.75
22	0.84	0.93	0.75
23	0.86	0.93	0.78
24	0.88	0.93	0.81
25	0.70	0.90	0.69
26	0.60	0.88	0.70
27	0.76	0.91	0.71
28	0.89	0.92	0.79
29	0.86	0.92	0.75
30	0.87	0.92	0.76
31	0.87	0.93	0.78
32	0.87	0.92	0.78
33	0.80	0.92	0.75
34	0.77	0.92	0.75

Table A.2: Correlation beween experimental and calculated outlet qualities for water continuous tests.

DSD#	ΔP=1 bar		ΔP=0.5 bar		ΔP=0.75 bar Unloading	
	m	s	m	s	m	s
1	1.89E+02	0.19	2.61E+02	0.22	1.48E+02	0.24
2	1.89E+01	0.23	2.69E+01	0.27	1.66E+01	0.36
3	6.54E-01	1.29	1.41E+00	0.92	1.64E+00	1.06
4	5.39E+00	0.59	9.21E+00	0.54	7.57E+00	0.80
5	4.00E+00	0.50	6.60E+00	0.47	4.87E+00	0.69
6	3.53E+00	0.66	6.20E+00	0.58	5.26E+00	0.82
7	6.43E+00	0.50	1.06E+01	0.47	7.58E+00	0.67
12	5.57E+01	0.30	8.32E+01	0.33	5.13E+01	0.43
13	5.31E+01	0.23	7.59E+01	0.26	4.47E+01	0.34
14	9.12E+01	0.20	1.27E+02	0.24	7.34E+01	0.28
15	7.94E+01	0.24	1.15E+02	0.27	6.67E+01	0.36
16	1.28E+02	0.32	1.95E+02	0.33	1.13E+02	0.47
17	9.44E+01	0.19	1.31E+02	0.22	7.29E+01	0.27
18	1.18E+02	0.21	1.67E+02	0.25	9.35E+01	0.32
19	1.36E+02	0.30	2.05E+02	0.32	1.18E+02	0.46
20	5.93E+01	0.21	8.43E+01	0.25	4.82E+01	0.32
21	8.65E+01	0.23	1.23E+02	0.26	7.28E+01	0.35
22	1.35E+02	0.22	1.92E+02	0.25	1.10E+02	0.32
23	7.20E+01	0.20	1.01E+02	0.24	5.82E+01	0.29
24	1.19E+02	0.20	1.65E+02	0.23	9.57E+01	0.28
25	6.82E+01	0.28	1.02E+02	0.31	5.86E+01	0.43
26	2.15E+00	0.41	3.39E+00	0.42	2.41E+00	0.62
27	8.32E+01	0.25	1.21E+02	0.28	7.05E+01	0.39
28	2.04E+02	0.19	2.81E+02	0.22	1.57E+02	0.25
29	8.75E+01	0.20	1.23E+02	0.23	6.85E+01	0.29
30	1.27E+02	0.20	1.78E+02	0.23	1.00E+02	0.28
31	1.06E+02	0.20	1.48E+02	0.24	8.53E+01	0.27
32	6.40E+01	0.20	8.96E+01	0.23	5.09E+01	0.28
33	4.18E+01	0.24	5.99E+01	0.27	3.62E+01	0.36
34	2.81E+01	0.25	4.08E+01	0.29	2.51E+01	0.40

Table A.3: Mean value and relative standard deviation for multiplier.

DSD#	ΔP=1 bar		ΔP=0.5 bar	
	m	s	m	s
1	6.16E+02	0.06	6.58E+03	0.07
2	6.01E+01	0.09	6.39E+02	0.10
3	1.25E+00	0.58	1.22E+01	0.74
4	1.55E+01	0.28	1.59E+02	0.34
5	1.21E+01	0.25	1.25E+02	0.31
6	9.91E+00	0.31	1.01E+02	0.38
7	1.94E+01	0.27	2.01E+02	0.32
12	1.76E+02	0.15	1.85E+03	0.18
13	1.71E+02	0.10	1.82E+03	0.12
14	2.95E+02	0.08	3.14E+03	0.09
15	2.58E+02	0.13	2.73E+03	0.16
16	4.14E+02	0.21	4.32E+03	0.25
17	3.09E+02	0.09	3.29E+03	0.10
18	3.84E+02	0.11	4.06E+03	0.13
19	4.39E+02	0.19	4.59E+03	0.23
20	1.93E+02	0.11	2.04E+03	0.13
21	2.78E+02	0.10	2.94E+03	0.12
22	4.36E+02	0.09	4.63E+03	0.11
23	2.33E+02	0.08	2.48E+03	0.10
24	3.85E+02	0.07	4.11E+03	0.08
25	2.20E+02	0.17	2.31E+03	0.20
26	**6.52E+00**	**0.20**	**6.80E+01**	**0.24**
27	2.69E+02	0.14	2.84E+03	0.17
28	6.65E+02	0.07	7.09E+03	0.09
29	2.86E+02	0.10	3.04E+03	0.11
30	4.15E+02	0.09	4.42E+03	0.10
31	3.42E+02	0.08	3.64E+03	0.09
32	2.09E+02	0.09	2.22E+03	0.11
33	1.33E+02	0.10	1.41E+03	0.12
34	9.00E+01	0.12	9.52E+02	0.14

Table A.4: Mean value and relative standard deviation for multiplier, feed WC 0.5 only.

DSD#	ΔP=1 bar		ΔP=0.5 bar	
	m	s	m	s
1	5.28E+02	0.14	1.02E+03	0.13
2	5.24E+01	0.23	1.06E+02	0.20
3	1.75E+00	1.59	5.99E+00	0.83
4	1.41E+01	0.78	3.66E+01	0.54
5	1.05E+01	0.66	2.58E+01	0.48
6	9.18E+00	0.87	2.46E+01	0.58
7	1.67E+01	0.68	4.16E+01	0.49
12	1.51E+02	0.37	3.26E+02	0.30
13	1.46E+02	0.24	2.97E+02	0.21
14	2.53E+02	0.18	4.98E+02	0.16
15	2.15E+02	0.28	4.46E+02	0.24
16	3.35E+02	0.44	7.52E+02	0.35
17	2.60E+02	0.17	5.10E+02	0.16
18	3.21E+02	0.22	6.46E+02	0.20
19	3.58E+02	0.41	7.91E+02	0.33
20	1.62E+02	0.23	3.27E+02	0.20
21	2.38E+02	0.24	4.83E+02	0.21
22	3.73E+02	0.21	7.47E+02	0.19
23	1.99E+02	0.18	3.93E+02	0.17
24	3.29E+02	0.16	6.42E+02	0.14
25	1.81E+02	0.37	3.93E+02	0.31
26	5.72E+00	0.53	1.33E+01	0.41
27	2.24E+02	0.31	4.71E+02	0.26
28	5.64E+02	0.15	1.09E+03	0.14
29	2.40E+02	0.19	4.76E+02	0.17
30	3.51E+02	0.18	6.93E+02	0.17
31	2.93E+02	0.18	5.77E+02	0.16
32	1.76E+02	0.19	3.48E+02	0.17
33	1.15E+02	0.25	2.34E+02	0.22
34	7.66E+01	0.28	1.59E+02	0.24

Table A.5: Mean value and relative standard deviation for multiplier, feed WC 0.6 only.

DSD#	ΔP=1.5 bar Unloading		ΔP=0.75 bar Unloading	
	m	s	m	s
1	6.43E+02	0.18	1.72E+03	0.30
2	6.72E+01	0.26	1.71E+02	0.40
3	4.26E+00	0.91	5.93E+00	1.38
4	2.37E+01	0.66	4.35E+01	1.08
5	1.65E+01	0.60	3.24E+01	0.98
6	1.63E+01	0.70	2.85E+01	1.14
7	2.63E+01	0.61	5.19E+01	1.04
12	2.04E+02	0.38	4.81E+02	0.61
13	1.85E+02	0.28	4.67E+02	0.45
14	3.13E+02	0.22	8.20E+02	0.36
15	2.75E+02	0.33	6.67E+02	0.59
16	4.45E+02	0.51	9.48E+02	1.05
17	3.13E+02	0.25	7.92E+02	0.48
18	3.93E+02	0.31	9.58E+02	0.59
19	4.67E+02	0.49	1.01E+03	1.01
20	2.02E+02	0.29	5.06E+02	0.50
21	2.99E+02	0.30	7.35E+02	0.52
22	4.61E+02	0.29	1.13E+03	0.50
23	2.47E+02	0.23	6.39E+02	0.38
24	4.06E+02	0.20	1.07E+03	0.31
25	2.35E+02	0.44	5.26E+02	0.87
26	8.55E+00	0.51	1.80E+01	0.78
27	2.87E+02	0.37	6.73E+02	0.69
28	6.81E+02	0.21	1.79E+03	0.38
29	2.91E+02	0.28	7.24E+02	0.53
30	4.28E+02	0.25	1.09E+03	0.46
31	3.65E+02	0.21	9.67E+02	0.32
32	2.17E+02	0.24	5.62E+02	0.41
33	1.48E+02	0.30	3.66E+02	0.46
34	1.00E+02	0.32	2.44E+02	0.52

Table A.6: Mean value and relative standard deviation for multiplier, feed WC 0.65 only.

DSD#	ΔP=1 bar		ΔP=0.5 bar	
	m	s	m	s
1	2.46E+02	0.16	3.84E+02	0.09
2	2.53E+01	0.26	3.89E+01	0.16
3	1.32E+00	1.30	1.73E+00	1.09
4	8.41E+00	0.76	1.28E+01	0.49
5	5.99E+00	0.66	9.33E+00	0.39
6	5.65E+00	0.83	8.52E+00	0.54
7	9.57E+00	0.67	1.50E+01	0.39
12	7.68E+01	0.39	1.20E+02	0.22
13	7.08E+01	0.26	1.11E+02	0.15
14	1.20E+02	0.20	1.87E+02	0.11
15	1.06E+02	0.29	1.69E+02	0.15
16	1.76E+02	0.43	2.86E+02	0.21
17	1.23E+02	0.18	1.94E+02	0.09
18	1.55E+02	0.23	2.46E+02	0.11
19	1.86E+02	0.41	3.00E+02	0.20
20	7.84E+01	0.24	1.24E+02	0.12
21	1.15E+02	0.26	1.80E+02	0.15
22	1.80E+02	0.23	2.81E+02	0.13
23	9.46E+01	0.20	1.48E+02	0.11
24	1.55E+02	0.18	2.42E+02	0.10
25	9.25E+01	0.37	1.49E+02	0.18
26	3.12E+00	0.55	4.81E+00	0.34
27	1.12E+02	0.32	1.78E+02	0.16
28	2.64E+02	0.16	4.15E+02	0.08
29	1.14E+02	0.20	1.81E+02	0.10
30	1.67E+02	0.20	2.63E+02	0.10
31	1.39E+02	0.20	2.17E+02	0.11
32	8.37E+01	0.20	1.32E+02	0.10
33	5.61E+01	0.28	8.71E+01	0.16
34	3.78E+01	0.31	5.94E+01	0.17

Table A.7: Mean value and relative standard deviation for multiplier, feed WC 0.70 only.

DSD#	ΔP=0.75 bar WC=0.75 Unloading		ΔP=0.75 bar WC=0.85 Unloading	
	m	s	m	s
1	3.02E+02	0.17	1.78E+02	0.15
2	3.41E+01	0.27	2.11E+01	0.30
3	3.45E+00	0.82	2.62E+00	0.88
4	1.58E+01	0.63	1.12E+01	0.67
5	1.02E+01	0.57	6.87E+00	0.58
6	1.11E+01	0.66	7.75E+00	0.69
7	1.59E+01	0.56	1.06E+01	0.56
12	1.07E+02	0.36	6.57E+01	0.35
13	9.20E+01	0.26	5.59E+01	0.25
14	1.51E+02	0.21	8.97E+01	0.19
15	1.38E+02	0.29	8.37E+01	0.26
16	2.35E+02	0.41	1.46E+02	0.33
17	1.50E+02	0.20	8.89E+01	0.16
18	1.93E+02	0.25	1.16E+02	0.20
19	2.45E+02	0.39	1.51E+02	0.32
20	9.91E+01	0.25	5.97E+01	0.22
21	1.50E+02	0.27	9.16E+01	0.26
22	2.28E+02	0.25	1.37E+02	0.23
23	1.19E+02	0.21	7.15E+01	0.20
24	1.95E+02	0.20	1.18E+02	0.20
25	1.22E+02	0.36	7.49E+01	0.30
26	5.01E+00	0.50	3.33E+00	0.53
27	**1.46E+02**	**0.32**	**8.92E+01**	**0.27**
28	3.23E+02	0.18	1.91E+02	0.15
29	1.41E+02	0.22	8.43E+01	0.18
30	2.06E+02	0.21	1.23E+02	0.18
31	1.75E+02	0.20	1.04E+02	0.19
32	1.04E+02	0.21	6.25E+01	0.19
33	7.48E+01	0.29	4.56E+01	0.28
34	5.17E+01	0.31	3.23E+01	0.32

Table A.8: Mean value and relative standard deviation for multiplier, feed WC 0.75 and 0.85.

OC DSD#	ΔP= 1 bar f	ΔP= 0.5 bar f	ΔP= 0.5 bar p	ΔP= 5 bar	ΔP= 1 bar	ΔP= 0.5 bar
1	0.87	0.98	0.58	0.82	0.98	0.55
2	0.87	0.98	0.58	0.82	0.98	0.59
3	0.89	0.99	0.58	0.83	0.99	0.44
4	0.84	0.96	0.56	0.81	0.97	0.78
5	0.83	0.97	0.58	0.80	0.96	0.73
6	0.82	0.96	0.57	0.82	0.96	0.80
7	0.84	0.97	0.56	0.81	0.97	0.77
12	0.86	0.98	0.56	0.80	0.97	0.68
13	0.87	0.98	0.57	0.82	0.98	0.59
14	0.87	0.98	0.57	0.82	0.98	0.59
15	0.85	0.98	0.55	0.79	0.97	0.70
16	0.73	0.91	0.50	0.59	0.90	0.89
17	0.84	0.98	0.53	0.76	0.97	0.75
18	0.82	0.97	0.53	0.75	0.96	0.78
19	0.74	0.91	0.50	0.62	0.91	0.90
20	0.86	0.98	0.57	0.81	0.98	0.64
21	0.85	0.98	0.56	0.81	0.97	0.70
22	0.86	0.98	0.58	0.83	0.98	0.65
23	0.87	0.98	0.57	0.82	0.98	0.57
24	0.87	0.98	0.58	0.83	0.98	0.53
25	0.80	0.95	0.52	0.74	0.94	0.84
26	0.87	0.98	0.56	0.80	0.98	0.64
27	0.83	0.97	0.54	0.77	0.96	0.78
28	0.87	0.98	0.54	0.79	0.98	0.66
29	0.81	0.97	0.51	0.73	0.95	0.79
30	0.83	0.98	0.52	0.75	0.96	0.75
31	0.88	0.99	0.58	0.83	0.99	0.52
32	0.87	0.98	0.56	0.81	0.98	0.62
33	**0.88**	**0.99**	**0.57**	0.82	**0.99**	**0.56**
34	**0.86**	**0.98**	**0.56**	0.81	**0.98**	**0.66**

Table A.9: Correlation beween experimental and calculated outlet qualities for oil continuous tests (using water continuous measured DSDs). "p" labels experiments with plates, "f" labels experiments with shear point close to the separator.

DSD#	ΔP= 1 bar "f"		ΔP= 0.5 bar "f"		ΔP= 0.5 bar "p"	
	m	s	m	s	m	s
1	4.3E+01	0.34	1.1E+02	0.65	7.1E+02	0.35
2	3.7E+00	0.37	9.2E+00	0.70	5.9E+01	0.36
3	5.8E-03	0.29	1.4E-02	0.54	9.9E-02	0.36
4	2.1E-01	0.46	5.7E-01	1.03	3.1E+00	0.39
5	2.4E-01	0.44	6.3E-01	0.86	3.5E+00	0.35
6	1.1E-01	0.48	3.0E-01	1.04	1.5E+00	0.37
7	2.9E-01	0.48	7.7E-01	1.02	4.2E+00	0.41
12	7.1E+00	0.45	1.7E+01	0.89	1.0E+02	0.42
13	9.6E+00	0.37	2.4E+01	0.72	1.5E+02	0.37
14	1.9E+01	0.36	4.6E+01	0.70	3.0E+02	0.36
15	9.2E+00	0.51	2.3E+01	1.03	1.3E+02	0.47
16	1.8E+00	1.15	7.6E+00	2.10	9.4E+00	0.74
17	1.0E+01	0.68	2.4E+01	1.40	1.2E+02	0.60
18	9.7E+00	0.73	2.4E+01	1.50	1.0E+02	0.62
19	2.1E+00	1.10	8.8E+00	2.09	1.2E+01	0.72
20	9.1E+00	0.41	2.3E+01	0.80	1.4E+02	0.39
21	1.2E+01	0.46	2.9E+01	0.92	1.7E+02	0.41
22	2.1E+01	0.37	5.3E+01	0.73	3.3E+02	0.36
23	1.5E+01	0.35	3.6E+01	0.68	2.4E+02	0.36
24	2.8E+01	0.31	7.0E+01	0.59	4.7E+02	0.33
25	2.7E+00	0.81	7.8E+00	1.67	2.6E+01	0.63
26	2.2E-01	0.43	5.3E-01	0.85	3.3E+00	0.42
27	6.4E+00	0.65	1.6E+01	1.35	7.6E+01	0.56
28	3.3E+01	0.53	7.4E+01	1.11	4.5E+02	0.55
29	7.5E+00	0.81	1.8E+01	1.63	7.3E+01	0.68
30	1.4E+01	0.73	3.2E+01	1.50	1.5E+02	0.65
31	2.5E+01	0.33	6.1E+01	0.62	4.1E+02	0.35
32	1.1E+01	0.42	2.7E+01	0.82	1.7E+02	0.42
33	**7.7E+00**	**0.37**	**1.9E+01**	**0.72**	**1.2E+02**	**0.40**
34	**4.1E+00**	**0.44**	**1.0E+01**	**0.86**	**6.1E+01**	**0.41**

Table A.10: Oil continuous tests, first set: mean value and standard deviation for multiplier. "p" labels experiments with plates, "f" labels experiments with shear point close to the separator.

#	Δ P=5 bar		ΔP=1 bar		ΔP=0.5 bar	
	m	s	m	s	m	s
1	2.8E+1	0.48	4.0E+1	0.41	1.7E+2	0.40
2	2.3E+0	0.48	3.4E+0	0.43	1.4E+1	0.42
3	3.9E-3	0.49	5.3E-3	0.36	2.2E-2	0.37
4	1.2E-1	0.53	2.0E-1	0.53	8.6E-1	0.59
5	1.4E-1	0.46	2.3E-1	0.49	9.4E-1	0.51
6	6.0E-2	0.50	1.0E-1	0.53	4.5E-1	0.61
7	1.5E-1	0.55	2.8E-1	0.55	1.2E+0	0.58
12	3.8E+0	0.59	6.7E+0	0.52	2.8E+1	0.51
13	5.9E+0	0.51	8.9E+0	0.44	3.7E+1	0.43
14	1.2E+1	0.49	1.7E+1	0.43	7.2E+1	0.42
15	4.4E+0	0.69	8.8E+0	0.58	3.6E+1	0.58
16	1.9E-1	1.45	2.1E+0	1.01	9.9E+0	1.45
17	3.4E+0	0.97	1.0E+1	0.74	4.1E+1	0.74
18	2.9E+0	1.01	9.8E+0	0.77	4.0E+1	0.81
19	2.7E-1	1.36	2.4E+0	0.98	1.2E+1	1.43
20	5.3E+0	0.53	8.5E+0	0.48	3.5E+1	0.47
21	6.3E+0	0.57	1.1E+1	0.53	4.5E+1	0.53
22	1.3E+1	0.49	1.9E+1	0.43	8.0E+1	0.44
23	9.2E+0	0.49	1.3E+1	0.42	5.6E+1	0.41
24	1.9E+1	0.44	2.6E+1	0.38	1.1E+2	0.38
25	7.3E-1	1.03	2.8E+0	0.82	1.2E+1	0.97
26	1.2E-1	0.60	2.1E-1	0.50	8.6E-1	0.49
27	2.4E+0	0.86	6.3E+0	0.71	2.6E+1	0.74
28	1.4E+1	0.86	3.1E+1	0.62	1.3E+2	0.59
29	1.9E+0	1.18	7.7E+0	0.83	3.1E+1	0.88
30	4.1E+0	1.11	1.4E+1	0.78	5.5E+1	0.79
31	1.6E+1	0.48	2.3E+1	0.40	9.5E+1	0.39
32	6.4E+0	0.59	1.1E+1	0.49	4.4E+1	0.47
33	4.7E+0	0.55	**7.1E+0**	**0.44**	**3.0E+1**	**0.43**
34	2.3E+0	0.58	**3.9E+0**	**0.51**	**1.6E+1**	**0.50**

Table A.11: Oil continuous tests, second set: mean value and standard deviation for multiplier.

DSD#	Ref. expm	Qt	WC	dP	Rosin-Rammler parameters	
					dm	n
1	o3.21	12	15	5	1.89E-04	3.09
2	o3.26	9.6	15	5	5.52E-04	2.09
3	o3.22	12	20	5	3.34E-04	1.69
4	o3.27	9.6	20	5	2.36E-04	1.58
5	o3.1	12	15	0.5	2.16E-04	2.67
6	o3.6	9.6	15	0.5	1.93E-04	1.74
7	o3.2	12	20	0.5	1.97E-04	1.76
8	o3.7	9.6	20	0.5	2.06E-04	2.04
9	o3.28	12	25	5	3.25E-04	1.53
10	o3.23	9.6	25	5	6.13E-04	2.56
11	o3.8	12	25	0.5	2.96E-04	3.09
12	o3.3	9.6	25	0.5	4.82E-04	2.50
13	o3.24	8	30	5	2.68E-04	2.19
14	o3.24.1	6.9	30	5	1.82E-04	4.38
15	o3.CC	8	35	5	4.24E-04	3.00
16	o3.25	6.9	35	5	5.47E-04	3.34
17	o3.4	8	30	0.5	2.97E-04	3.03
18	o3.A	6.9	30	0.5	3.49E-04	2.08
19	o3.C	8	35	0.5	2.92E-04	3.45
20	o3.5	6.9	35	0.5	5.16E-04	2.53
21	o3.21	12	15	5	3.54E-04	2.23
22	unlisted	12	15	5	1.93E-04	2.78

Table A.12: Drop size distribution measurements for oil continuous tests, fluid system 3.

OC DSD#	ΔP= 5 bar		ΔP= 1 bar		ΔP= 0.5 bar	
	m	s	m	s	m	s
1	**1.22E+01**	**0.53**	1.87E+01	0.45	7.77E+01	0.44
2	**2.86E+00**	**0.63**	5.03E+00	0.53	2.08E+01	0.51
3	**5.06E+00**	**0.63**	8.82E+00	0.52	3.65E+01	0.51
4	**8.72E+00**	**0.61**	1.44E+01	0.49	5.98E+01	0.48
5	5.29E+00	0.68	1.00E+01	0.57	**4.14E+01**	**0.56**
6	6.00E+00	0.75	1.29E+01	0.62	**5.30E+01**	**0.62**
7	7.06E+00	0.81	1.61E+01	0.65	**6.57E+01**	**0.64**
8	1.67E+00	1.01	6.30E+00	0.82	**2.61E+01**	**0.95**
9	**2.14E+00**	**0.78**	4.84E+00	0.65	2.00E+01	0.66
10	**6.40E-01**	**0.64**	1.20E+00	0.57	4.98E+00	0.57
11	8.22E-01	0.71	1.83E+00	0.65	**7.59E+00**	**0.68**
12	9.48E-01	0.67	1.80E+00	0.57	**7.48E+00**	**0.57**
13	**1.82E+00**	**0.68**	3.65E+00	0.60	1.51E+01	0.61
14	**4.13E-02**	**1.36**	3.76E-01	1.00	1.80E+00	1.47
15	**1.34E-01**	**0.54**	2.22E-01	0.50	1.00E+00	0.65
16	**3.40E-01**	**0.61**	6.63E-01	0.59	2.77E+00	0.62
17	2.57E-01	0.80	8.21E-01	0.78	**3.45E+00**	**0.92**
18	4.67E-01	0.86	1.27E+00	0.73	**5.33E+00**	**0.80**
19	1.23E-01	0.78	4.99E-01	0.86	**2.16E+00**	**1.12**
20	1.96E-01	0.65	3.64E-01	0.56	**1.52E+00**	**0.57**
21	**5.38E+00**	**0.52**	8.11E+00	0.45	3.37E+01	0.43
22	**1.25E+01**	**0.52**	1.86E+01	0.44	7.75E+01	0.43

Table A.13: Oil continuous tests, oil continuous DSD, experimental points under standard separator operation.

OC DSD#	ΔP= 1 bar f		ΔP= 0.5 bar f		ΔP= 0.5 bar p	
	m	s	m	s	m	s
1	2.02E+01	0.38	4.93E+01	0.74	3.18E+02	0.39
2	5.35E+00	0.45	1.29E+01	0.90	7.87E+01	0.44
3	9.40E+00	0.45	2.25E+01	0.90	1.39E+02	0.44
4	1.55E+01	0.42	3.72E+01	0.83	2.36E+02	0.43
5	1.06E+01	0.49	**2.55E+01**	**0.99**	**1.50E+02**	**0.47**
6	1.34E+01	0.56	**3.24E+01**	**1.13**	**1.77E+02**	**0.50**
7	1.66E+01	0.58	**3.96E+01**	**1.18**	**2.15E+02**	**0.53**
8	6.02E+00	0.82	**1.68E+01**	**1.64**	**5.76E+01**	**0.62**
9	4.98E+00	0.58	1.23E+01	1.21	6.45E+01	0.52
10	1.26E+00	0.50	3.12E+00	1.01	1.78E+01	0.45
11	1.87E+00	0.59	**4.77E+00**	**1.21**	**2.40E+01**	**0.49**
12	1.89E+00	0.50	**4.65E+00**	**1.02**	**2.67E+01**	**0.46**
13	3.79E+00	0.53	9.48E+00	1.08	5.17E+01	0.47
14	3.26E-01	1.13	1.38E+00	2.12	1.75E+00	0.75
15	2.34E-01	0.44	6.89E-01	1.10	3.51E+00	0.39
16	6.83E-01	0.53	1.80E+00	1.08	9.28E+00	0.43
17	7.90E-01	0.77	**2.28E+00**	**1.56**	**8.07E+00**	**0.55**
18	1.27E+00	0.68	**3.35E+00**	**1.43**	**1.47E+01**	**0.55**
19	4.56E-01	0.92	**1.54E+00**	**1.75**	**3.78E+00**	**0.53**
20	3.83E-01	0.49	**9.59E-01**	**1.01**	**5.44E+00**	**0.45**
21	8.77E+00	0.37	2.14E+01	0.72	1.39E+02	0.38
22	2.02E+01	0.37	4.93E+01	0.71	3.22E+02	0.38

Table A.14: Oil continuous tests, oil continuous DSD, experimental points with moved shear point (labelled f) and "dispersion dividers" (labelled p).

OC DSD#	ΔP= 0.5 bar f		ΔP= 0.5 bar p		ΔP= 5 bar		ΔP= 0.5 bar	
	m	s	m	s	m	s	m	s
1	8.46E+1	0	3.15E+2	0.30	**2.04E+1**	**0.17**	9.87E+1	0.23
2	1.83E+1	0	6.33E+1	0.43	**4.10E+0**	**0.25**	2.04E+1	0.32
3	3.20E+1	0	1.12E+2	0.40	7.25E+0	0.24	3.60E+1	0.30
4	5.69E+1	0	2.01E+2	0.39	1.30E+1	0.23	6.42E+1	0.29
5	**3.23E+1**	**0**	**1.06E+2**	**0.52**	6.88E+0	0.31	**3.50E+1**	**0.38**
6	**3.36E+1**	**0**	**1.09E+2**	**0.56**	6.97E+0	0.34	**3.60E+1**	**0.40**
7	3.69E+1	0	1.12E+2	0.68	7.17E+0	0.43	3.81E+1	0.48
8	6.03E+0	0	1.60E+1	0.99	9.78E-1	0.69	5.77E+0	0.66
9	1.15E+1	0	3.61E+1	0.62	2.31E+0	0.39	1.21E+1	0.44
10	3.95E+0	0	1.42E+1	0.36	9.13E-1	0.21	4.51E+0	0.27
11	4.64E+0	0	1.61E+1	0.42	1.03E+0	0.26	5.19E+0	0.31
12	5.79E+0	0	1.97E+1	0.46	1.27E+0	0.28	6.39E+0	0.34
13	1.10E+1	0	3.75E+1	0.45	2.41E+0	0.27	1.21E+1	0.33
14	1.44E-2	0	5.79E-2	0.17	3.75E-3	0.09	1.76E-2	0.14
15	9.14E-1	0	3.41E+0	0.29	2.19E-1	0.17	1.07E+0	0.22
16	2.19E+0	0	7.81E+0	0.38	5.06E-1	0.22	2.49E+0	0.28
17	1.21E+0	0	4.45E+0	0.32	2.86E-1	0.19	1.40E+0	0.24
18	2.15E+0	0	7.02E+0	0.53	4.31E-1	0.38	2.31E+0	0.39
19	6.09E-1	0	2.21E+0	0.34	1.40E-1	0.22	6.99E-1	0.26
20	1.23E+0	0	4.18E+0	0.46	2.70E-1	0.27	1.36E+0	0.34
21	3.73E+1	0	1.41E+2	0.27	**9.11E+0**	**0.15**	4.39E+1	0.21
22	8.71E+1	0	3.29E+2	0.27	**2.13E+1**	**0.15**	1.03E+2	0.21

Table A.15: Oil continuous tests, second set: mean value and standard deviation for multiplier. WC 0.15 only. A s-value of 0 implies that experiments were only available for one flow rate.

OC DSD#	ΔP= 1 bar f m	s	ΔP= 0.5 bar p m	s	ΔP= 5 bar m	s	ΔP= 0.5 bar m	s
1	2.44E+1	0	3.53E+2	0.22	2.90E+1	0.17	1.28E+2	0.17
2	6.22E+0	0	8.55E+1	0.31	6.94E+0	0.25	3.16E+1	0.23
3	1.10E+1	0	1.51E+2	0.32	**1.22E+1**	**0.25**	5.59E+1	0.24
4	1.85E+1	0	2.59E+2	0.28	**2.11E+1**	**0.22**	9.51E+1	0.22
5	1.20E+1	0	1.61E+2	0.35	1.29E+1	0.29	6.01E+1	0.27
6	1.45E+1	0	1.85E+2	0.43	1.47E+1	0.36	7.05E+1	0.32
7	1.79E+1	0	**2.22E+2**	**0.49**	1.74E+1	0.41	**8.54E+1**	**0.36**
8	5.01E+0	0	**5.50E+1**	**0.75**	4.10E+0	0.65	**2.23E+1**	**0.52**
9	5.31E+0	0	6.69E+1	0.47	5.28E+0	0.39	2.56E+1	0.34
10	1.41E+0	0	1.90E+1	0.34	1.53E+0	0.27	7.09E+0	0.26
11	1.95E+0	0	2.50E+1	0.43	1.98E+0	0.35	9.48E+0	0.32
12	2.13E+0	0	2.86E+1	0.35	2.31E+0	0.28	1.07E+1	0.26
13	4.15E+0	0	5.51E+1	0.37	4.42E+0	0.30	2.06E+1	0.28
14	1.62E-1	0	1.38E+0	1.36	8.78E-2	1.35	6.30E-1	0.84
15	2.69E-1	0	3.89E+0	0.22	3.20E-1	0.18	1.41E+0	0.17
16	7.29E-1	0	1.01E+1	0.30	8.16E-1	0.24	3.72E+0	0.23
17	6.77E-1	0	7.85E+0	0.63	5.94E-1	0.53	3.11E+0	0.45
18	1.24E+0	0	1.47E+1	0.57	1.14E+0	0.48	5.77E+0	0.41
19	3.14E-1	0	3.77E+0	0.56	2.90E-1	0.46	1.47E+0	0.40
20	4.32E-1	0	5.89E+0	0.32	4.76E-1	0.26	2.19E+0	0.25
21	1.06E+1	0	1.55E+2	0.21	1.27E+1	0.16	5.60E+1	0.17
22	2.45E+1	0	3.59E+2	0.21	2.95E+1	0.16	1.30E+2	0.16

Table A.16: Oil continuous tests, second set: mean value and standard deviation for multiplier. WC 0.20 only. A s-value of 0 implies that experiments were only available for one flow rate.

OC DSD#	ΔP= 1 bar f m	s	ΔP= 0.5 bar p m	s	ΔP= 1 bar m	s	ΔP= 0.5 bar m	s
1	2.90E+01	0	3.93E+02	0	2.55E+01	0	1.24E+02	0.16
2	8.20E+00	0	1.00E+02	0	7.19E+00	0	3.42E+01	0.21
3	1.43E+01	0	1.77E+02	0	1.26E+01	0	5.99E+01	0.20
4	2.29E+01	0	2.98E+02	0	2.01E+01	0	9.72E+01	0.18
5	1.68E+01	0	1.93E+02	0	1.47E+01	0	6.88E+01	0.24
6	2.23E+01	0	2.33E+02	0	1.95E+01	0	8.94E+01	0.28
7	2.81E+01	0	2.87E+02	0	2.46E+01	0	1.12E+02	0.29
8	1.22E+01	0	8.05E+01	0	1.07E+01	0	4.49E+01	0.46
9	8.45E+00	0	8.55E+01	0	7.41E+00	0	3.37E+01	0.30
10	2.00E+00	0	2.27E+01	0	1.76E+00	0	8.19E+00	0.24
11	3.20E+00	0	**3.13E+01**	**0**	2.81E+00	0	**1.27E+01**	**0.31**
12	3.02E+00	0	**3.43E+01**	**0**	2.64E+00	0	**1.23E+01**	**0.24**
13	6.21E+00	0	6.68E+01	0	5.44E+00	0	2.51E+01	0.27
14	7.98E-01	0	2.60E+00	0	6.99E-01	0	2.70E+00	0.65
15	3.57E-01	0	4.34E+00	0	3.13E-01	0	1.48E+00	0.21
16	1.13E+00	0	1.17E+01	0	9.87E-01	0	4.52E+00	0.28
17	1.56E+00	0	1.09E+01	0	1.37E+00	0	5.78E+00	0.44
18	2.34E+00	0	1.99E+01	0	2.05E+00	0	8.98E+00	0.37
19	9.89E-01	0	5.04E+00	0	8.68E-01	0	3.51E+00	0.54
20	6.05E-01	0	6.96E+00	0	5.31E-01	0	2.48E+00	0.24
21	1.26E+01	0	1.71E+02	0	1.10E+01	0	5.39E+01	0.15
22	2.87E+01	0	3.96E+02	0	2.52E+01	0	1.23E+02	0.15

Table A.17: Oil continuous tests, second set: mean value and standard deviation for multiplier. WC 0.25 only. A s-value of 0 implies that experiments were only available for one flow rate.

OC DSD#	WC 0.30, ΔP= 0.5 bar		WC 0.35, ΔP= 0.5 bar	
	m	s	m	s
1	9.85E+01	0.26	3.62E+02	0.14
2	2.72E+01	0.35	9.71E+01	0.20
3	4.76E+01	0.34	1.71E+02	0.19
4	7.72E+01	0.30	2.80E+02	0.16
5	5.55E+01	0.40	1.93E+02	0.22
6	7.30E+01	0.48	2.45E+02	0.27
7	9.09E+01	0.49	3.06E+02	0.28
8	4.14E+01	0.80	1.11E+02	0.50
9	2.82E+01	0.53	9.15E+01	0.29
10	6.75E+00	0.43	2.28E+01	0.23
11	1.08E+01	0.55	3.42E+01	0.31
12	1.01E+01	0.43	3.45E+01	0.23
13	2.09E+01	0.47	6.91E+01	0.26
14	3.56E+00	1.14	5.86E+00	0.79
15	1.48E+00	0.56	4.16E+00	0.19
16	3.89E+00	0.51	1.23E+01	0.27
17	**5.46E+00**	**0.79**	1.45E+01	0.47
18	**8.02E+00**	**0.67**	2.34E+01	0.38
19	3.73E+00	0.94	**8.23E+00**	**0.61**
20	2.07E+00	0.43	**6.95E+00**	**0.23**
21	4.25E+01	0.25	1.57E+02	0.14
22	9.76E+01	0.24	3.61E+02	0.13

Table A.18: Oil continuous tests, second set: mean value and standard deviation for multiplier. WC 0.30 and 0.35.

A.5 Grade efficiency from CFD simulation: example

Table A.19 shows an example calculation for grade efficiencies based on CFD simulation of case 28 (laminar) described in table 3.1.

Origin	Fate	d [m] 1.0E-05	2.0E-05	3.0E-05	4.0E-05	5.0E-05	6.0E-05
I	end	0	0	0	0	0	0
I	I	6	14	22	29	35	655
I	out	2176	2184	2186	2187	2185	1563
end	end	0	0	0	0	0	0
end	I	0	0	0	0	0	0
end	out	189	186	189	190	190	190
Sum		2371	2384	2397	2406	2410	2408
P end-I		0	0	0	0	0	0
P I-I		0.003	0.006	0.010	0.013	0.016	0.295
η_i		0.002	0.004	0.006	0.008	0.009	0.177

Origin	Fate	d [m] 7.0E-05	8.0E-05	9.0E-05	1.0E-04	1.1E-04
I	end	0	0	0	0	0
I	I	2181	2261	2261	2261	2261
I	out	80	0	0	0	0
end	end	0	0	0	0	0
end	I	3	56	106	162	189
end	out	186	132	83	27	0
Sum		2450	2449	2450	2450	2450
P end-I		0.016	0.300	0.561	0.857	1
P I-I		0.965	1	1	1	1
η_i		0.585	0.719	0.824	0.943	1

Table A.19: Example: grade efficiency calculation based on Lagrangian particle tracking for case 28, table 3.1 (laminar)

Appendix B

Experimental data

This appendix contains all the experimentally measured data from the various tests, as described.

B.1 Macro data

This section contains the outlet quality measurements, dispersion layer height measurements and dispersion sample qualities. They are split into oil continuous- and water continuous tests. All the experiments are labelled by a letter signifying the continuous phase and a number representing the fluid system ID# (see section 2.3.2), totalling to the first part of the label. After the period, an index system is used where a set of $Q_t, \phi_{w,i}, \Delta P$ is labelled with a number, a capital letter or a variation ("var[1]") over an earlier test. A letter represent a mechanical variation in the test set-up, as shown in table B.1. Repetitions of a test is labelled by a second period, and a new number signifying the repetition. Furthermore, an oiw-value "peak" suggests that the content of the water effluent were higher than 1440 ppm, the maximum for the measuring device. A value "NaN" suggests that this value is missing (for any particular reason).

p	Horizontal dispersion dividers
f	Shear close to the separator (at position 6 in figure 2.4)
u	Unloading

Table B.1: Index system for the experimental work

Thus o3.1f.1 is the same set of $Q_t, \phi_{w,i}, \Delta P$ as o3.1, but the experiment was performed with the "Horizontal dispersion divider" set-up described in chapter 5, and it is also a repetition of test o3.1f.

[1]The including of this "variation" comes from a test set-up that was initially a factorial design, but later points were added as the observations indicated the need of further exploration. The including of capital letters was to combine several factorial designs, caused by the joint experimental work with UiB.

B.1.1 Oil continuous runs

Tables B.2 – B.10 contains performance values from oil continuous runs for the pilot separator. Table B.4 also contains some data with variations in inlet configuration.

Outlet quality data

test#	Q_t	$\phi_{w,\mathsf{i}}$	ΔP	NIL	Inlet config#	$\phi_{w,\mathsf{oo}}$	$\phi_{w,\mathsf{wo}}$	$\phi_{w,\mathsf{d3}}$	$\phi_{w,\mathsf{d2}}$	$\phi_{w,\mathsf{d1}}$
o1.1	17.3	0.15	7	191	7	0.005	0.995	0.005	0.005	0.339
o1.2	17.4	0.17	7	199	7	0.005	0.995	0.005	0.005	0.995
o1.3	17.4	0.17	7	239	7	0.005	0.995	0.005	0.990	0.995
o1.4	17.5	0.37	7	237	7	0.005	0.990	0.005	0.970	0.980
o1.5	20.4	0.31	7	-87	7	0.005	0.990	0.005	0.895	0.990
o1.6	17.5	0.37	7	192	7	0.005	0.995	0.005	0.990	0.995
o1.7	18.7	0.25	7	228	7	0.005	0.995	0.005	0.995	0.995

Table B.2: Outlet quality data for fluid system 1, oil continuous tests

test#	Q_t	$\phi_{w,\mathsf{i}}$	ΔP	NIL	Inlet config#	$\phi_{w,\mathsf{oo}}$	$\phi_{w,\mathsf{wo}}$	$\phi_{w,\mathsf{d3}}$	$\phi_{w,\mathsf{d2}}$	$\phi_{w,\mathsf{d1}}$
w1.1	19.2	0.51	7	190	7	0.005	0.995	0.364	0.438	0.491
w1.2	19.3	0.50	7	149	7	0.005	0.990	0.286	0.383	0.417
w1.3	17.3	0.83	7	195	7	0.005	0.990	0.005	0.159	0.587
w1.4	17.3	0.83	7	233	7	0.005	0.990	0.113	0.600	0.990
w1.5	18.0	0.83	7	167	7	0.005	0.990	0.005	0.059	0.288
w1.6	18.0	0.83	7	232	7	0.005	0.990	0.022	0.551	0.990
w1.7	17.8	0.83	7	249	7	0.005	0.990	0.005	0.177	0.870
w1.8	17.8	0.83	7	310	7	0.005	0.990	0.493	0.980	0.990
w1.9	17.7	0.83	7	197	7	0.005	0.990	0.005	0.192	0.606
w1.10	17.7	0.83	7	231	7	0.005	0.990	0.143	0.980	0.990

Table B.3: Outlet quality data for fluid system 1, water continuous tests

test#	Q_t	$\phi_{w,\mathsf{i}}$	ΔP	NIL	Inlet config#	$\phi_{w,\mathsf{oo}}$	$\phi_{w,\mathsf{wo}}$	$\phi_{w,\mathsf{d3}}$	$\phi_{w,\mathsf{d2}}$	$\phi_{w,\mathsf{d1}}$
o2.1	12.4	0.17	3	182	7	0.018	1.001	-0.016	0.985	0.997
o2.2	12.4	0.17	3	153	7	0.000	1.010	-0.001	0.836	1.005
o2.3	19.7	0.16	3	151	7	0.001	1.010	0.001	0.963	0.993
o2.4	18.7	0.15	7	205	7	-0.008	0.983	0.000	0.164	0.993
o2.5	17.4	0.26	7	206	7	-0.001	0.998	-0.011	0.973	1.001
o2.6	18.3	0.36	7	206	7	-0.004	0.943	0.404	0.947	0.940
o2.7	19.7	0.35	3	207	7	0.002	0.992	0.572	0.967	0.985
o2.8	19.5	0.25	7	228	7	0.007	0.985	0.017	0.851	0.989
o2.9	21.3	0.25	3	228	7	-0.010	1.001	-0.008	0.964	0.986
o2.10	18.1	0.16	7	219	6	0.001	1.012	-0.003	0.176	1.003
o2.11	19.8	0.16	3	219	6	0.006	0.988	0.033	0.875	0.990
o2.12	19.9	0.26	3	221	6	0.004	1.006	-0.006	0.604	0.989
o2.13	18.3	0.26	7	220	6	0.001	1.002	-0.004	0.907	1.008
o2.14	12.0	0.24	3	219	6	-0.009	0.996	-0.010	0.993	1.001
o2.15	19.6	0.35	3	220	6	-0.008	0.982	0.179	0.987	0.980
o2.16	17.7	0.36	7	219	6	-0.010	0.987	0.106	0.940	0.968
o2.17	10.7	0.23	7	221	6	0.003	1.002	0.109	0.998	0.992
o2.18	17.8	0.14	7	192	7	0.012	0.983	-0.005	0.009	0.950
o2.19	20.5	0.16	3	193	7	0.005	0.999	-0.011	0.491	0.959
o2.20	11.8	0.15	7	205	7	0.003	1.006	-0.002	0.033	0.974
o2.21	20.0	0.25	3	204	7	0.013	0.998	-0.006	0.991	0.991
o2.22	18.2	0.25	7	205	7	0.001	0.999	-0.001	0.991	0.999
o2.23	19.8	0.35	3	203	7	0.005	1.005	-0.005	0.984	0.970
o2.24	17.8	0.36	7	203	7	-0.001	0.996	0.037	0.958	0.990
o2.25	17.5	0.13	7	184	8	-0.003	1.002	0.101	0.958	0.968
o2.26	20.0	0.25	3	183	8	0.002	1.003	0.029	1.007	1.014
o2.27	17.6	0.25	7	184	8	0.004	0.999	0.199	0.986	0.993
o2.28	19.8	0.35	3	185	8	0.001	0.999	0.173	0.975	0.997
o2.29	18.0	0.37	7	185	8	0.005	0.972	0.242	0.973	0.964
o2.30	19.8	0.16	3	185	8	0.009	0.986	0.444	0.956	0.957

Table B.4: Outlet quality data for fluid system 2, oil continuous tests

test#	Q_t	$\phi_{w,\mathsf{i}}$	ΔP	NIL	NOL	$\phi_{o,\mathsf{w-low}}$	$\phi_{o,\mathsf{w-high}}$	$\phi_{o,\mathsf{w-avg}}$
o3.1	12.0	0.15	0.5	4.5	52	35	60	47.5
o3.2.1	12.0	0.20	0.5	26	52	30	36	33
o3.3	9.8	0.24	0.5	26	52	57	68	62.5
o3.4	8.0	0.30	0.5	26	52	86	95	90.5
o3.4.1	8.0	0.30	0.5	28	52	59	68	63.5
o3.5	6.9	0.35	0.5	27	52	49	65	57
o3.6	9.6	0.15	0.5	27	52	11	18	14.5
o3.7	9.6	0.20	0.5	27	52	25	35	30
o3.8	11.8	0.25	0.5	27	52	85	100	92.5
o3.9	10.0	0.30	0.5	24	52	65	85	75
o3.10	8.6	0.35	0.5	24.5	52	101	119	110
o3.A	7.0	0.30	0.5	22	52	55	70	62.5
o3.5.1	7.1	0.34	0.5	22	52	66	75	70.5
o3.C	8.0	0.35	0.5	23	52	74	88	81
o3.21	12.0	0.15	5	27	52	1300	1400	1350
o3.21.1	12.0	0.15	5	27	52	420	450	435
o3.22	11.6	0.20	5	33	52	550	630	590
o3.23	9.3	0.25	5	31	52	950	1030	990
o3.24	8.0	0.30	5	28	52	600	900	750
o3.25	6.9	0.35	4.5	29	52	peak	peak	NaN
o3.26	9.5	0.15	5	30	52	320	380	350
o3.27	9.5	0.20	5	30	52	410	460	435
o3.28	12.0	0.25	5	30	52	peak	peak	NaN
o3.1.1	12.0	0.15	0.5	30	52	66	82	74
o3.24.1	7.8	0.28	5	30	52	1200	1400	1300
o3.CC	8.0	0.35	5	25	52	peak	peak	NaN

Table B.5: Outlet quality data for fluid system 3, oil continuous batch 1

test#	Q_t	$\phi_{w,\mathsf{i}}$	ΔP	NIL	NOL	$\phi_{o,\mathsf{w-low}}$	$\phi_{o,\mathsf{w-high}}$	$\phi_{o,\mathsf{w-avg}}$
o3.19	10.0	0.30	1	30	52	1274	peak	1372
o3.16	10.0	0.15	1	30	52	339	425	382
o3.16ns	10.0	0.15	0	29	52	53	78	65.5
o3.1.2	12.0	0.15	0.5	30	52	80	108	94
o3.2.2	12.0	0.20	0.5	27	52	123	167	145
o3.8.2	12.0	0.25	0.5	27	52	216	276	246
o3.var1	12.0	0.30	0.5	27	52	328	408	368
o3.var1.1	12.0	0.30	0.5	27	52	349	407	378
o3.18	12.0	0.25	1	32	52	1092	1281	1186.5
o3.12	12.0	0.20	1	30	52	856	967	911.5
o3.11	12.0	0.15	1	29	52	422	458	440
o3.18	12.0	0.25	1	29	52	1206	1398	1302
o3.var2	12.0	0.30	1	29	52	peak	peak	1600

Table B.6: Outlet quality data for fluid system 3, oil continuous batch 2

test#	Q_t	$\phi_{w,\mathsf{i}}$	ΔP	NIL	NOL	$\phi_{o,\mathsf{w-low}}$	$\phi_{o,\mathsf{w-high}}$	$\phi_{o,\mathsf{w-avg}}$
o3.1p	12.0	0.15	0.5	24	52	8	12	10
o3.2p	12.0	0.20	0.5	24	52	27	32	29.5
o3.3p	9.7	0.25	0.5	31	52	29	41	35
o3.3p1	9.7	0.25	0.5	31	52	33	42	37.5
o3.3p2	9.7	0.25	0.5	32	52	59	680	63
o3.3p3	9.7	0.25	0.5	32	52	55	73	64
o3.3p4	9.7	0.25	0.5	26	52	88	peak	88
o3.4p	8.1	0.30	0.5	30	52	35	50	42.5
o3.6p	9.6	0.15	0.5	27	52	25	30	27.5
o3.7p	9.6	0.20	0.5	27	52	47	53	50

Table B.7: Outlet quality data for fluid system 3, oil continuous batch 1, Horizontal dispersion dividers

test#	Q_t	$\phi_{w,\mathsf{i}}$	ΔP	NIL	NOL	$\phi_{o,\mathsf{w-low}}$	$\phi_{o,\mathsf{w-high}}$	$\phi_{o,\mathsf{w-avg}}$
o3.1f	12.0	0.15	0.5	27	52	108	139	123.5
o3.2f	12.0	0.20	0.5	27	52	181	222	201.5
o3.8f	12.0	0.25	0.5	27	52	250	310	280
o3.var1f	12.0	0.30	0.5	27	52	341	441	391
o3.1f.1	12.0	0.15	0.5	32	52	45	87	66
o3.1f.2	12.0	0.15	0.5	32	52	85	107	96
o3.1f.3	12.0	0.15	0.5	32	52	99	118	108.5
o3.1f.4	12.0	0.15	0.5	32	52	111	134	122.5
o3.11f	12.0	0.15	1	32	52	268	297	282.5
o3.12f	12.0	0.20	1	32	52	565	722	643.5
o3.var2f	12.0	0.30	1	32	52	1312	peak	1312
o3.18f	12.0	0.25	1	32	52	700	961	830.5
o3.18f.1	12.0	0.25	1	31	52	1052	1226	1139
o3.12f.1	12.0	0.20	1	30	52	707	758	732.5
o3.12f	12.0	0.20	1	29	52	734	940	837

Table B.8: Outlet quality data for fluid system 3, oil continuous batch 2, shear at position close to separator

Dispersion layer quality data

Here are the quality data measured from samples taken within the dispersion layer.

test#	$\phi_{w,\mathsf{d1}}$	$\phi_{w,\mathsf{d2}}$	$\phi_{w,\mathsf{d3}}$
o3.1	0.963	0.916	0.836
o3.2.1	0.781	0.676	0.619
o3.3	0	NaN	NaN
o3.4.1	0.873	0.824	0.815
o3.5	0.814	0.824	0.849
o3.6	1.000	0.835	0.679
o3.7	0.916	0.853	0.808
o3.8	0.903	0.812	0.722
o3.9	0.961	0.875	0.794
o3.10	0.885	0.806	0.800
o3.A	0.930	0.866	0.839
o3.5.1	0.886	0.855	0.845
o3.C	0.878	0.846	0.838
o3.21.1	0.938	0.868	0.759
o3.22	0.956	0.936	0.913
o3.23	0.984	0.953	0.941
o3.24	0.939	0.920	0.898
o3.25	0.996	0.996	0.881
o3.26	0.996	0.947	0.835
o3.27	1.000	0.988	0.953
o3.24.1	0.996	0.992	0.950
o3.CC	1.000	0.972	0.726
o3.19	NaN	NaN	0.976
o3.16	NaN	NaN	0.996

Table B.9: Dispersion layer quality data for fluid system 3, oil continuous batch 1

test#	$\phi_{w,\mathsf{d1}}$	$\phi_{w,\mathsf{d2}}$	$\phi_{w,\mathsf{d3}}$
o3.1p	0.867	0.752	0.674
o3.2p	0.852	0.813	0.754
o3.3p	0.916	0.886	0.835
o3.3p4	0.902	0.919	0.938
o3.4p	0.900	0.864	0.835
o3.6p	0.946	0.927	0.900
o3.7p	0.953	0.933	0.909

Table B.10: Dispersion layer quality data for fluid system 3, oil continuous batch 1, mechanical alteration: plates

Dispersion cross-areas

This section contains the dispersion cross-areas, calculated by the height measured along the wall of the separator and the position of these heigths.

test#	$A_{z,\mathsf{dw}}$	$A_{z,\mathsf{dm}}$	$A_{z,\mathsf{dp}}$	$A_{z,\mathsf{dbp}}$	$A_{z,\mathsf{di}}$
o3.1p	0.0396	0.0372	0.0242	0.0250	0.0170
o3.2p	0.0461	0.0423	0.0237	0.0291	0.0232
o3.3p	0.0508	0.0446	0.0329	0.0308	0.0318
o3.3p1	0.0571	0.0506	0.0309	0.0364	0.0346
o3.3p2	0.0585	0.0501	0.0329	0.0395	0.0374
o3.3p4	0.0576	0.0486	0.0329	0.0395	0.0375
o3.4p	0.0574	0.0486	0.0317	0.0375	0.0357
o3.6p	0.0454	0.0405	0.0235	0.0331	0.0332
o3.7p	0.0532	0.0480	0.0317	0.0403	0.0393

Table B.11: Dispersion cross-areas for fluid system 3, oil continuous batch 1

test#	$A_{z,\mathsf{dw}}$	$A_{z,\mathsf{dm}}$	$A_{z,\mathsf{dp}}$	$A_{z,\mathsf{dbp}}$	$A_{z,\mathsf{di}}$
o3.1p	0.0396	0.0372	0.0242	0.0250	0.0170
o3.2p	0.0461	0.0423	0.0237	0.0291	0.0232
o3.3p	0.0508	0.0446	0.0329	0.0308	0.0318
o3.3p1	0.0571	0.0506	0.0309	0.0364	0.0346
o3.3p2	0.0584	0.0501	0.0329	0.0395	0.0374
o3.3p4	0.0575	0.0486	0.0329	0.0395	0.0375
o3.4p	0.0574	0.04861	0.0317	0.0375	0.0357
o3.6p	0.0454	0.04047	0.0235	0.0331	0.0332
o3.7p	0.0532	0.0480	0.0317	0.0403	0.03933

Table B.12: Dispersion cross-areas for fluid system 3, oil continuous batch 1, mechanical alteration: plates

test#	$A_{z,\mathsf{dw}}$	$A_{z,\mathsf{dm}}$	$A_{z,\mathsf{dp}}$	$A_{z,\mathsf{dbp}}$	$A_{z,\mathsf{di}}$
o3.19	0.0026	0.0035	0.0072	0.0246	0.0369
o3.16	0.0074	0.0080	0.0108	0.0202	0.0333
o3.16ns	0.0019	0.0043	0.0090	0.0217	0.0345
o3.1.2	0.0084	0.0109	0.0101	0.0240	0.0311
o3.2.2	0.0086	0.0075	0.0112	0.0297	0.0311
o3.8.2	0.0069	0.0064	0.0101	0.0291	0.0311
o3.var1	0.0080	0.0094	0.0110	0.0318	0.0336
o3.var1.1	0.0110	0.0097	0.0098	0.0334	0.0299
o3.18	0.0094	0.0076	0.0086	0.0259	0.0362
o3.12	0.0140	0.0125	0.0080	0.0145	0.0298
o3.11	0.0113	0.0124	0.0085	NaN	0.0293
o3.18	0.0132	0.0126	0.0079	0.0198	0.0320
o3.var2	0.0140	0.0135	0.0114	0.0230	0.0233

Table B.13: Dispersion cross-areas for fluid system 3, oil continuous batch 2

test#	$A_{z,\mathsf{dw}}$	$A_{z,\mathsf{dm}}$	$A_{z,\mathsf{dp}}$	$A_{z,\mathsf{dbp}}$	$A_{z,\mathsf{di}}$
o3.1f	0.0070	0.0093	0.0104	0.0295	0.0287
o3.2f	0.0114	0.0085	0.0105	0.0309	0.0281
o3.8f	0.0123	0.0093	0.0107	0.0308	0.0291
o3.var1f	0.0143	0.0102	0.0102	0.0308	0.0286
o3.1f.1	0.0171	0.0135	0.0145	0.0273	0.0311
o3.1f.3	0.0104	0.0101	0.0107	0.0215	0.0304
o3.11f	0.0098	0.0092	0.0132	0.0201	0.0310
o3.12f	0.0098	0.0092	0.0063	0.0163	0.0337
o3.var2f	0.0101	0.0101	0.0098	0.0250	0.0377
o3.18f	0.0111	0.0116	0.0116	0.0280	0.0362
o3.18f.1	0.0079	0.0098	0.0091	0.0272	0.0320
o3.12f.1	0.0136	0.0139	0.0081	0.0200	0.0326
o3.12f	0.0149	0.0145	0.0102	0.0231	0.0340

Table B.14: Dispersion cross-areas for fluid system 3, oil continuous batch 2, shear at position close to separator

B.1.2 Water continuous runs

Tables B.15 – B.24 contains performance values from oil continuous runs for the pilot separator. Table B.18 also contains some data with variations in inlet configuration.

Outlet quality data

test#	Q_t	$\phi_{w,\mathrm{i}}$	ΔP	NIL	NOL	$\phi_{o,\mathrm{w-low}}$	$\phi_{o,\mathrm{w-high}}$	$\phi_{o,\mathrm{w-avg}}$
w3.1	12.5	0.50	0.5	21.5	52	23	34	28.5
w3.1.1	12.5	0.50	0.5	19.5	52	20	29	24.5
w3.2	12.5	0.60	0.5	19	52	231	334	282.5
w3.2.1	12.5	0.60	0.5	21	52	222	345	283.5
w3.8	12.5	0.80	0.5	28.5	52	peak	peak	2500
w3.3	10.7	0.70	0.5	26	52	700	1050	875
w3.4	9.4	0.80	0.5	28	52	870	1428	1149
w3.5	10	0.50	0.5	23	52	26	42	34
w3.6	8.3	0.60	0.5	26	52	118	135	126.5
w3.7	8.3	0.70	0.5	28	52	229	282	255.5
w3.7.1	8.3	0.70	0.5	23	52	280	325	302.5
w3.9	12.5	0.50	1.5	23	52	77	114	95.5
w3.10	12.5	0.60	1.5	23	52	453	560	506.5
w3.11	10.7	0.70	1.5	28	52	1200	1500	1350
w3.12	9.4	0.80	1.5	30	52	peak	peak	3500
w3.13	10	0.50	1.5	23	52	85	98	91.5
w3.14	8.3	0.60	1.5	27	52	190	200	195
w3.14.1	8.3	0.60	1.5	23	52	200	218	209
w3.15	7.1	0.70	1.5	29	52	492	527	509.5
w3.16	6.25	0.80	1.5	30	52	1415	1480	1447.5
w3.1n	12.5	0.50	0	21	52	324	410	367
w3.1n.1	12.5	0.50	0	22	52	311	406	358.5

Table B.15: Outlet quality data for fluid system 3, water continuous

test#	Q_t	$\phi_{w,\mathsf{i}}$	ΔP	NIL	NOL	$\phi_{o,\mathsf{w-low}}$	$\phi_{o,\mathsf{w-high}}$	$\phi_{o,\mathsf{w-avg}}$
w3.1f	12.5	0.50	0.5	22	52	85	104	94.5
w3.2f	12.5	0.60	0.5	22	52	501	847	674
w3.8f	12.5	0.80	0.5	27.5	52	peak	peak	NaN
w3.3f	10.7	0.70	0.5	26	52	peak	peak	NaN
w3.5f	10	0.50	0.5	22	52	92	114	103
w3.6f	8.3	0.60	0.5	26	52	292	376	334
w3.7f	8.3	0.70	0.5	28	52	918	1268	1093
w3.4f	9.4	0.80	0.5	28.5	52	peak	peak	NaN
w3.1f	12.5	0.50	0.5	22	52	95	115	105
w3.1/9f	12.5	0.50	1	22	52	100	123	111.5
w3.9f	12.5	0.50	1.5	22	52	113	144	128.5
w3.9fx	12.5	0.50	2	22	52	111	144	127.5
w3.10f	12.5	0.60	1.5	22	52	1084	peak	1300
w3.13f	10	0.50	1.5	22	52	109	131	120
w3.14f	8.3	0.60	1.5	26	52	308	401	354.5
w3.15f	7.1	0.70	1.5	28	52	845	1155	1000

Table B.16: Outlet quality data for fluid system 3, water continuous, shear at position close to the separator

test#	Q_t	$\phi_{w,\mathsf{i}}$	ΔP	NIL	NOL	$\phi_{o,\mathsf{w-low}}$	$\phi_{o,\mathsf{w-high}}$	$\phi_{o,\mathsf{w-avg}}$
w3.1p	12.6	0.50	0.5	18	52	36	111	73.5
w3.2p	12.5	0.60	0.5	18	52	150	210	180
w3.3p	10.7	0.70	0.5	18	52	360	481	420.5
w3.4p	9.4	0.80	0.5	18	52	850	1250	1050
w3.4p1	9.4	0.80	0.5	23	52	400	447	423.5
w3.8p	12.1	0.80	0.5	28	52	709	957	833
w3.6p	8.3	0.60	0.5	27	52	105	108	106.5
w3.7p	8.3	0.70	0.5	27	52	192	201	196.5
w3.5p	10	0.50	0.5	23	52	28	36	32

Table B.17: Outlet quality data for fluid system 3, water continuous, mechanical alteration: plates

test#	Q_t	$\phi_{w,\mathsf{i}}$	ΔP	NIL	Inlet config#	$\phi_{w,\mathsf{oo}}$	$\phi_{w,\mathsf{wo}}$	$\phi_{w,\mathsf{d3}}$	$\phi_{w,\mathsf{d2}}$	$\phi_{w,\mathsf{d1}}$
w2.1	12.1	0.50	3	153	D	-0.002	0.462	0.289	0.384	0.431
w2.2	11.8	0.51	7	152	D	0.207	0.986	0.371	0.457	0.462
w2.3	11.8	0.84	7	235	D	-0.009	0.990	0.360	0.961	0.981
w2.4	12.3	0.84	3	192	D	-0.002	0.995	0.158	0.500	0.925
w2.5	17.5	0.83	3	190	D	-0.001	0.849	0.326	0.431	0.528
w2.6	17.0	0.83	7	170	D	0.000	0.847	0.267	0.364	0.407
w2.7	11.9	0.84	3	184	B	-0.002	0.996	0.109	0.397	0.459
w2.8	11.4	0.84	7	184	B	0.012	0.988	0.288	0.475	0.983
w2.9	11.5	0.52	7	127	B	0.009	0.628	0.425	0.458	0.491
w2.10	11.5	0.51	7	154	B	0.262	1.032	0.478	0.540	1.003
w2.11	12.0	0.52	3	136	B	0.307	1.027	0.486	0.510	0.511
w2.12	12.4	0.84	7	175	F	-0.003	0.998	0.142	0.358	0.588
w2.13	12.8	0.84	3	173	F	0.001	0.997	0.182	0.394	0.653
w2.14	11.8	0.49	3	143	F	0.202	0.982	0.447	0.479	0.475
w2.15	11.5	0.49	7	142	F	0.172	1.019	0.447	0.460	0.479
w2.16	11.8	0.50	3	142	C	0.004	0.484	0.100	0.391	0.468
w2.17	11.7	0.84	3	183	C	-0.003	0.962	0.226	0.895	0.918
w2.18	11.5	0.84	7	185	C	-0.011	0.971	0.323	0.937	0.932
w2.19	11.9	0.49	3	152	C	0.266	1.011	0.542	0.566	0.662
w2.20	11.5	0.49	7	151	C	0.290	1.006	0.464	0.496	0.531

Table B.18: Outlet quality data for fluid system 2, water continuous tests

Dispersion layer quality data

test#	$\phi_{w,\mathsf{d1}}$	$\phi_{w,\mathsf{d2}}$	$\phi_{w,\mathsf{d3}}$
w3.1	0.457	0.452	0.407
w3.1.1	0.460	0.423	0.393
w3.2	0.483	0.422	0.373
w3.2.1	0.461	0.410	0.354
w3.5	0.393	0.403	0.352
w3.6	0.263	0.835	1.000
w3.9	0.449	0.440	0.392
w3.10	0.458	0.407	0.355
w3.13	0.410	0.377	0.327

Table B.19: Dispersion layer quality data for fluid system 3, water continuous

test#	$\phi_{w,\mathsf{d1}}$	$\phi_{w,\mathsf{d2}}$	$\phi_{w,\mathsf{d3}}$
w3.1f	0.440	0.403	0.388
w3.2f	0.435	0.397	0.351

Table B.20: Dispersion layer quality data for fluid system 3, water continuous, shear at position close to the separator

test#	$\phi_{w,\mathsf{d1}}$	$\phi_{w,\mathsf{d2}}$	$\phi_{w,\mathsf{d3}}$
w3.1p	0.4	0.392	0.345
w3.2p	0.405	0.395	0.348
w3.3p	0.323	0.272	0.238
w3.4p	0.283	0.155	0
w3.4p1	NaN	NaN	0.593

Table B.21: Dispersion layer quality data for fluid system 3, water continuous, mechanical alteration: plates

Dispersion cross-area measurements

test#	$A_{z,\mathsf{dw}}$	$A_{z,\mathsf{dm}}$	$A_{z,\mathsf{dp}}$	$A_{z,\mathsf{dbp}}$	$A_{z,\mathsf{di}}$
w3.1	0.0468	0.0522	0.0383	0.0497	0.0610
w3.1.1	0.0529	0.0583	0.0421	0.0483	0.0620
w3.2	0.0515	0.0555	0.0374	0.0430	0.0534
w3.2.1	0.0524	0.0526	0.0379	0.0427	0.0519
w3.8	0.0103	0.0091	NaN	0.0388	0.0550
w3.3	0.0147	0.0181	0.0102	0.0376	0.0510
w3.4	0.0052	0.0089	0.0000	0.0328	0.0475
w3.5	0.0454	0.0460	0.0317	0.0418	0.0528
w3.6	0.0131	0.0181	0.0108	0.0362	0.0443
w3.7	0.0109	0.0138	0.0048	0.0346	0.0432
w3.7.1	0.0116	0.0133	0.0057	0.0284	0.0384
w3.9	0.0527	0.0591	0.0401	0.0460	0.0590
w3.10	0.0406	0.0403	0.0307	0.0398	0.0531
w3.11	0.0134	0.0142	NaN	0.0362	0.0440
w3.12	0.0052	0.0075	NaN	0.0306	0.0386
w3.13	0.0441	0.0474	0.0323	0.0407	0.0487
w3.14	0.0158	0.0173	0.0120	0.0366	0.0434
w3.14.1	0.0184	0.0191	0.0106	0.0307	0.0398
w3.15	0.0064	0.0088	NaN	0.0288	0.0348
w3.16	NaN	0.0027	NaN	0.0183	0.0267
w3.1n	0.0516	0.0519	0.0346	0.0503	0.0698
w3.1n.1	0.0394	0.0410	0.0303	0.0464	0.0698

Table B.22: Dispersion cross-areas for fluid system 3, water continuous

test#	$A_{z,\mathsf{dw}}$	$A_{z,\mathsf{dm}}$	$A_{z,\mathsf{dp}}$	$A_{z,\mathsf{dbp}}$	$A_{z,\mathsf{di}}$
w3.1f	0.0525	0.0594	0.0426	0.0471	0.0590
w3.2f	0.0536	0.0567	0.0420	0.0414	0.0534
w3.8f	0.0118	0.0157	0.0027	0.0389	0.0496
w3.3f	0.0154	0.0225	0.0229	0.0379	0.0450
w3.5f	0.0362	0.0428	0.0284	0.0355	0.0490
w3.6f	0.0117	0.0194	0.0080	0.0369	0.0449
w3.7f	0.0074	0.0122	NaN	0.0350	0.0403
w3.4f	0.0023	0.0078	NaN	0.0359	0.0490
w3.1f	0.0557	0.0634	0.0480	0.0480	0.0590
w3.1/9f	0.0570	0.0606	0.0452	0.0475	0.0590
w3.9f	0.0545	0.0575	0.0379	0.0482	0.0588
w3.9fx	0.0500	0.0563	0.0379	0.0471	0.0575
w3.10f	0.0395	0.0390	0.0281	0.0375	0.0505
w3.13f	0.0336	0.0410	0.0229	0.0357	0.0487
w3.14f	0.0134	0.0169	0.0077	0.0314	0.0393
w3.15f	0.0000	0.0096	0.0000	0.0292	0.0372

Table B.23: Dispersion cross-areas for fluid system 3, water continuous, shear at position close to the separator

test#	$A_{z,\mathsf{dw}}$	$A_{z,\mathsf{dm}}$	$A_{z,\mathsf{dp}}$	$A_{z,\mathsf{dbp}}$	$A_{z,\mathsf{di}}$
w3.1p	0.0523	0.0534	0.0387	0.0548	0.0605
w3.2p	0.0516	0.0548	0.0379	0.0482	0.0580
w3.3p	0.0354	0.0375	0.0261	0.0383	0.0450
w3.4p	0.0151	0.0144	0.0105	0.0153	0.0251
w3.4p1	0.0042	0.0066	0.0196	0.0316	0.0290
w3.8p	0.0064	0.0079	0.0183	NaN	0.0000
w3.6p	0.0096	0.0135	0.0188	0.0390	0.0469
w3.7p	NaN	0.0057	0.0196	0.0335	0.0416
w3.5p	0.0385	0.0441	0.0287	0.0454	0.0506

Table B.24: Dispersion cross-areas for fluid system 3, water continuous, mechanical alteration: plates

B.2 UV absorbance measurements

This section contains all the UV absorbance measurements for samples at different runs (described above), performed by Dr. Kallevik at Statoil's Research Centre. Figures B.1 and B.2 show the resulting model from reference measurements. The absorbance correlates very well with concentration.

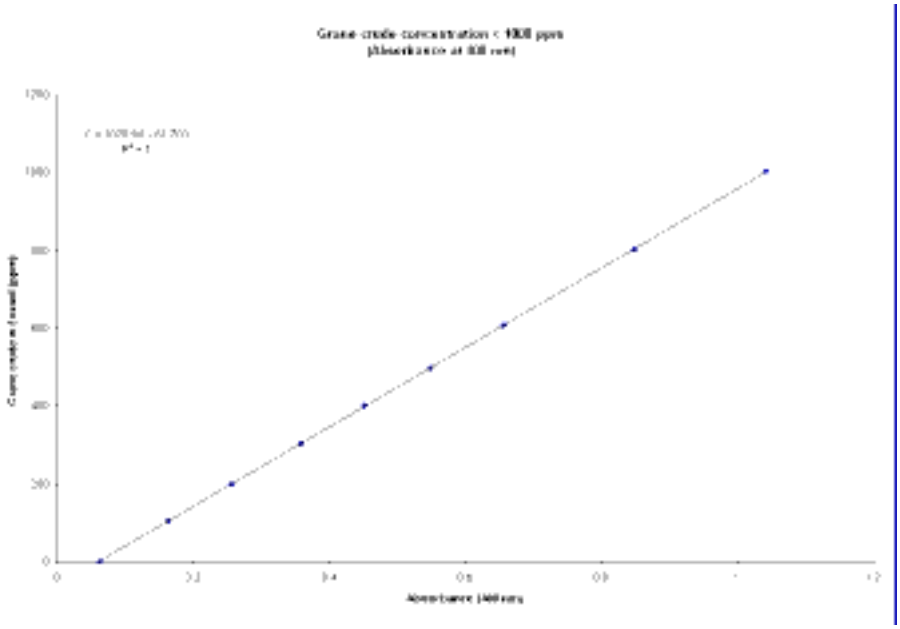

Figure B.1: Linear UV absorbance model for Grane crude concentrations below 1000 ppm, at 400 nm.

Tables B.25, B.26, and B.27 shows the measured UV absorbance for different samples from the pilot separator. See table 2.1 for sample point details.

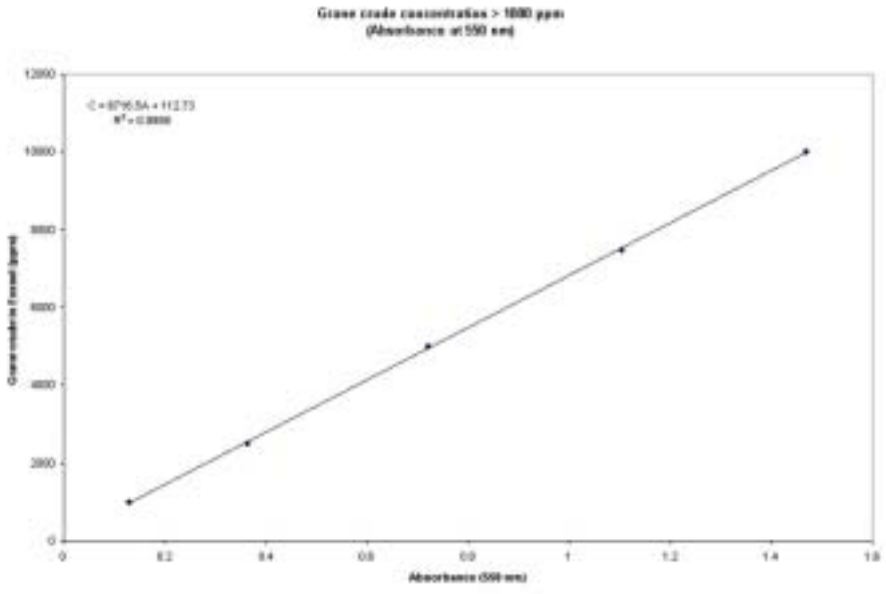

Figure B.2: Linear UV absorbance model for Grane crude concentrations above 1000 ppm, at 550 nm.

Test #	Sp1 [ppm]		Sp4 [ppm]		Sp3 [ppm]		Sp2 [ppm]		Sp6 [ppm]	
	400 [nm]	550 [nm]	400 [nm]	550 [nm]	400 [nm]	550 [nm]	400 [nm]	550 [nm]	400 [nm]	550 [nm]
26	643	475			4249	6561	2357	3202		
27	634	482					3972	5902		
28	615	455					3650	5526		
1.1	589	408	2605	3055	3243	4257	2881	3820		
24.1	620	462					1311	4774		
CC	695	496			1468	5217	1522	1899		
1p			2556	3028	1514	3773	2544	3377		
2p			2089	2652	1420	1651	1424	1631		
3p	659	449	1686	2081	1361	1590	1137	1187	616	455
3p3	740	502					1847	2524	610	415
3p4	619	449	1353	1550	1455	1718	1884	2369	620	422
4p	614	415	1720	2094	1275	1422	1109	1167	605	422
6p	629	657	2636	3538	1788	2208	1357	1993		
7p	644	684	2223	2940	1552	2309	1480	1738	621	442

Table B.25: Measured UV absorbance for samples from tests with fluid system 3, oil continuous batch 1

Test	Sp1 [ppm]		Sp4 [ppm]		Sp3 [ppm]		Sp2 [ppm]		Sp6 [ppm]	
#	400 [nm]	550 [nm]	400 [nm]	550 [nm]	400 [nm]	550 [nm]	400 [nm]	550 [nm]	400 [nm]	550 [nm]
19							716	731	645	596
16									649	637
var1									617	422

Table B.26: Measured UV absorbance for samples from tests with fluid system 3, oil continuous batch 2

Test	Sp1 [ppm]		Sp4 [ppm]		Sp3 [ppm]		Sp2 [ppm]		Sp6 [ppm]	
#	400 [nm]	550 [nm]	400 [nm]	550 [nm]	400 [nm]	550 [nm]	400 [nm]	550 [nm]	400 [nm]	550 [nm]
1p	643	462	647	489	611	845	669	643	665	670
2p	659	677	634	563	624	428	631	469	638	543
3p	635	442	645	509	640	710	635	442	654	616
4p	698	690	652	596	648	731	626	435	660	583
4p1	683	482	646	455					636	482
1			642	543	631	489	637	449	673	610
9			623	442	630	522	640	563		

Table B.27: Measured UV absorbance for samples from tests with fluid system 3, water continuous